AD-A107 339 WESTINGHOUSE DEFENSE AND ELECTRONIC SYSTEMS CENTER B--ETC F/G 9/5
ESTABLISHMENT OF PRODUCTION TECHNIQUES FOR TRANSDUCER ACOUSTIC --ETC(U)
JUN 81 A F ZAHORCHAK, R A MOORE, R N SUNDELIN DAAB07-77-C-0569

UNCLASSIFIED HDL-CR-81-569-1 NL

1 of 2
AD A
107 339

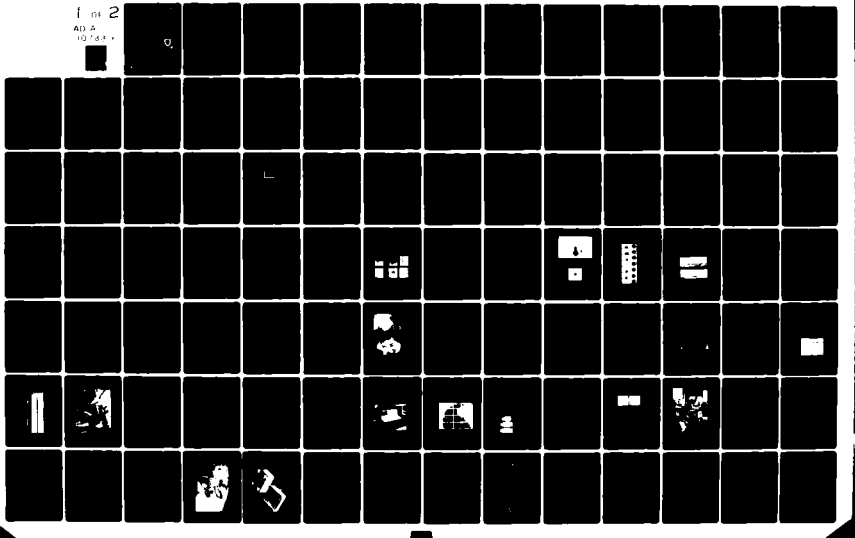

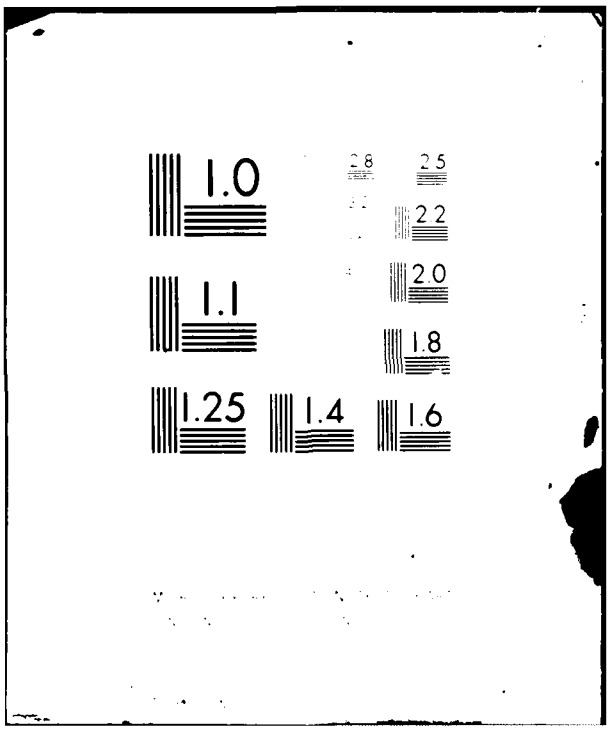
1.0
2.8
2.5
2.2
2.0
1.1
1.8
1.25
1.4
1.6

(12)

HDL-CR-81-500-1

LEVEL II

AD A107339

June 1981

Establishment of Production Techniques for Transducer Acoustic Delay Lines on a Pilot-Line Basis

by: A.F. Zahorchak, R.A. Moore, R.N. Sundelin, J.B. Goodell, B.R. McAvoy, and H.L. Salvo, Jr.

Prepared by

Westinghouse Electric Corporation
Defense and Electronics Systems Center
Baltimore, Maryland 21203

Under contract

DAAB07-77-C-0569

Contracting Officer's Representative
S. Lieberman

U.S. Army Electronics Research and Development Command
Harry Diamond Laboratories
Adelphi, MD 20783

The findings of this report are not to be construed as an official Department of the Army position, unless so designated by other authorized documents.

When this report is no longer needed, Department of the Army organizations will destroy it in accordance with the procedure given in AR 380-5. Navy and Air Force elements will destroy it in accordance with applicable directives. Department of Defense contractors will destroy the report according to the requirements of section 14 of the Industrial Security Manual for Safeguarding Classified Information. All others will return the report to Harry Diamond Laboratories.

SECURITY CLASSIFICATION OF THIS PAGE (When Data Entered)

REPORT DOCUMENTATION PAGE

READ INSTRUCTIONS BEFORE COMPLETING FORM

1. REPORT NUMBER: HDL-CR-81-569-1	2. GOVT ACCESSION NO.: AD-A107 339
3. RECIPIENT'S CATALOG NUMBER:	
4. TITLE (and Subtitle): Establishment of Production Techniques for Transducer Acoustic Delay Lines on a Pilot Line Basis.	5. TYPE OF REPORT & PERIOD COVERED: Final rep't. Sept 1977 - April 1980
6. PERFORMING ORG. REPORT NUMBER: (15)	
7. AUTHOR(s): A. F. Zahorchak, R. A. Moore, R. N. Sundelin, J. B. Goodell, B. R. McAvoy and H. L. Salvo, Jr.	8. CONTRACT OR GRANT NUMBER(s): DAAB07-77-C-0569
9. PERFORMING ORGANIZATION NAME AND ADDRESS: Westinghouse Electric Corporation, Defense and Electronics Systems Center, Baltimore, Maryland 21803	10. PROGRAM ELEMENT, PROJECT, TASK AREA & WORK UNIT NUMBERS: Program Element: P, PRON: 1F0P46750LCTA9
11. CONTROLLING OFFICE NAME AND ADDRESS: Harry Diamond Laboratories, 2800 Powder Mill Road, Adelphi, Maryland 20783	12. REPORT DATE: June 1981
	13. NUMBER OF PAGES: 128
14. MONITORING AGENCY NAME & ADDRESS (if different from Controlling Office)	15. SECURITY CLASS. (of this report): Unclassified
	15a. DECLASSIFICATION DOWNGRADING SCHEDULE: N/A

16. DISTRIBUTION STATEMENT (of this Report)

Approved for public release; distribution unlimited

17. DISTRIBUTION STATEMENT (of the abstract entered in Block 20, if different from Report)

18. SUPPLEMENTARY NOTES

HDL Project: 337035
DRCMS Code: 5297 0H3510

19. KEY WORDS (Continue on reverse side if necessary and identify by block number)

Delay Lines, Acoustics, Zinc Oxide, Bulk wave, Sputtering, Mosaic Transducer

20. ABSTRACT (Continue on reverse side if necessary and identify by block number)

For about the past decade the development of microwave acoustic delay lines has seen few innovations. It is primarily for this reason that opportunities in the production of these lines leading to lower cost and improved performance was not realized. Such innovations include monolithic matching, mosaic transducers and an intensive investigation of processing steps and systems operation. All aspects of delay line design have been reexamined including media loss and anisotropy, transduction efficiency, diffraction and transducer film analysis.

DD FORM 1 JAN 73 1473 EDITION OF 1 NOV 65 IS OBSOLETE

SECURITY CLASSIFICATION OF THIS PAGE (When Data Entered)

Abstract Continued

The net result of this effort is an essentially new approach to delay line design. This design lends itself well to batch fabrication processes with resulting cost reductions and performance improvement.

TABLE OF CONTENTS

TABLE OF CONTENTS
(Continued)

FIGURES
(Continued)

FIGURES
(Continued)

FIGURES
(Continued)

TABLES

SUMMARY

The purpose of this Manufacturing Methods and Technology project is to verify production-line techniques for the manufacture of low cost, reliable, and rugged bulk acoustic wave delay lines using a mosaic transducer with matching networks on the end of the delay line. The production techniques will be proven with a pilot-line capable of producing bulk acoustic wave delay lines at an equivalent rate of 500 acceptable units a month, in accordance with ECIPPR No. 15, revised August 1976, and the requirements of Specification No. 2779834, 29 June 1976. The pilot line will provide the production capability for military needs for a period of 2 years after the completion of the contract. The project will establish a base and plans for meeting expanded requirements.

The initiation of a pilot line requires the solution of problems and development of good performance in the following areas:

1. Design of the delay line
   - material selection
   - transducer design
   - multiple transit suppression
   - feedthrough suppression
   - impedance matching
   - compatibility to low cost and high-volume fabrication

2. Low-cost fabrication
   - high-yield fabrication techniques
   - efficient production flow
   - material costs and flow
   - automatic testing

3. Meeting production volume
   - high yield fabrication techniques
   - station capacity
   - efficient production flow

1. INTRODUCTION

1.1 Object of Program

The object of this program, as stated in the Request for Proposal (RFP), identifies these considerations toward production of microwave delay lines.

- series-connected mosaic transducers
- metal mask deliniation process to eliminate wet photo-processing
- control of processes
- elimination of hand tuning

All of the above aimed at achieving low-cost production. Viewed broadly, the objective of the program was to transfer the microwave delay lines into a microwave integrated circuit (MIC) in which all elements are fabricated through common processing steps. Approaching this goal required examining all aspects of delay-line design. It is felt that, at least in terms of confirming feasibility, all necessary elements have been verified. Thus, although low-cost production would require significant facility advances, the key elements have been established.

Of those elements that constitute a microwave delay line, a propagation media, and input and output transducers, the most process-dependent elements are the metal-piezoelectric film transducers at each end. At the outset of the program, the standard production transducer was a single-element transducer covering the required acoustical aperture. The electrical impedance was typically very low--often less than one ohm--and difficult to match. (Typically, lines required individual matching.)

A major accomplishment of this program was the verification of the series-connected mosaic transducer with integral tuning as a feasible

production element. This included geometric analysis, electrical analysis, and computer modeling for design purposes. It also included establishing both wet and dry mask process procedures compatible with dimensional requirements of the transducer.

The monolithically matched transducer consists of a series-connected mosaic transducer and either series or parallel monolithic inductors. Two separate models were used to describe the structure for design purposes. A three-dimensional diffraction analysis was carried out to assure that the mosaic transducer provided an equivalent acoustic aperture to a continuous transducer. A single dimension model was used to parameterize all elements of the delay line in a form simple enough to be useful for design. The analysis models the substrate, material, and physical parameters of each of the films and the monolithic matching element. One feature of the model is the ability to identify and make adjustment for variation in material parameters. This allows design optimization for the material parameters available. It also allows optimal redesign to new parameters and requirements without iterations.

Identifying an optimum approach toward zinc oxide deposition began with surveying those methods then in use. The Westinghouse approach at that time was rf diode sputtering. Although this was continued, it was felt that considerable analysis of the method and results was called for. Systematic analysis of results was carried out using reflection electron diffraction. By the end of the program a mass analyzer was made a part of the setup for on-line monitoring. Improved mechanization was developed in key areas, such as the laser thickness monitor, to allow operation by less skilled production operators. Finally key areas for further investigation were identified toward achieving a totally mechanized zinc oxide process. With completion of these activities, along with present metal film mechanization, it will be possible to completely computer control the process portion of microwave delay line fabrication.

Both wet and dry process approaches were carried out. Wet processing using photolithographic techniques allows a rapid generation of new patterns as required during a development phase. Once a pattern is established it appears low cost production may be available through dry processing using metal masks.

Besides substrate design, packaging is critical to acnieving isolation. At an early stage in the program it was discovered that the epoxy used to mount the substrate did not achieve full conductivity within a temperature range acceptable for processing metallized zinc oxide films. Extensive testing established that a polyimide achieved both very low resistivity and very low outgassing after curing at an acceptable temperature (under 200 ^{o}C).

Electrical testing is the final time consuming area in which a mechanized approach was feasible. The key difficulty has been availability of probes suitable for test at the wafer level which could provide a reliable measure of delay line performance. Such a probe was developed as a part of this program. This probe proved so successful that the effect of the added lead inductance in the package can be identified and therefore compensated in the design. Mechanization of wafer testing thus depends only on the development of a mechanical probe transporter analogous to that used by IC processors.

1.2 One-Dimensional Analysis

The piezoelectric transducer used for the bulk of this work launches a parallel, longitudinal wave at the surface. Not until the wave moves away from the transducer does the geometry shift due to diffraction effects. When analyzing the transducer, variables change in only one direction. Only the area in the nonpropagating direction is needed for the analysis. The one-dimensional analysis uses a Mason model

as its basis. The basic program can be run on almost any computer. We have programs for programmable calculators, desk-top computers, and main-frame computers. The speed of execution and degree of complexity possible are determined by the machine used.

1.2.1 Purpose of Computer Program

Three different computer programs were used in this contract. The first calculates the input impedance and estimates the insertion loss. It uses the Winslow-Reeder-Mason model. In this program the substrate is represented by a resistance and the input impedance is calculated. By computing the power transfer into the substrate, the transducer insertion loss is calculated. By adding substrate losses, the total insertion loss can be estimated. The second program incorporates the first and finds the values of physical parameters which best fit the data. The third program uses the same model as the first but uses a lossy transmission line for the substrate. The program calculates and plots the insertion loss versus frequency.

1.2.2 Transducer Equivalent Circuit

The transducer theory presented here is based on the Winslow-Reeder-Mason model where the piezoelectric material, sandwiched between two electrodes, is treated as a center-tapped transmission line. figure 1 shows the Winslow-Reeder schematic. The (assumed lossless) piezoelectrical conversion is represented by a negative capacitance together with a 1:1 transformer.

The basic equations for computing the three layer transducer electrical impedance are:

$$Z = \frac{V}{I} = \frac{1}{j\omega C_o} + \frac{P(f)}{R_o(\omega C_o)^2} \qquad (1)$$

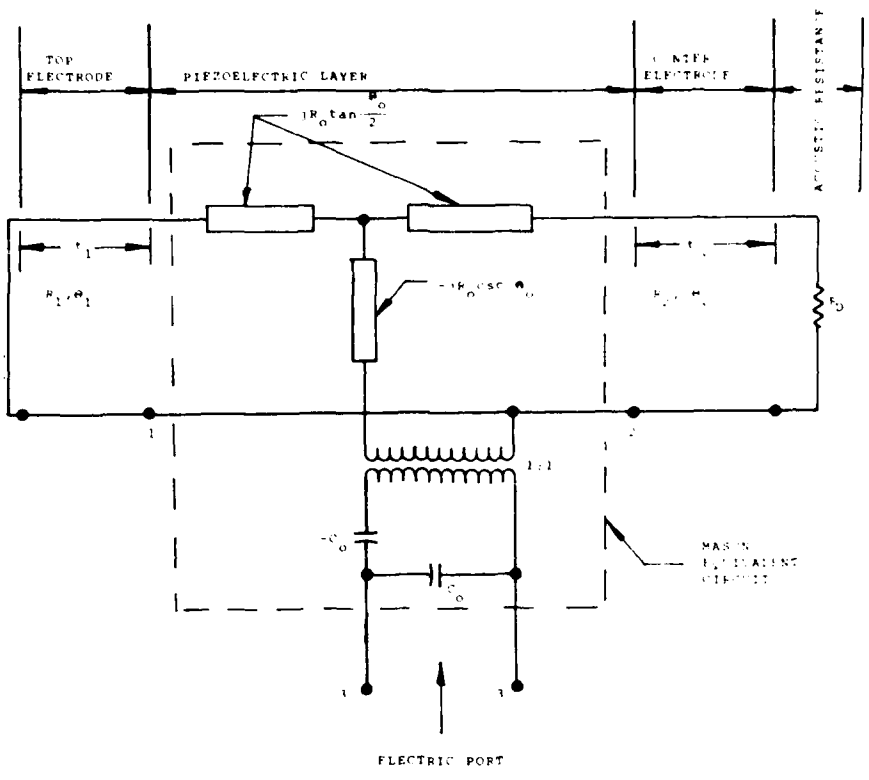

Figure 1. Winslow-Reeder-Mason transducer model.

where ω is the angular frequency, C_o is the piezo-layer capacitance, R_o is $\pi/\omega_o C_o k^2$, k^2 is the acousto-electric coupling efficiency, and $r_D = R_D/R_o$, with R_D the electrical unit equivalent of the transducer substrate acoustic impedance.

$$P(f) = \frac{2j(1-\cos\theta_o)+(Z_1+Z_2)\sin\theta_o}{(1+Z_1Z_2)\sin\theta_o - j(Z_1+Z_2)\cos\theta_o}, \qquad (2)$$

where $\theta_o = \pi\omega/\omega_o$,

$$Z_1 = jr_1 \tan \theta_1,$$

$$Z_2 = r_2 \frac{r_D \cos\theta_2 \sin\theta_2}{\cos\theta_2 + jr_D \sin\theta_2},$$

$$r_1 = R_1/R_o,$$

$$r_2 = R_2/R_o,$$

$$\theta_1 = \pi d_1 \omega/\omega_o,$$

$$\theta_2 = \pi d_2 \omega/\omega_o,$$

R_1 and R_2 are electrical equivalents of the electrode acoustic impedance, and d_1 and d_2 are the corresponding normalized electrode thicknesses. The quantity of interest is the real part of equation (1); namely,

$$R = \frac{4k^2}{\pi r_o} \frac{1}{\omega C_o} \frac{\omega_o}{\omega} \frac{(r_D/2)^2(1-\cos\theta_o)^2}{\sin^2\theta_o + (r_D\cos\theta_o)^2} \qquad (3)$$

By setting R equal to some desired input impedance value, e.g., 50 Ω, transducer areas can be determined based on electrode thickness and substrate.

R is, of course, frequency dependent, the pulse frequency being primarily determined by the piezo layer thickness. Equation (1) also takes into account the electrode thickness through the transition angles, $\theta_0, \theta_1, \theta_2$. Thus, by adjusting thickness, frequency response characteristics can be predetermined over wide ranges.

The adaptation, figure 2, for the present analysis extends the Winslow-Reeder-Mason circuit in order to account for multiple sandwich layers. For example, a typical transducer of the present study comprises the following materials in the following thicknesses: Aluminum, (2000 Å); Silicon dioxide, (200 Å); chromium, (50 Å); zinc oxide, (3000 Å); gold, (1200 Å). The chromium and gold are at one end of the transducer, the aluminum, silicon dioxide, chromium are at the other. The first end terminates in the delay-line material. The second terminates in the air. The model also allows acoustic losses in the metal films and delay line material.

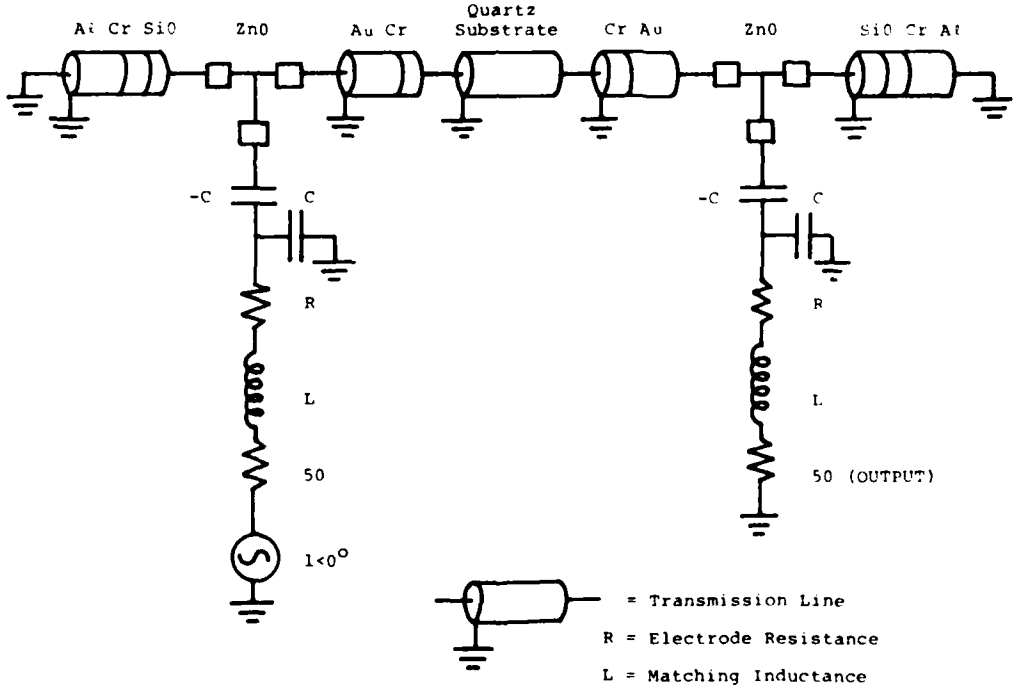

Figure 2. Transmission-line model

The modified circuit is the one used for the third program discussed in section 1.2.1. The first two programs would use only one half of the circuit. The circuit shown has both input and output transducers. The analysis transforms the Thevenin equivalent generator through the circuit. The resultant Thevenin equivalent circuit is then placed across the output load resistor. This analysis gives the bandpass charactreristic of the delay line which includes ripple from multiple transits.

1.2.3 Computer Fit of Physical Parameters

The computer programs did not predict the proper resonant frequency. When the actual thicknesses were used, as measured by a Sloan Dektak, the frequency was about 10% off. A new program was written which varied the physical constants of the films until the best fit was achieved with the frequency thickness data. Using these numbers for the physical parameters, new designs can be generated with an expected error of less than 2%.

It was also discovered that different systems required different correction factors. The two different zinc oxide sputtering systems required a 10% correction for one and zero correction for the other.

1.2.4 Computer-Calculated Insertion Loss and Input Impedance

The computer programs previously described have special features which are used in calculating the insertion loss and input impedance. The effective area of the transducer is one of the input variables. This is used to calculate the capacitance used for the equivalent circuit. Also the number of squares of each electrode is entered. This information, along with the thickness, is used to calculate a series resistance. The capacitance and resistance are

calculated each time any of the film thicknesses are changed. Starting with the substrate acoustic impedance represented as a resistance, the impedance at the substrate side of the zinc oxide is calculated. Starting with a short for the unloaded surface of the top electrode, the impedance at the other side of the zinc oxide is calculated. The equivalent circuit for the zinc oxide is used to compute the electrical input impedance of the transducer. The series resistance described above and the tuning and bonding elements are added to find the inputs of the device. This single transducer program keeps track of the power going into the radiation resistance relative to the input power in a 50 Ω system. This loss is then doubled for the delay line. The absolute value is not correct because diffraction and material losses are not calculated, but the shape of the curve with respect to frequency agrees well with experimental results. The input impedance also agrees with experimental results.

1.2.5 Frequency Sensitivity Due to Variation of Physical Parameters

A set of curves has been generated which gives sensitivity of each of the parameters to variation. Examples shown in figures 3 and 4 show the change in center frequency, for example, for variation in thickness and acoustic impedance for each of the constituent films.

1.3 Transducer Design

The three device specifications which have the greatest effect on the transducer design are the input VSWR, the maximum insertion loss, and the bandwidth. These specifications tend to interact during the design. A good input impedance and bandwidth can be obtained at the expense of the insertion loss. This is especially true for single-element transducers where reducing the area for impedance considerations increases the diffraction losses. With a mosaic

transducer, the interaction between input impedance and insertion loss is greatly reduced.

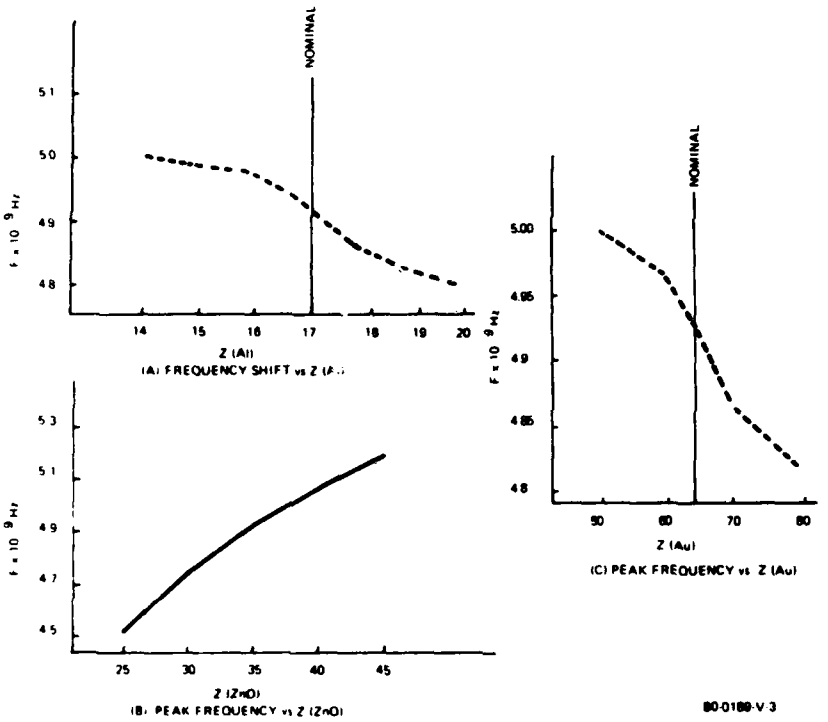

Figure 3. Variation in center frequency versus acoustical impedance (Z) of transducer constituent films.

1.3.1 Series Mosaic

A mosaic transducer is formed by dividing the active area into sections. If the sections are connected in parallel, the input impedance would be the same, but the wave pattern would be altered by the position of the sections. By connecting the sections in series, the input impedance increases, but the acoustic wave pattern can be kept almost the same. The acoustic wave pattern is changed slightly by the inactive

region between the sections. If a transducer is broken into N sections which are connected in series, the impedance will be N^2 times greater than the unbroken transducer. For this contract a series mosaic was used.

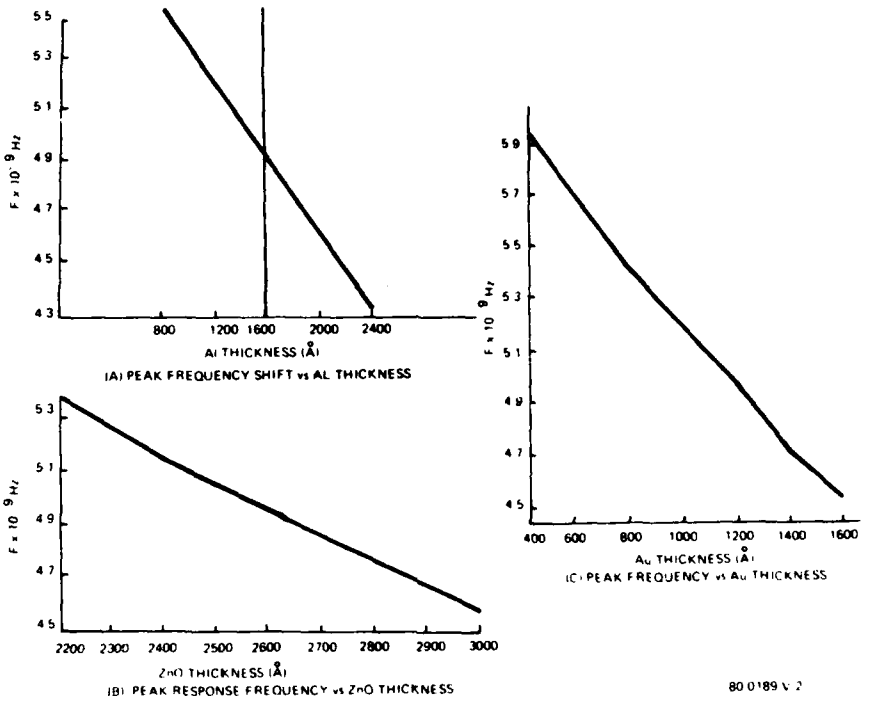

Figure 4. Variation in center frequency versus thickness of transducer constituent films.

The transducer appears mainly capacitive with some resistance. A typical Q would be around five. In order to match the transducer with a single inductor, the impedance has to be high. On a Smith Chart, the inductor has to swing the impedance into the center.

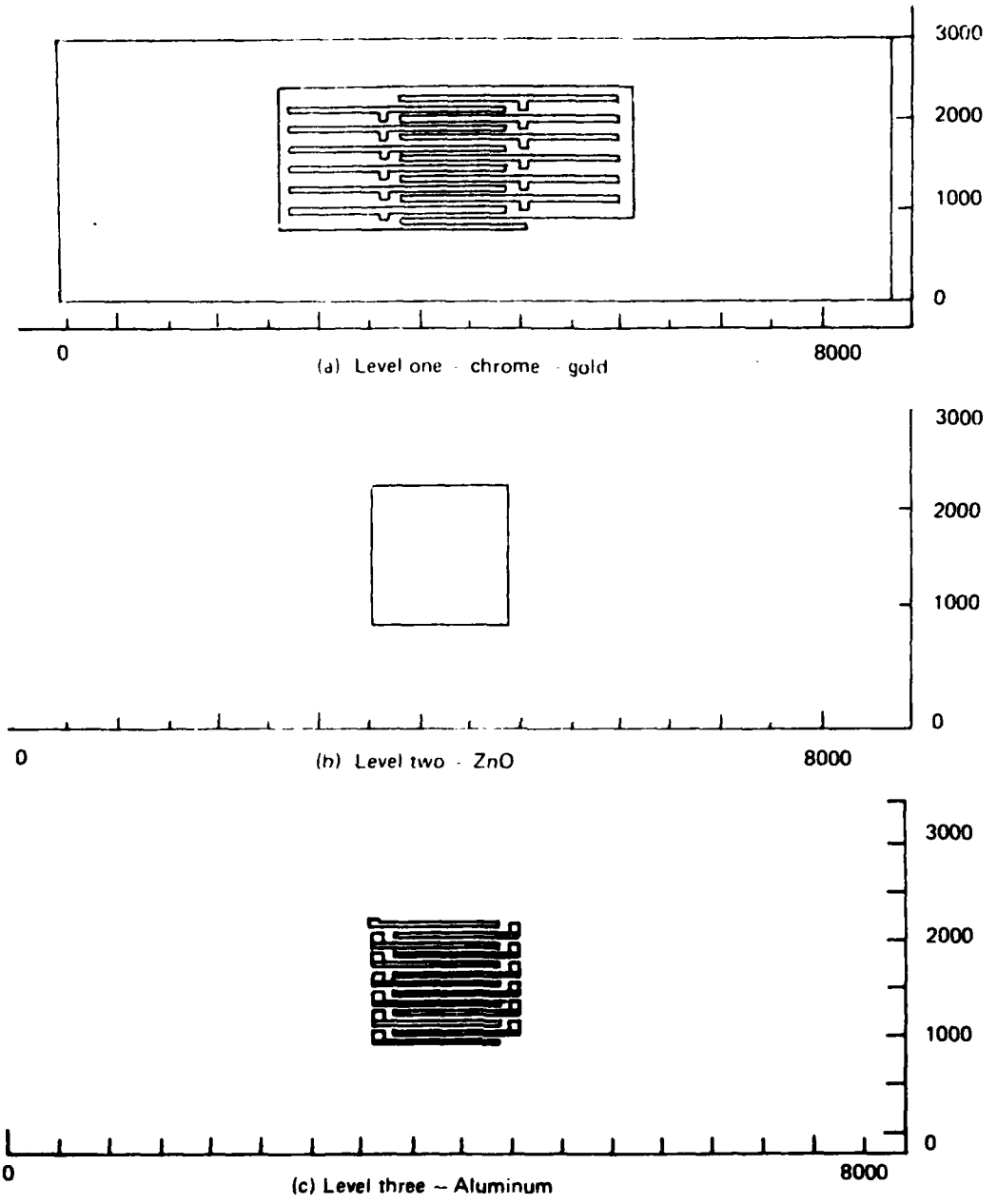

Figure 5. Initial mosaic transducer design (1 grid unit = 0.5 μm).

1.3.2 Initial Mosaic Transducer Design

The initial mosaic transducer design used to fabricated Type A and B delay lines is shown in figure 5. It features 13 series-connected transducer elements and no monolithic matching inductor. The single-ended input/output wire is attached to a pad area at the beginning of the first top surface electrode; the ground plane extends completely around the transducer and is connected to the walls of the package by conductive epoxy. The acoustic aperture is 21.65 mils x 24.1 mils while the area of one element is 10 $(\text{mils})^2$. The acoustic aperture is sufficiently large to place operation in the acoustic near zone for both types of delay lines being fabricated. A set of flying fingers was incorporated in the design to reduce feedthrough due to capacitive coupling. The first devices fabricated were made with these cancellation elements disconnected. The feedthrough from port one to port two has been found to be well within specification; therefore, subsequent transducer designs will not incorporate capacitance cancellation elements.

1.3.3 Transducer Design: Second Iteration

Devices from the initial mosaic transducer design were fabricated using photolithographic masking techniques. The details were reported in the first quarterly report, March 1978. The results obtained with devices fabricated from the first mask set indicated the need for a second generation of transducer designs before committing the program to metal masks. Four transducer designs were formulated and combined into a single photolithographic mask set. Devices were then fabricated and tested. The techniques of combining several geometric designs into one mask set allowed direct performance comparison of devices made at the same time, but with different transducers. The combined transducer designs are shown in figure 6. The mask includes two designs which are optimized for Type B device parameters. Each set of

two designs is further divided into one series inductor and one parallel inductor design. Each transducer was designed to have a 50 Ω real impedance at center frequency and a 10 dB bandwidth of 20%, the center frequency value. The following paragraphs describe the unique features of the individual designs.

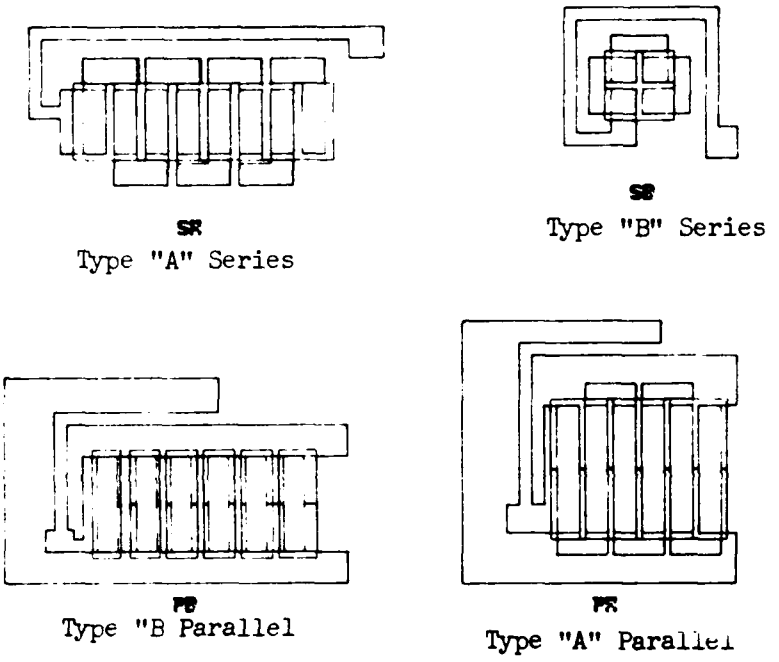

Figure 6. Combined transducer mask set: second iteration

The geometry of the parallel inductor transducer design optimized for operation of Type A frequency and delay is shown in figure 6. The design consists of six series connected transducer elements. Each element is 20 mils by 3.52 mils. Series connection is made at the end of the transducers by overlaying the aluminum upper electrode over the gold lower electrode. The total acoustic aperture is sufficient to place the receiving transducer in the acoustic near field zone of the

transmitting array. Interference effects due to fine structure can arise because the spacing between individual elements of the array have not been considered in setting the displacement between elements. The parallel inductance required to match the capacitive reactance of the transducer is 1.05×10^{-9} H. The resulting dimensions of the inductor are then 2 mils wide by 47.5 mils long by 0.011 mils thick.

The geometry of the series inductor transducer design optimized for operation at Type A frequency and delay is shown in figure 6. The design has eight series connected transducer elements each, 10 mils by 3.57 mils. The interconnection between array elements is made at the end of the transducer similar to the parallel design described above. The total series inductance necessary to resonate the circuit at the center frequency is 2.71×10^{-9} H. Approximately one nanohenry of series inductance is obtained by the wire bond between package terminal and device. The remaining series inductance of 1.62×10^{-9} H is supplied by the on-chip inductor.

The geometry of the parallel inductor transducer design optimized for operation at Type B frequency and delay is shown in figure 6. The design consists of six series connected transducers each 15 mils by 3.18 mils. The interconnection between elements is made by overlapping of aluminum and gold electrodes along the long edge of the transducers. This design leads to the lowest possible series resistance for the individual elements. In practice, however, the over-throw of the zinc oxide causes problems in achieving contact between top and bottom electrodes. The parallel inductance necessary to achieve resonance is 0.9×10^{-9} H in series, which is provided by the bond wire length, and 0.94×10^{-9} H in parallel, which is supplied by the on-chip inductor.

The geometry of the series inductor design optimized for operation at Type B frequency and delay is shown in figure 6. The design

consists of four square series connected transducers. Each element is 3.89 mils on a side. This design represents an optimum compromise in minimizing the losses due to resistance of the electrodes. The total inductance necessary to achieve resonance at the required center frequency is 2.03×10^{-9} H. Approximately 0.4×10^{-9} H of series inductance results from the bond lead, while the remaining 1.63×10^{-9}H results from the on-chip series inductor. Although more series inductance could be supplied by the bond wire, the intent is to minimize this inductance because it is substantially less controllable than the on-chip inductor.

1.3.4 Transducer Design: Third Iteration

The second iteration of transducer design did not yield devices which met all the specifications. Improved computer programs were written to fit the data by minor variations in the physical properties. Material constants such as velocity and acoustic coupling were varied. With thin deposited films one would not expect the material constants to be bulk values. The main program, which computes bandwidth and input impedance, was also enlarged to automatically include electrode resistance. Diffraction and material loss could be added to this program for an absolute insertion loss. The diffraction losses were computed by separate program and found to be nearly independent of frequency. Using the impedance bandwidth program, new designs were derived which incorporate the better physical constants. There are two designs, one for a parallel matching inductor and one for a series matching inductor. This design was optimized for the "B" frequency, but the program predicts it will also be satisfactory for the "A" frequency. The reason both frequencies should work is because "tapped" inductors were included in the design.

Feedthrough has also been a problem with the larger transducer designs. At first, the feedthrough was masked by the test fixture, but after the fixtures was corrected the devices could be accurately measured. The test fixture has a feed through suppression of 70 dB. The capacitive coupling was analyzed from the input to the output transducer of mosaic structures. An upper bound on area was obtained from this analysis and is incorporated in the new designs.

The two new designs, one parallel and one series, for the transducers were completed, and photolithographic masks were made to test the design. The design criteria are as follows: For diffraction loss effects, an aperture dimension of 9 mils was used. To limit capacitive feedthrough, the maximum electrode pattern width is 15 mils. A 2 mil tolerance is used between the active area and the interconnects to allow for underthrow or overetching. Based on the computer program, the number of squares in the electrodes was kept to a maximum.

Series Tuning.--With the basic rules described above, the series device was designed with six series sections of 6.55 $mils^2$ area each. The sections are positioned in a circula: pattern in order to maximize the number of squares of interconnects. The pattern is positioned so that the highest potential part of the electrode is above the ground at the other transducer. The second highest is above the lowest, etc. The inductor is on one side of the transducer so that coupling between inductors is minimimal. The complete inductance is on the chip, but there are three bonding pads to allow for the bonding wire in the package. Figure 7 shows the series transducer with the 6 nH inductor.

Parallel Tuning.--The parallel inductor design requires a much lower transducer impedance than the series tuned device. This led to three sections of 24 $mils^2$ in series. The relative impedance between the series and the parallel is over 7:1. A 1.5 nH inductor is used for

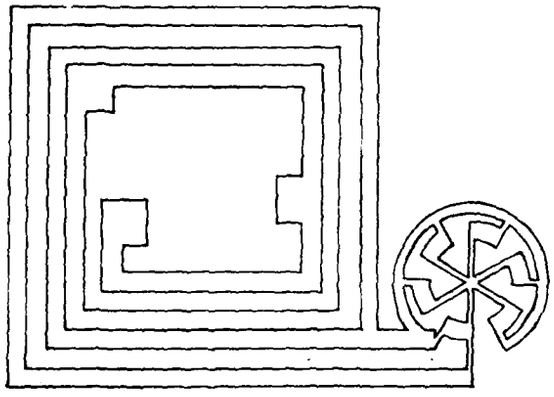

Figure 7. Series transducer with a 6 nH inductor

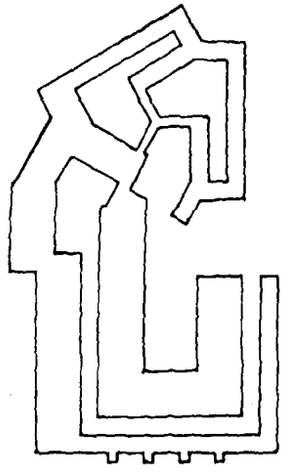

Figure 8. Parallel tuned transducer

parallel tuning. This inductor can be changed by shorting to ground. Figure 8 shows this design. The computer program indicates that this design is very sensitive to the series resistance in the electrodes. This sensitivity is not expected to be a problem in processing because of the controls used during depositions. It could, however, require a few fabrication iterations in order to optimize the electrical performance.

Isolation.--Signal isolation requires both capacitive and magnetic isolation--both significant in the delay line package. Because of the approximately 30 dB insertion loss of the delay line, isolation should be at least 60 dB and preferably 70 or 80 dB to assure a reasonable margin for manufacturing.

The lack of isolation can be from both capacitive and magnetic coupling. Capacitive coupling is illustrated in figure 9. It is the result of the transducers being opposite each other and cannot be made

zero for the multi-element series-connected configuration. The mosaic design is arranged such that capacitive coupling is minimized. Isolation is greater than 80 dB, and therefore is great enough that it is not a design problem.

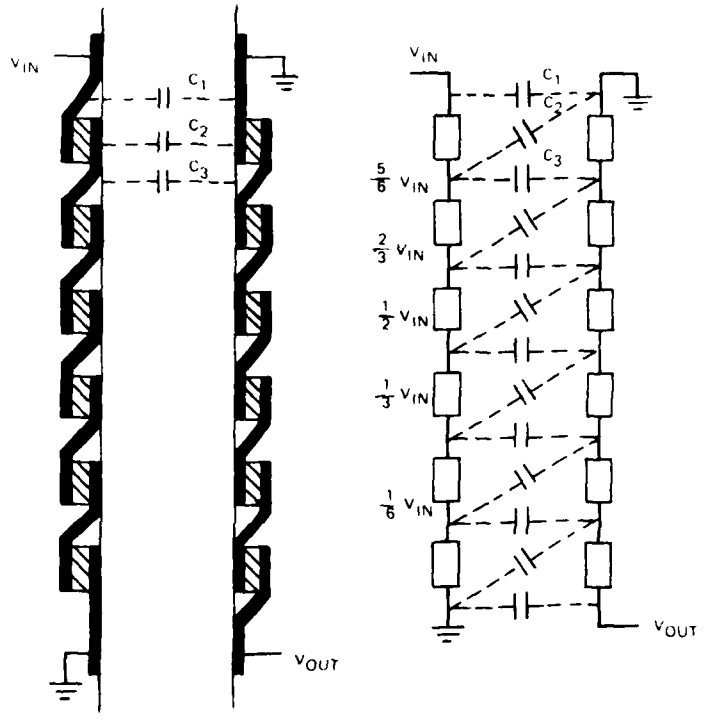

Figure 9. Linear representation of the six-section mosaic showing feedthrough capacitance elements and the equivalent circuit.

Magnetic isolation is normally the greater problems and it is illustrated in figure 10. The magnetic coupling of prime importance results from breaking current loops in the shield of the substrate or between the substrate and ground or causing current loops to occur which generate rf magnetic fields.

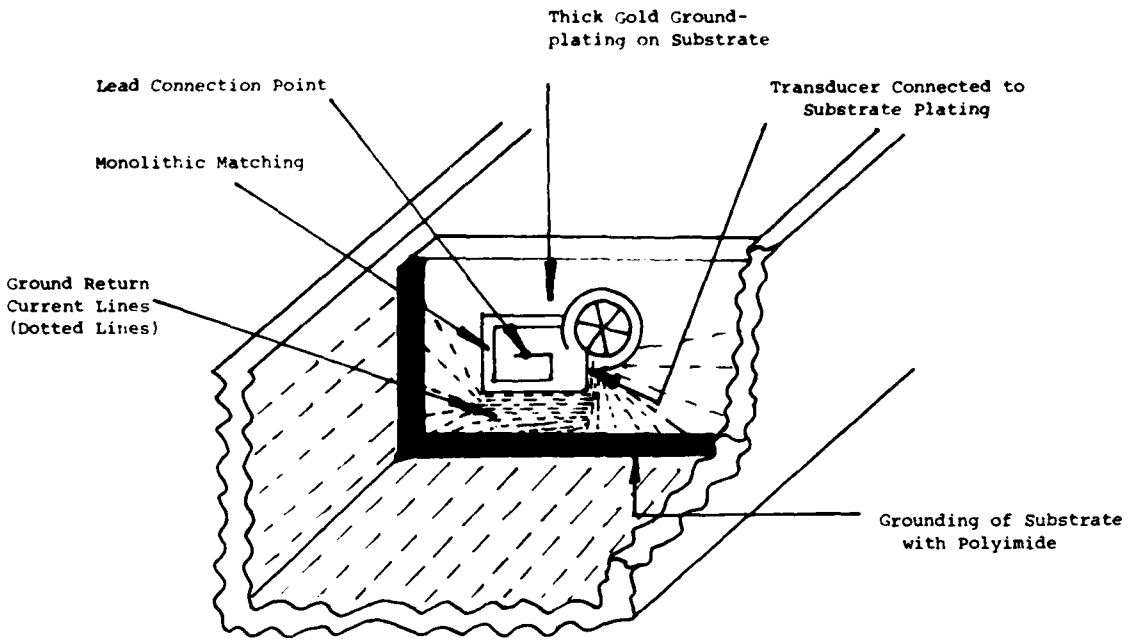

Figure 10. Diagram of ground return currents which can cause magnetic coupling.

Isolation has been solved by the use of an extremely thick film on the ground surface so that currents opposite each other are fully isolated and by high conductivity polyimide used to couple the substrate ground to the package ground. With the polyimide this is done continuously on the periphery of the substrate which gives a maximum of current transfer. At times there has been a problem of breaking the current filaments at the top of the substrate. At those times this was solved by a gold leaf between each substrate and its respective ground close to the package ground at the appropriate feed thru. This is not necessary if a sufficiently thick ground is used. The remaining possible source of magnetic coupling is in the monolithic tuning elements themselves. This coupling can be eliminated with proper positioning of the monolithic tuning elements and has never been a serious problem.

It should be pointed out that the polyimide used by Westinghouse for grounding the substrate has a full curing temperature of less than 200 ^{o}C. Complete curing and specified conductivity can be achieved at a temperature well below the safety temperature of the piezoelectric films. This is extremely important because an epoxy, H31, cures at greater than 200 ^{o}C and we have found that this temperature adversely affects zinc oxide piezoelectric films. In curing below 200 ^{o}C the H31 is only partially cured and the resistivity is too high. The degree of conductivity achieved is highly dependent on the exact mixture and the cure temperature used, and thus can vary considerably from run to run. In this case the H31 cannot be depended upon for isolation, and extra parallel bonds are required. Extra labor and lower reliability are the result.

1.4 Three-Dimensional Analysis

Delay line performance prediction requires a knowledge of the acoustical wave diffraction from the transmitting electrodes. Diffraction determines not only insertion losses but triple and higher order transits as well. In turn, transducer configuration and delay-line bulk geometries as well as crystal wave propagation properties control diffraction. Optimum delay-line design requires obtaining maximum throughput and minimum triple transit. Throughput depends on transducer piezoelectric properties as well as diffractions, but the ratio of triple transit to throughput depends only on diffraction. Thus, three-dimensional diffraction analysis is an important step in delay-line design.

1.4.1 Scalar Wave Propagation

Diffraction analysis is conceptually simple but the computations require computers. The basic equation for scalar wave propagation in an isotropic, homogeneous acoustic medium is

$$U(x,y,z,) = \frac{jk}{4\pi} \iint \frac{U_a \, e^{-jkR}}{R} (1+\cos\theta) \, ds \qquad (4)$$

where $j = -\sqrt{-1}$, $k = 2\pi$ /wavelength, $R = \sqrt{(x-y')^2 + (y-y')^2 + (z-z')^2}$ x', y', and z' are the coordinates of the receiving plane, x, y, and z are the coordinates of the transmitting plane, U_a is a function of the transmitting plane, θ is the angle between the propagation vector and the normal to the transmitting plane, and S is the transmitting surface. Usually is very small so that cos almost exactly equals unity. Equation (4) occurs often in all types of diffraction situations.

The principal difficulty with solving (4) is that no closed form solutions exist. Second-order integrals (Fresnel approximations) lead to sin and cos integral approximations which have been extensively tabulated. First-order integrals (Fraunhofer approximations) lead to very convenient Fourier Transform solutions which are often easy to obtain in closed form and, depending on transducer aperture dimensions and delay-line thickness, can provide good approximations to rigorous solutions. For example, figure 11 compares a "rigorous solution" of a square aperture to the solution obtained by Fourier transforming the aperture. Here, mainly because of the large separation between transmitting and receiving planes, the Fraunhofer approximation is a very good approximation to the actual solution. In other cases, where the delay-line thickness is not great, the transducer aperture is large, or the wavelength approaches the aperture or thickness dimensions, the Fourier transform approximation provides a good initial solution. The exact solution requires either a series solution or some numerical algorithum. Previous experience at Westinghouse favors a numerical algorithum over a series solution because the answer can be obtained with less computer time.

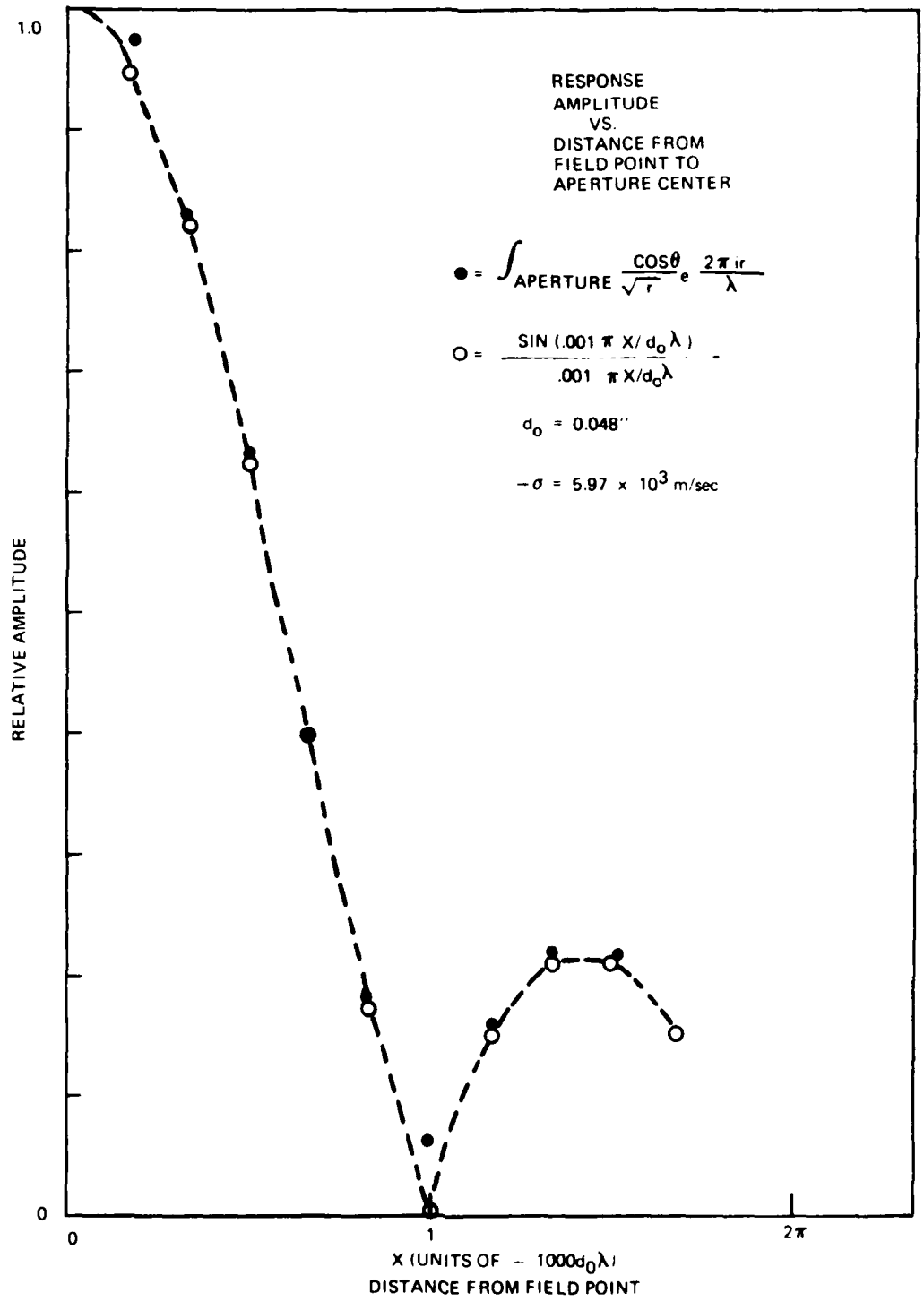

Figure 11. Comparison of rigorous solution to Fourier transforming solution.

A typical solution uses basically a trapezoidal or Simpson's rule quadrature. The two constraints which increase computation time are Nyquist sampling and limits of integration. Thus, to avoid aliasing, lattice points must be close enough so that phase changes between two successive points do not exceed the Nyquist limit of 180 degrees. Experience has shown that phase intervals no greater than 30 degrees give better solutions to these nonlinear equations. On the other hand, the limits of integration, (the sampling window width) must be large enough to avoid large truncation errors. In the final stages of each real design these two constraints were balanced to provide sufficiently accurate solutions in reasonable computation times.

Simplifications due to symmetries in transducer geometries can drastically reduce computation time while often providing exactly the same solutions as the long algorithms. The following examples illustrate design approaches and typical results.

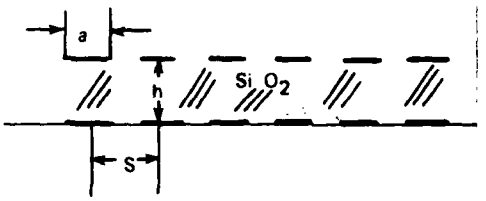

S = 1.716567689

a = 0.5

h = 16 mil

Figure 12. Square-wave transducer.

1.4.2 Square Wave Type Transducer Arrays

Figure 12 depicts a typical, in this case six-finger, array of transmitting electrodes over an identical set of receiving electrodes. Each electrode has the same width and separation from its nearest neighbor. In this configuration, the receiving electrodes lie directly under the transmitting electrodes (i.e. no offset). Alternate electrodes may or may not alternate the sign of voltage. The design objective is to adjust electrode widths and spacing so as to minimize triple transit relative to throughput. The thickness determines the amount of delay. Figure 13 shows a computer calculated result of triple transit versus wavelength in the case where the design is optimized for a normalized wavelength (denoted by 1.0 on figure 13). The results show that designs of this type which operate solely on interference and diffraction mechanisms do not make good broad bandwidth delay lines.

1.4.3 Single Aperture, Tilted Plane

A single aperture transducer has a main lobe and side lobes, a property which offers several promising design possibilities. One of these is a delay line with input and output faces tilted with respect to each other. Tilting the faces causes the triple transit signal, after the two reflections it experiences, to strike the output plane at an angle corresponding as nearly as possible to a diffraction minimum. This requires the angle between the faces to be 1/3 of the angular distance to the first minimum of the diffraction patterns. Thus, a long narrow input transducer of width "a" has a first order zero at an angle, $\theta = \lambda/a$ radians.

A typical design started with a 0.0002" wide transducer and a relative tilt between plates equal to 0.00256 rad. In general, a first-order relation between transducer aperture width, wavelength, and relative tilt is: $a = \lambda/3\theta$, where λ is the wavelength, θ is the

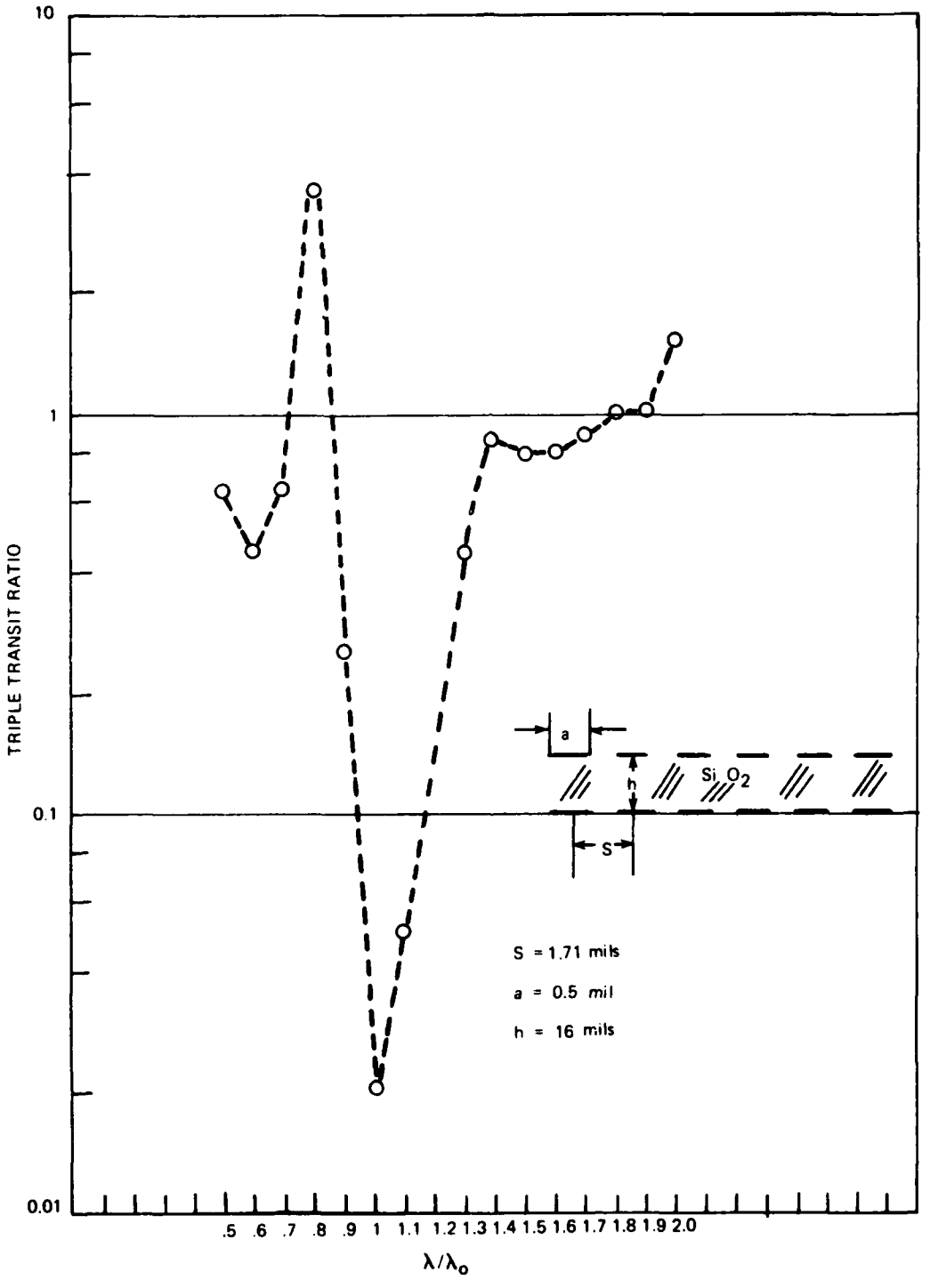

Figure 13. Computer results for triple transit versus normalized wavelength.

relative tilt angle, and "a" is the aperture width. A more rigorous solution, the one used to optimize, requires first a computation of the diffracted field over the entire slanted output surface (the output surface can be assumed to slope relative to the input face, as shown in figure 14). This field is integrated over the input surface and once again over the output surface. A constraint is that voltages are constant over the input and output electrodes. Thus, the output voltage is the vector sum of the voltages across the output transducer.

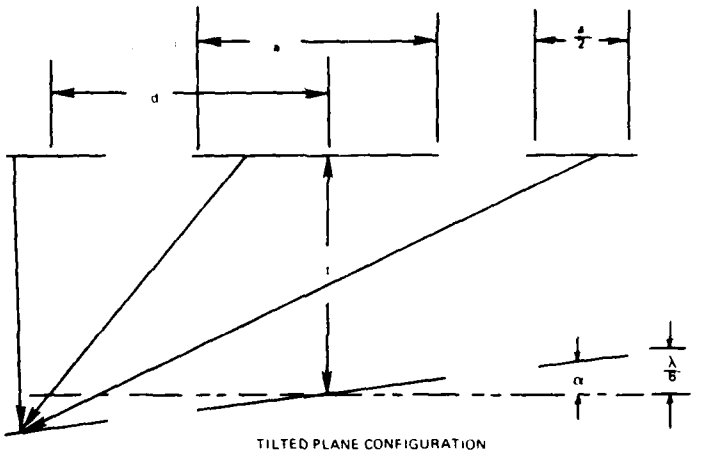

Figure 14. Single aperture, tilted plane transducers.

1.4.4 *Three Finger Configuration*

This arrangement places three transmitting electrodes above three identical receiving electrodes. The central electrode has the same length but is twice as wide as each of the side electrodes. The lower face is sloped so that one side electrode advances the phase by 60 degrees relative to the central electrode, while the other side electrode retards the phase relative to the central electrode by the same amount.

The input, central, and side electrodes are connected as are the output electrodes, so the output voltage is the vector sum of the voltages across the three electrodes. Because of this and because after a triple transit the phase differences triple, the configuration suppresses triple transit by destructive interference. This design, one of the more successful ones, was analyzed and optimized using the previously described procedures.

1.4.5 Output Offset Relative to Input

This configuration uses equal size input and output electrodes. Both are square-wave configurations, but the output electrodes are offset relative to the input electrodes. The analysis resembles the other configurations. Poor diffraction efficiency reduced the practicality of this design.

1.4.6 Efficient Diffraction Algorithm Development

This effort became necessary after considering the results of computation cost and time needed for diffraction calculations. The calculations themselves are critical steps in optimizing all parameters (bandwidth, insertion loss, etc.) associated with all acoustic devices under study.

The basic difficulty is that device dimensions place all diffraction patterns in the Fresnel zones, even within very near zones. This latter fact was determined by noting the relative magnitudes of the terms in power series expansions of the radius vectors. This causes field amplitudes to oscillate faster and faster as the radius vector increases. However, these oscillations are not rapid enough to apply the stationary phase method. The only approach with these integrals, since no closed form exists, is numerical integration on a computer using

enough sample points, at least 100, across each of the two dimensions of the transmitting electrodes and across the two dimensions of the receiving electrodes. This entails 100^4 or 100^8 sine and cosine calculations, far too many for practicality.

Diffraction Integral.--Knowledge of the field amplitudes on the receiving plate are absolutely necessary, thus necessitating the development of the fast algorithm described below. The basic function to be integrated is quite simple; namely,

$$\varepsilon(f,x,x',y,y',T,v) = \frac{T^2}{R^3} e^{i2\pi fR/v(1+\cos\theta)} \qquad (5)$$

where f is frequency, v is the velocity of the compressional wave in the acoustic medium, x and y are coordinates on the lower (receiving) electrodes, T is the electrode separation, θ is the off axis angle, x' and y' are coordinates on the upper (transmitting) electrode, and $R = \sqrt{(x-x')^2+(y-y')^2 + T^2}$; that is, the distance between one element on the transmitting electrode and an element on the receiving electrode.

The output on the receiving electrode, of course, is the integral of ε over both the upper and lower electrodes;

$$\text{Output} = \int\int\int\int \varepsilon\,(f,x,x',y,y',T,v)\; dx\;\; dx'\;\; dy\;\; dy' \qquad (6)$$

Fast Algorithm.--This impressive integral can be drastically reduced by collecting all x and x' for which $(x-x')^2$ is a constant, thus exploiting the convolution properties of (1). (Note that the only variable quantity is R.)

A computer, which performs the numerical integration, employs running integers for the x and y coordinates with a scale factor multiplication to relate the integers to the physical dimensions of the electrode. Thus, the integral (4) becomes the four fold sum

$$\text{Output} \simeq \frac{jk}{4\pi} \sum_{xx'} \sum_{yy'} \frac{\varepsilon U_a e^{-jkR}}{R} (1+\cos\theta)\, \Delta s \qquad (7)$$

where $x = I\,W/N$; $y = JW/N$; $x' = K\,W/N$; $y' = L\,W/N$, I,J,K,L are integers, W is the width and length of the (square) electrodes, and N is the number of increments. As I,J,K,L vary from 0 to N, the corresponding physical coordinates vary from 0 to N.

The computer program begins by counting all I and J such that the absolute value of the difference I-J is a constant. The set of sums is then stored. The sum corresponding to the $(y-y')$ difference is the same in the present electrode design so that all the ways in which $(x-x')^2 + (y-y')^2$ equal the same value are the products of the stored values, doubled when $(x-x')^2$ does not equal $(y-y')^2$.

Let A(N) equal the number of ways $(x-x')^2$ can equal N (also the number of ways $(y-y')^2$ can equal the same value). Then the number of ways the function $(x-x')^2 + (y-y')^2$ can equal a value, $N^2 + M^2$ is the product A(N) A(M) if N=M and 2A(N)A(M) if $N \neq M$.

This operation reduces the number of computations from approximately N_T^4, where N_T is the number of divisions to about $N_T(N_T+1)/2$. The reduction is exact in the sense that it gives identical answers as the long algorithm. It allows one to calculate values of the argument in equation (7) and multiply them by the corresponding weighting factors. Each weighting factor reduces the number of evaluations indicated by the weighting factor to 1.

Reduction To One Dimensional Integral.--The reduction above does not quite achieve the full simplifications desired for feasible electrode optimization. The following continuation, while not exact achieves very high accuracy which increases with the number of intervals.

The computer finds all $(I-K)^2$, $(J-L)^2$ combinations for which the sum, $(I-J)^2 + (K-L)^2$ has the same value. The algorithm uses the A(N) obtained in the first reduction. Thus, for each integer value of $(I-J)^2 + (K-L)^2$, a new, final weighting function results from combinations of all the weighting values, the A(N). This final reduction reduces the integration to a one-dimensional integration, or on the computer, to a single sum. Thus,

$$\epsilon = \int W(r) \frac{T^2}{R^3} \exp \frac{j2\pi fR}{V} \, dr, \tag{8}$$

where $r = \sqrt{(x-x')^2+(y-y')^2}$ and $R = \sqrt{r^2 + T^2}$. The r's are scaled to integers for numerical computation.

Results.--The results indicate a very flat spectral dependence for an electrode pattern which consists of two identical configurations, one over the other, separated by 25 mils. Each configuration is constructed of four square electrodes, 4 mils on a side having one mil gaps. The large aperture size relative to the electrode separation places the diffraction well within the near field so that the acoustic wave pattern over the bottom electrode is almost constant for all frequencies. A slight falloff at higher frequencies is attributed to destructive interference, which is greater when more cycles (due to higher frequencies) enter into the calculation.

A different geometry will require a new weighting function determination. The reduction principle, however, will be the same in all cases.

1.5 Delay-Line Media Selection

The selection of the delay line medium is primarily determined by the following factors: (1) propagation loss, (2) anisotropy[1], (3) acoustic impedance, and (4) velocity. Other factors are also considered, such as: (1) mechanical and chemical stability, (2) relative ease of polishing and cleaning, (3) temperature coefficient of delay and (4) cost and availability of material.

1.5.1 Propagation Loss

An overview of the propagation loss parameter is provided in figure 15, which shows the longitudinal wave attenuation in decibels per centimeter versus frequency (GHz) for selected material at room temperature, and in figure 16 which is a plot of the media attenuation coefficient (decibels per wavelength) with the associated material Q versus frequency from 1 to 10 GHz.

The Westinghouse design philosophy for echo and spurious acoustic mode suppression is to set the single transit loss via propagation attenuation to approximately 5 dB. S Band delay lines therefore generally employ fused quartz or cultured crystalline quartz with a propagation loss of about 20 to 30 dB/cm.

---

[1] J. Murphy and M. Gad, "A Versatile Program for Computing and Displaying the Bulk Acoustic Wave Properties of Anisotropic Crystals", 1978 Ultrasonics Symposium Proceedings, IEEE Cat. 78CH 1344-15SU.

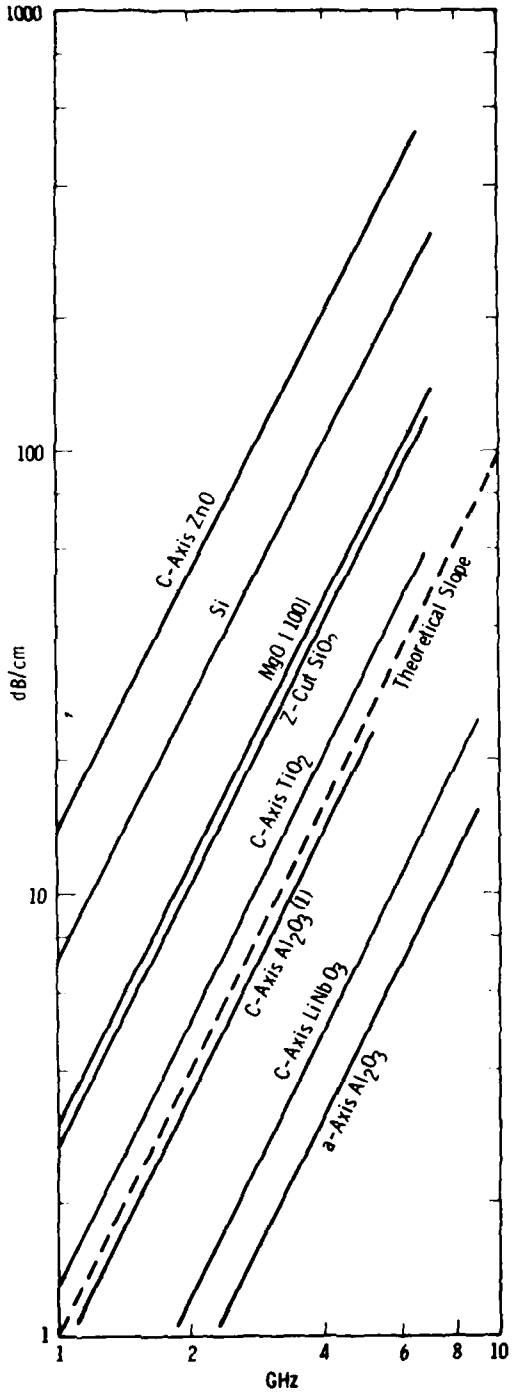

Figure 15. Longitudinal wave attenuation versus frequency for selected materials.

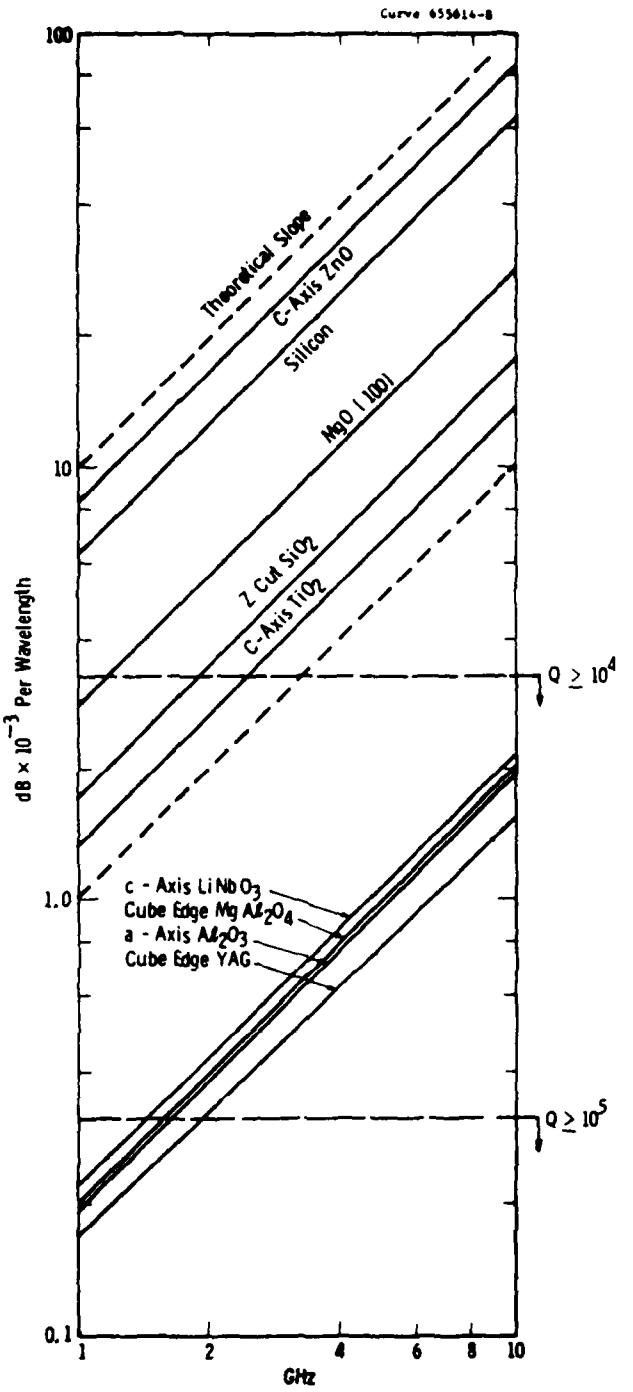

Figure 16. Longitudinal wave loss per wavelength versus frequency for selected materials.

1.5.2 Anisotropy

The anisotropy factors in alpha quartz were examined in detail using the Westinghouse media modeling program.[1] This program provides a comprehensive portrayal of the slowness (inverse velocity), power flow angle, temperature coefficient of delay, and the power flow angle out of the scan plane. Representative scans for quartz are shown in appendix A. Both polar and rectilinear plots are provided in this representation for the bulk mode longitudinal (L) and the two bulk shear modes (T_1 and T_2). The scan planes are shown as rotation about the Z axis of the crystal in 5 degree increments. The first scan, reproduced here as figure 17, has the normal to the scan plane along the positive Y-axis: direction cosines (90,0,0) and Miller (0,1,0), may be used to justify our choice of the X-direction at propagation for the longitudinal mode.

As can be seen in the first scan, the power flow direction varies very rapidly for small angles away from the X axis. The small circle (target) in the polar plots identifies the zero coordinate (zero power flow). The essential point is that the power flow is spread sharply away from the X direction for small deviations in angle. Power is therefore dispersed for small diffraction angles and for small angular spreads at boundary reflections. This effect assists in triple transit suppression and disperses the unwanted modes.[2]

---

[2] J. B. Goodell and R. Sundelin, "Frequency Characteristics of Bulk Microwave Acoustic Resonators," 1979 Ultrasonics Symposium Proceedings, IEEE Cat. No. 79 CH 1482-9.

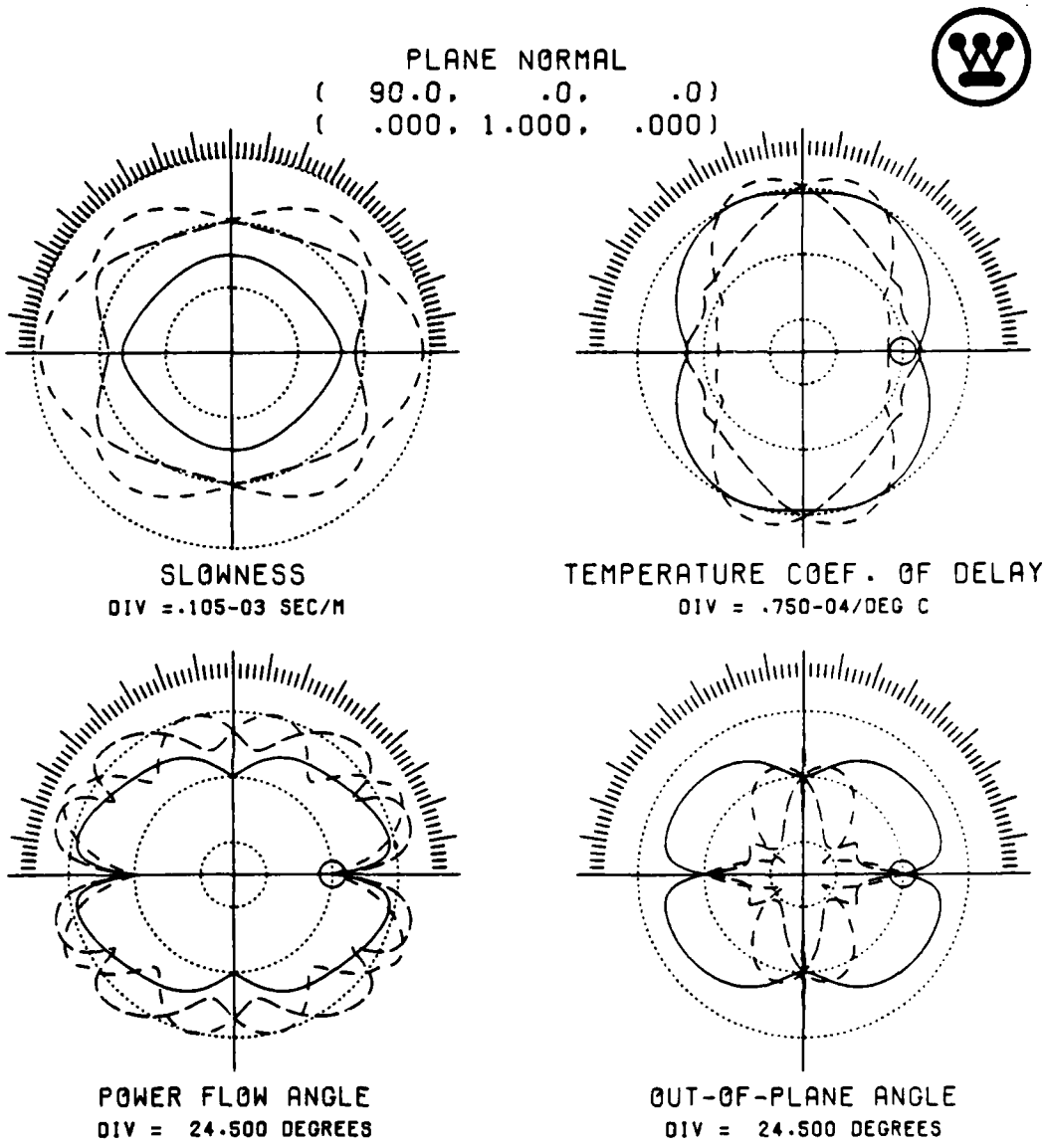

Figure 17. Media modeling of quartz.

1.0 Zinc Oxide Film Growth

1.0.1 Substrate Preparation

The growth of the zinc oxide piezoelectric transducer film is known to be sensitive to many factors. In this section is discussed the influence of substrate preparation, polishing, and cleaning, together with bottom contact preparation.

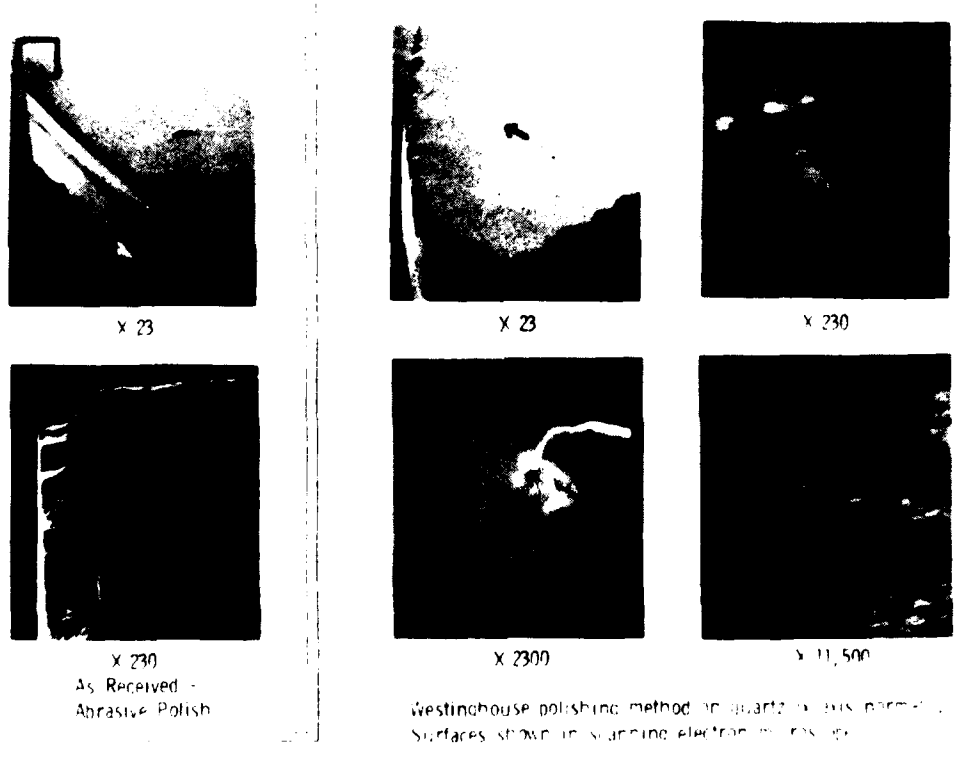

Figure 18. Surfaces of X-cut quartz as received and as prepared by Westinghouse process.

Westinghouse has developed a substrate polishing technique which provides exceptional results for virtually all acoustic media. This technique provides-scratch and damage-free surfaces essential to good zinc oxide growth. In addition, ultra-flat plane parallel surfaces are obtained in the process. Figure 18 shows a sample substrate of X-cut quartz. The contrast between the surface texture of the as-received material (230X scanning electron micrograph) and that provided by the Westinghouse process is very marked. The preparation of such surfaces is essential to low-loss high-frequency zinc oxide film transducers.

1.6.2 Bottom Contact Preparation

As recently discussed[3], it is suggested that a change in surface energy of the substrate due to contamination is the main reason for the different growth modes observed. It is therefore imperative that substrate cleanliness be maintained at all levels of transducer processing. Substrate cleaning procedures are described in Section 1.9.1 of this report. The bottom contact of the active transducer area is prepared by the flash evaporation of chromium-gold. A typical 1000 Å thick deposition should proceed in about 20 seconds. The chromium adhesion layer of 100 Å to 200 Å is evaporated first with a short interval of coevaporation with the gold. This procedure is known to produce ordered gold films.

1.6.3 Ordered Growth

Well-ordered gold is essential to the ordering of the zinc oxide. The transducer fabrication process must include monitoring of the degree of ordering of the gold before the zinc oxide deposition

---

[3] W. C. Bilings and H. Wurlingham, J. Vac. Sci Technical 17 (4), July/Aug., 1980.

proceeds. Westinghouse has initiated a test slug (mini substrate) program to check the ordering of gold and zinc oxide. The degree of gold order is determined primarily by reflection electron diffraction (RED) and by transmission electron diffraction (TEM). An example of well-ordered gold on fused quartz is shown in figure 19. A TEM pattern of well ordered gold on a glass slide is shown in figure 20.

1.7 Zinc Oxide Film Analysis

1.7.1 Reflection Electron Diffraction

Test slugs on which proven ordered gold has been deposited are run with the delay-line substrates for subsequent (and immediate) analysis in the RED microscope. The zinc oxide RED evaluation is facilitated by division into category types. These categories are shown in figure 21. Type 1 zinc oxide for which the ordering angle does not exceed 60 degrees generally provides acceptable transducers with efficiencies in the 15 to 20 dB range. The type 2 category, with an ordering angle of 20 degrees or less provides transduction efficiencies of 12 to 15 dB per transduction. Type 3 ordering is considered excellent zinc oxide (ordering angle of 6 degrees or less), with resulting transduction efficiences which are about 10 dB per transduction. Larger transduction efficiencies are to be expected of types 4 through 7, all of which are near heteroepitaxial films with ordering angles of a few degrees.

1.7.2 Scanning Electron Microscope

Macroscopic features of the zinc oxide film such as crystallite size and dead layer thickness are evaluated with a scanning electron microscope (SEM). This examination mode depends upon the synchronous collection of secondary electrons excited from the specimen

Figure 19. EDM pattern of well ordered (111) gold on fused quartz.

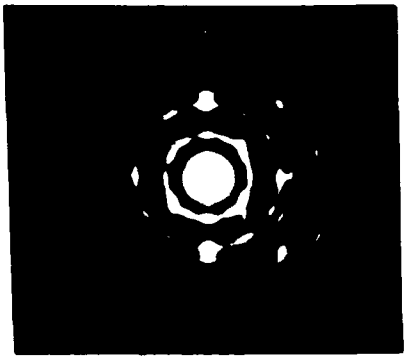

Figure 20. TEM diffraction pattern of a well ordered (111) gold film on a glass slide.

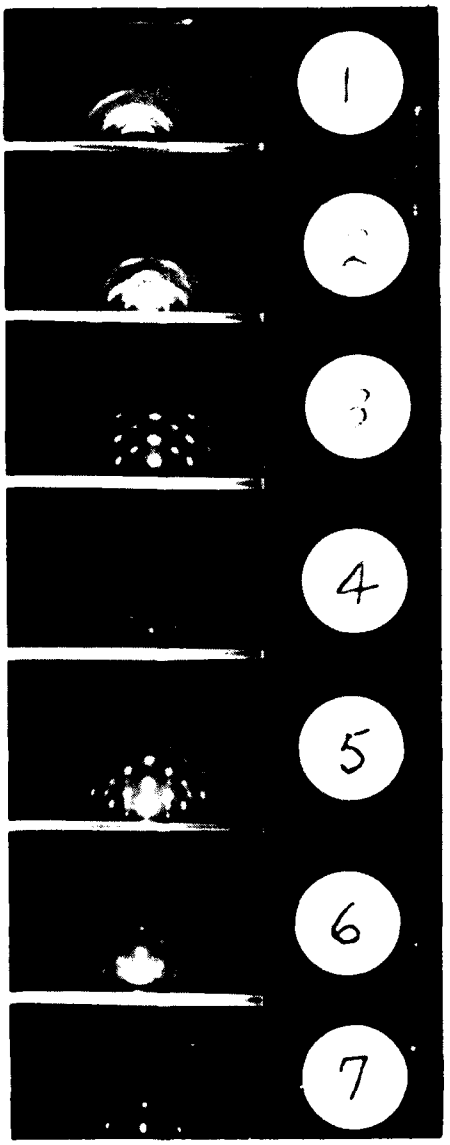

Figure 21. Zinc oxide cell evaluation category types.

surface by the primary, high voltage, electron beam. The wavelength of the primary beam is typically of the order of 0.1 Å. Resolution of this mode is generally limited by beam stiffness (self repulsion), which restricts the minimum diameter to about 200 Å. High SEM magnifications (50,000X or more) are used to examine individual zinc oxide crystallites and thickness of the dead layer. The dead layer is the initial, early growth of ZnO next to the substrate bed. If this initial growth is not well ordered it is parasitic to transducer efficiency. Methods for the consistent elimination of this layer are not well understood. Figure 22 is an SEM micrograph of a 3000 Å thick zinc oxide film.

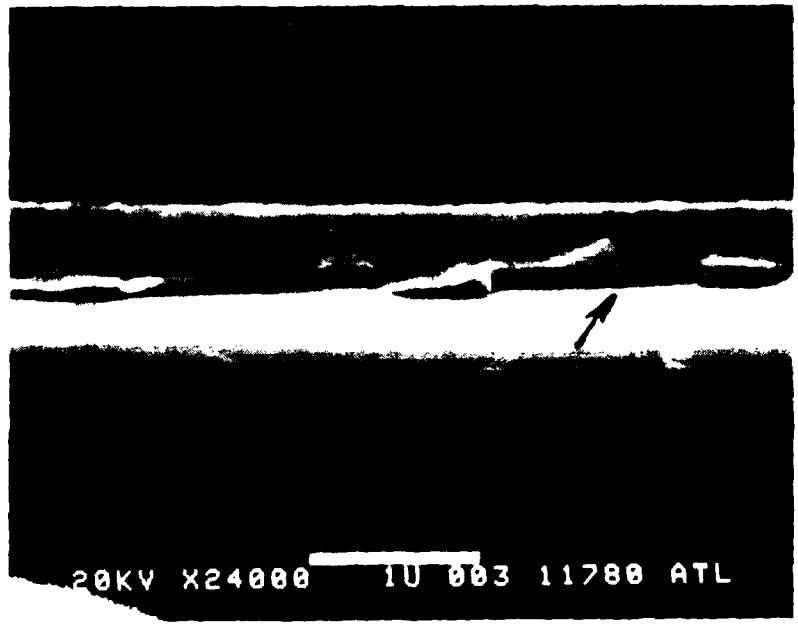

Figure 22. Scanning electron micrograph of zinc oxide film on gold on quartz (24,000X). Arrow points to initial layer of 3000 Å thick film (vertical and horizontal magnifications are not the same).

1.7.3 Auger Analysis

Auger analysis of transducer films is used to assess the stability of the sputtering system during the period of film deposition. Ideally, the oxygen to zinc ratio should remain constant at unity throughout the entire thickness of the film. A diffusion-pumped system with long-term instability is compared to a cryogenically pumped system for a one 1 μm thick zinc oxide film in figure 23. The film deposition run times analyzed in figure 23 were about 2.5 hours for both the diffusion pumped and cryopumped rf diode systems.

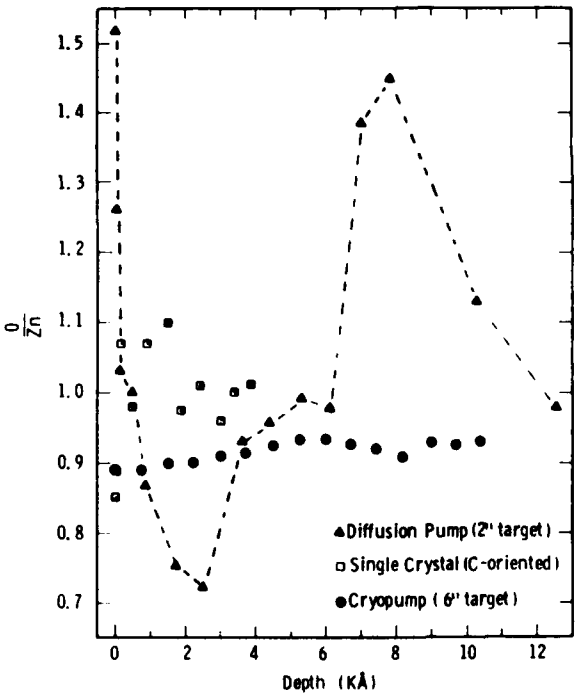

Figure 23. Auger analysis of progressively etched back zinc oxide film.

1.7.4 Test Slugs

To facilitate the zinc oxide film analysis program as described above, mini substrates or test slugs are used for monitoring. Slugs 0.25 inches in diameter are cavitron cut from fused quartz or X-cut quartz. These slugs then receive the same cleaning and metallization processes as the delay-line substrates. The slugs are conveniently used in the RED, SEM and auger analysis to monitor gold ordering, zinc oxide ordering, and thin film diagnostics described previously.

1.8 Zinc Oxide Sputtering Systems

1.8.1 Types of Systems

During the course of this program, three rf diode sputtering systems were used to fabricate transducer films.

RF System	Vacuum System	Target	Monitoring
System 1			
Westinghouse Side arm entry J-Head, sputter up	Glass and stainless steel with Meissner trap. 6 in. oil diffusion pump with LN_2 trap.	2-in. diameter, no cooling	Thermocouple and ionization gauge
System 2			
Westinghouse Bottom plate entry. sputter up	Glass and stainless steel. 6 in. oil diffusion pump with Ln_2 trap.	2-in. diameter, no cooling	MKS Baratron capacitance manometer and ionization gauge.

RF System	Vacuum System	Target	Monitoring
System 3			
Materials Research Corp. Model, SEM-8620 J-Head, sputter up	Stainless steel 6-in. oil diffusion pump, LN_2 trap with venetian blind gate	6-in. diameter	Inficon IQ 100 Mass Analyzer Sampling system. MKS Baratron capacitance manometer and ionization gauge

The principal system is number 3, which because of its larger target size provides a deposition of more uniform thickness. It is able to process up to four 1-in. square substrates at a time. The two 2 in. systems are employed as backups and have less elaborate process fixturing.

Temperature.--The temperature of the substrate fixturing during sputtering deposition currently is being controlled by two different methods. System 1 and 2 employ iron-constantin thermocouples embedded in the substrate holders, which are brought to temperature equilibrium before deposition begins. System 3 uses hot circulating water to maintain the substrates at 100 ^{o}C. The temperature is held constant in systems 1 and 2 by a heater power supply controlled by a thermocouple. Substrate temperatures have generally ranged from 40 ^{o}C (no heater power) to 150 ^{o}C.

Interferometer ZnO Thickness Monitor.--Zinc oxide film thickness control is accomplished with a laser interferometer which is used in two configurations. Systems 1 and 2 employ setups which are shown schematically in figure 24. The top schematic in figure 24 shows a

low-power laser (1 to 5 mW) which illuminates an angled mirror. The reflected light shines through a vacuum sealed window illuminating a sapphire rod. The end of the sapphire rod is close to the substrate, which is clamped to the holder. The reflected laser beam falls on a second mirror which directs it to a detector. The output of the detector is displayed on a strip-chart recorder. An improvement in this technique is described in section 1.9.3. As installed in system 3, little if any adjustment is required in the optical path through the use of light pipes and lenses.

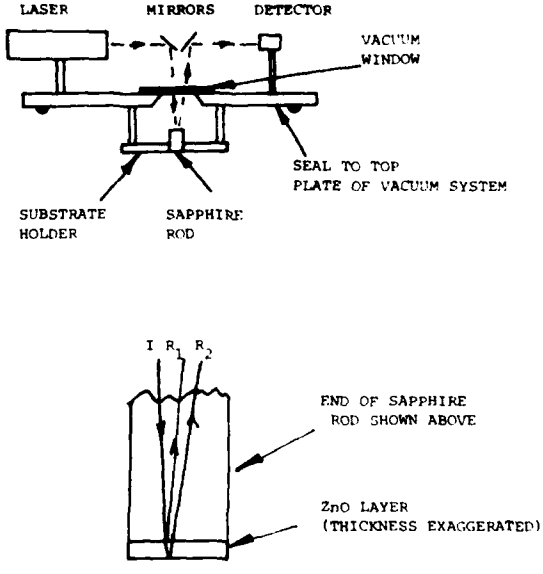

Incident Beam (I) is reflected twice at the end of the rod, R_1, and at film surface, R_2. R_2 changes phase as film thickness increases causing constructive and destructive interference at the detector.

Figure 24. Schematic of lasar monitor system.

1.8.2 System Parameters

Sputtering systems parameter controls are used to insure the quality of the zinc oxide film from run to run. The key components used in the control program are as follows.

Mass Analysis: Measures vacuum condition and contaminant levels to 10^{-11} Torr absolute. By use of a differentially pumped sampling system the sputtering atmosphere is monitored during a run.

Laser Thickness Monitor: Provides a high resolution measurement of the rate of change of the zinc oxide deposition as the deposition proceeds. In addition, this method is used to detect changes in the optical (scattering) properties of the film.

Reflection Electron Diffraction: A dedicated electron microscope is used to provide near immediate (10 minutes) evaluation of gold, bottom contact, and zinc oxide transducer films. Quantitative numbers relative to zinc oxide film fiber orientation are immediately available with respect to a given run.

1.8.3 Target Types

The sputter up configuration allows various zinc oxide targets to be evaluated with ease. Used successfully during the course of this program are the following target types: (1) Materials Research, MARS grade compacted zinc oxide (2) powdered zinc oxide (Alpha Chemicals 5 nines purity), and (3) zinc metal (5 nines). If target contamination is suspected as the source of low yield then the flexibility of the sputter up system offers a very distinct advantage for quick change of target types.

1.9 Manufacturing Process

1.9.1 Photolithographic Process

A photolithographic process uses the techniques that have evolved in silicon wafer and microwave integrated-circuit processing. Because these processes use photographic masks, new designs can be evaluated quickly. The disadvantages are that the process is more labor intensive and that there is a greater chance for chemical contamination. The chemical contamination would affect the lifetime of the delay line.

When a design for a delay line is developed, the necessary levels are digitized and entered into a computer. The computer generates a magnetic tape which is used to control the pattern generator. The pattern generator produces a glass mask for a single device, usually at 10X. This is used in a step and repeat machine to generate the final master mask. Alignment aids and device numbering are added as needed. From the master plate the working plates are made by contact printing.

Four levels of masks were required. The first level is a heavy gold layer (10K Å), which is used to form the ground plane and inductor. Two different masks are used for this level. One has the alignment marks for the first side and includes device numbers. The other is for the second side. The active portions of these two masks are identical. The second level defines the gold for the bottom electrode. The third level defines the zinc oxide islands. The last level defines the top aluminim electrode.

Once the masks are made the process is as follows. The substrates are ultrasonically cleaned in semiconductor-grade solvents to remove oils, waxes, and salts. Next, the substrates are cleaned in aqua regia to remove any metals from the surface. A final cleaning in 5:1:1

(H_2SO_4,H_2O_2, H_2O) follows to remove any residual organics. The substrates are rinsed in deionized water (D.I.) and methanol and then blown dry with filtered nitrogen. After loading the substrates into an evaporator, 50 Å of chromium and the 10K Å of gold are deposited on the substrates at a temperature of 200 °C. Standard evaporation techniques are used. When both sides have had 10K Å of gold evaporated on them, the first level masks are used to photoengrave the chromium-gold. Both sides are done in the same step for better front to back alignment. Also, both sides are processed in parallel instead of sequentially because the cleaning and etching steps of the second side would damage the first. After stripping the photoresist, the second layer of chromium-gold is deposited. The thickness of the gold is determined by the transducer design. The procedure used is the same as for the first-layer gold. The second-layer gold is then photoengraved to form the lower electrode. This layer of gold covers the numbers etched in the gold of the first side, but the numbers are still legible. The second-level mask also includes the inductor because it is shorted out during the evaporation. A pattern to pattern alignment is used for the second and succeeding levels. The front to back alignment is achieved during the first-level alignment. After etching of the second layer gold, the photoresist is stripped. This is a very critical step and we have only had success with chemical strippers. The zinc oxide is sputtered on the gold which has been cleaned by the stripping step. Depending on the system in which the zinc oxide is deposited, either silicon dioxide is sputtered or silicon monoxide is evaporated on top of the zinc oxide as a passivation layer. The zinc oxide and silicon oxide are then photoengraved. A positive resist is used so that it can be removed without using a stripper. The top electrode is deposited by using a rejection process. The substrates are coated with a positive resist (Shipley 13505), baked, aligned, exposed, and developed. Then chromium-aluminum is evaporated on the surface. 50 Å of chromium is used and the thickness of the aluminum is

determined by the transducer design. Using acetone and an ultrasonic cleaner, the unwanted chromium-aluminum is removed. Following a final visual inspection of the substrates, the electrical tests are begun.

1.9.2 Metal Mask Process

Metal aperture masks provide a clean process for zinc oxide device fabrication. A wet etching process provides a quick turnaround on testing new geometries. However, once a geometry is finalized, metal aperture masks reduce the labor and improve the yield. Westinghouse has had good success with both a wet process and a metal mask system.

The metal mask system which Westinghouse developed and is using was designed to the following criterion: The masks can be repositioned automatically to within 5 μm (0.2 mils). The holder works with rf for back sputtering. Substrates occupy a minimum diameter for maximum uniformity. The fixture has a laser thickness monitor which does not require alignment. The frames that hold the masks are not interchangeable so that each has to be used in its proper place. The final criterion was that the same masks be used for both sides. Figure 25 shows the fixture developed to meet these criteria. Because the coefficient of expansion between the substrate and fixture is not the same, there are spring-loaded plungers to push the substrate against pins. When the substrate is turned over for side two the other plunger is used. The mask frame uses precision pins for location. The pin pattern is different for each of the locations. The masks are expansion compensated so that they do not warp when heated. This is especially important for the zinc oxide mask because of under-throw during sputtering. The mask does not expand the same amount as the fixture. Therefore, the mask is clamped at one location and the rest is permitted to expand and contract.

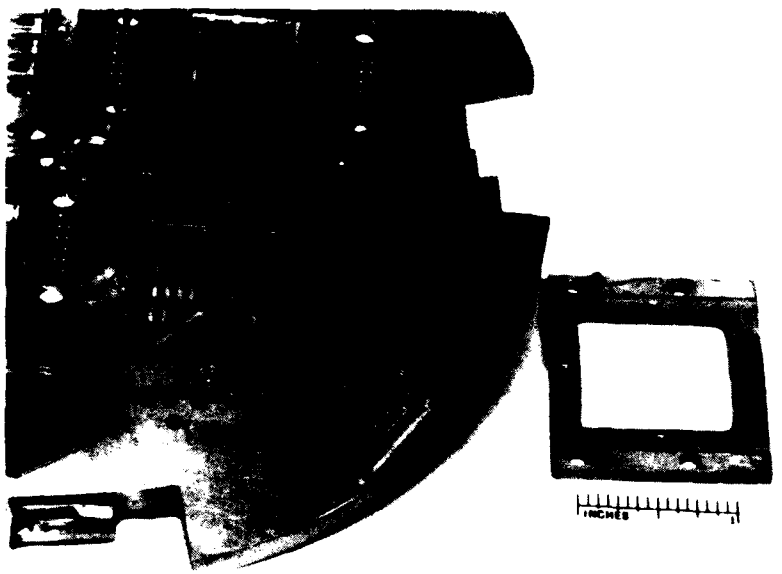

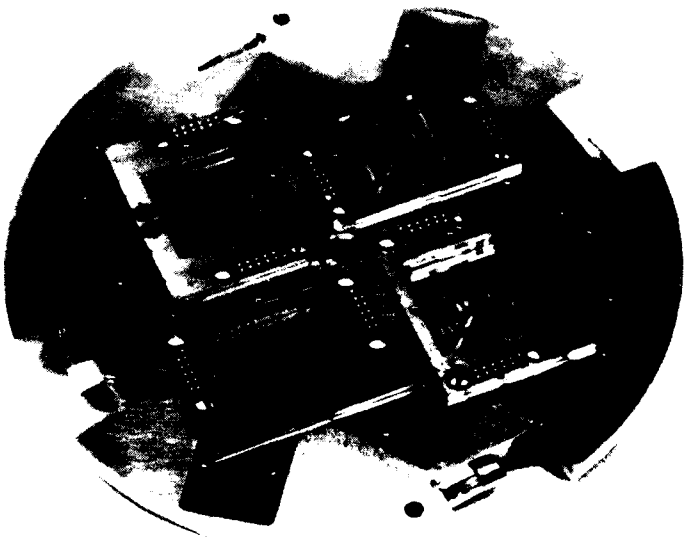

Figure 20. Zinc oxide metal mask fixturing

In order to make a device with a heavy metal ground plane with individual device numbers, six masks are required. The first two masks are the same, except one contains numbers and the other does not. The first is used on side one and the other on side two. This mask pair generates half the ground plane and part of the monolithic tuning inductor. The third mask completes the ground plane and inductor. The fourth mask forms the bottom electrode. The fifth defines the zinc oxide island. The sixth mask forms the top electrode. Figure 26 shows an exploded view of the mask series.

1.9.3 System Integration of Laser Monitor

It is critical to control the thickness of the layers as they are deposited. If all the thicknesses are 5% high, then the center frequency will be 5% low. For some layers, 5% can be as little as 30 Å. Westinghouse uses either a resistance monitor or crystal microbalance to monitor and control the thickness and rate of deposition of the metals. A laser interference monitor is used to measure the thickness and deposition rate of the zinc oxide.

The microbalance technique for opaque films uses standard equipment; however for zinc oxide, Westinghouse has made an innovation in the laser monitoring technique. The original system (see figure 24) used mirrors to reflect the laser through a sapphire rod and monitor the reflection from the end which received the deposition. Because the laser beam has to pass through a vacuum window, there are four reflections--top and bottom of window and both ends of the rod. Three of these reflections have to be blocked. This normally required readjusting the optics each time the system is loaded. The new method was developed because of a matching network on top of the new sputtering module. Lenses are used to focus the laser light after it leaves the fiber optics. The geometry of the system is such that the window reflections

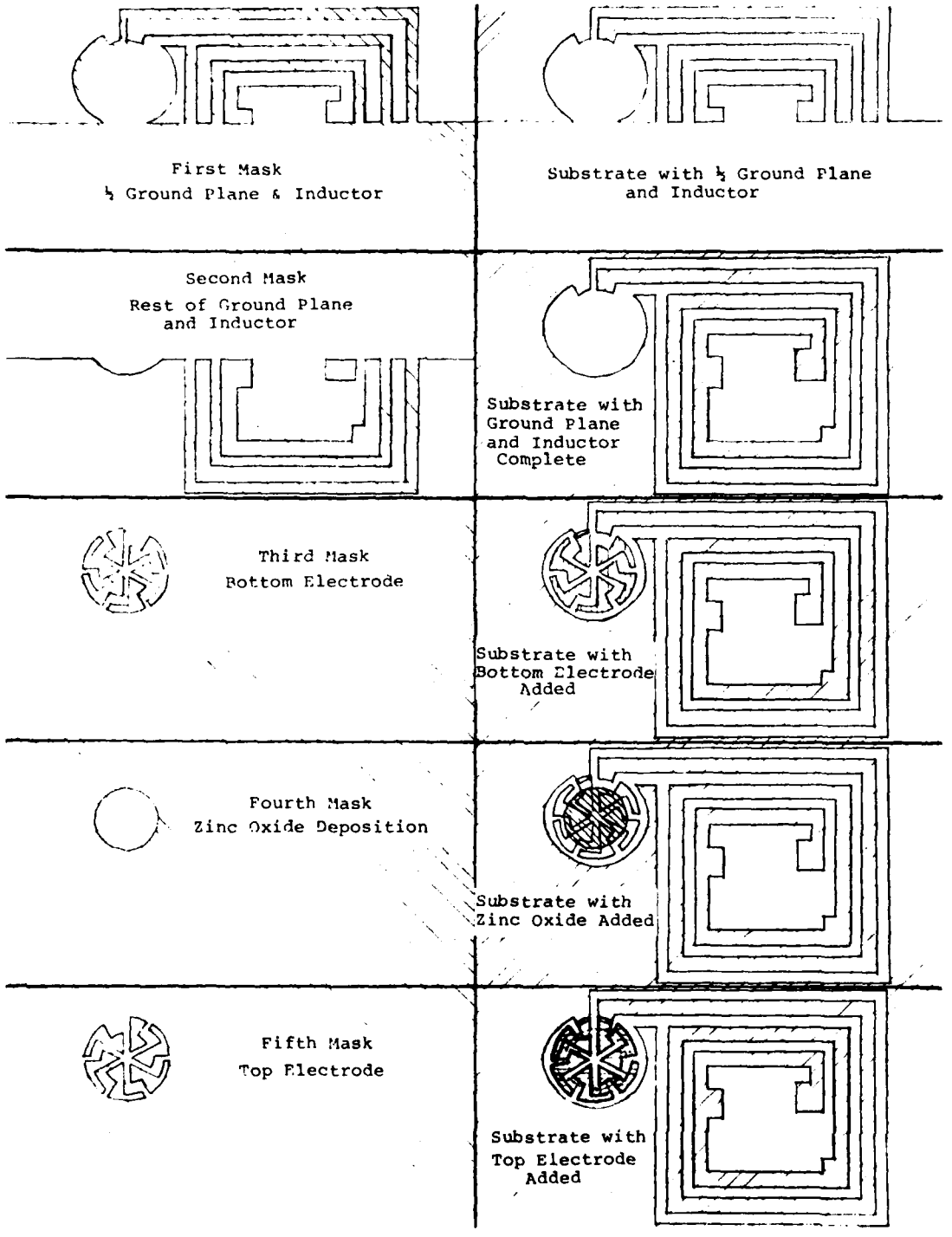

Figure 26. Exploded view of metal mask series.

do not enter the detection system. Also, a special sapphire rod is used which has tilted ends. This rod dumps the first reflection but keeps the second one. A diagram of this system is shown in figure 27.

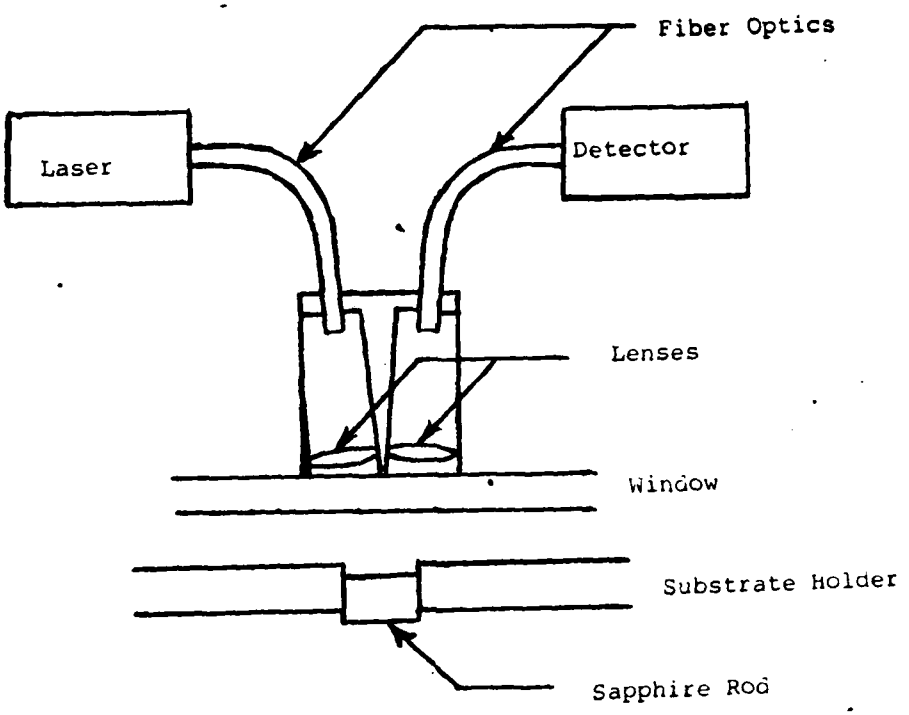

Figure 27. Diagram of the improved laser system which does not require any alignment.

1.9.4 Comparison of Wet Process and Dry Process

When setting up production of delay lines, both the wet and dry processes are useful. The wet process gives a method of fast turn-around for design evaluation. The dry process gives a lower cost method of producing the final lines. Even if outside vendors are used for all masks, the photographic masks should have a shorter delivery because an interim step of the metal masks is a photographic mask.

A comparison of the labor required to complete a run using each method was done. The wet process took 1.7 times as much labor as the dry. The reason for the significantly larger time for the wet process is the four photoe.. _ aving steps required. The extra evaporation step used in the dry process due to the split ground plane has been included.

1.9.5 Preliminary Electrical Test

After the wafer has been processed, it is electrically probed to determine which devices will meet specifications. However, at this time only the pulse attenuation measurements are performed. These tests are very good indicators of device quality. Delay lines which meet pulse specifications will generally pass all other specifications.

The wafer is a 1 x 1 in. quartz substrate. There are 80 individual devices on each wafer. A typical metal mask processed wafer is illustrated in figure 28. There are actually only 74 delay lines on the wafer because six of the positions are occupied by test patterns. All of the delay lines pictured in figure 28 are series tuned devices.

Pulse Test Specifications.--The pulse characteristics of a delay line are illustrated in figure 29 along with an oscilloscope photograph of a typical output pulse. The amplitude scale on the photograph is neither linear nor logarithmic. The tests are done in the time domain by exciting the delay lines with an rf modulated pulse and displaying the detector output on an oscilloscope. The insertion loss, feedthrough suppression and triple transit suppression are measured at center frequency and upper and lower band edges. The pulse specifications illustrated in figure 29 were to be met over $\pm$ 5% bandwidth. During this program, achieving more than 12 dB triple transit suppression was no problem. However, achieving the combination of 30 to 40 dB insertion

loss and a minimum of 20 dB feedthrough suppression over the required bandwidth proved to be more difficult. Measurement results are presented in Section 2.

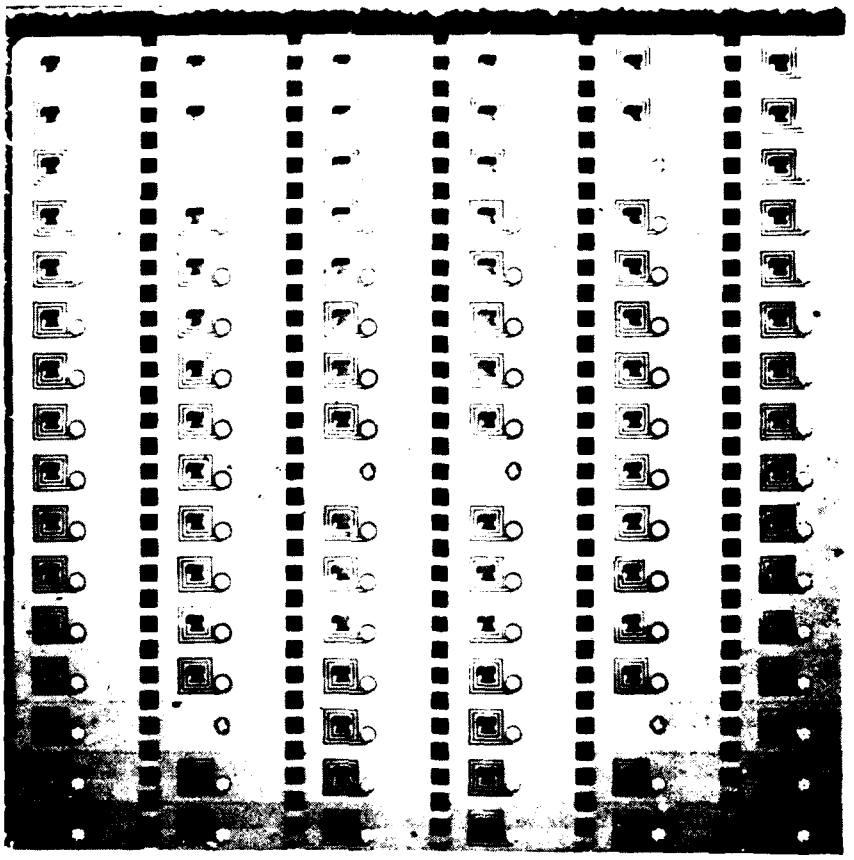

Figure 28. Typical metal mask processed wafer.

RF Probe.--Each of the delay lines on the wafer is pulse tested by using a special probe, shown in figure 30. This probe has been designed to be a 50Ω transmission line right up to the delay line transducer. The three prongs have spring-loaded telescoping contacts. These insure constant pressure on the wafer and reduce the possibility of damaging the transducer with the probe. The impedance of the three-prong probe was approximated by using a conformal mapping technique. Practical

dimensions were determined and the resulting probes work quite well. It should be emphasized that these probes measure rf performance directly. In many cases, dc probing is used to infer rf performance. However, these probes measure insertion loss, feedthrough suppression, and triple transit suppression directly at microwave frequencies. To illustrate how well the preliminary probing predicts final electrical performance, Table 1 compares probed wafer measurements to final packaged delay line measurements. There is excellent correlation for the insertion loss and triple transit suppression. In most cases, preliminary and final tests differ only by a few decibels. However, there is a discrepancy between feedthrough suppression measurements. This is not surprising, since feedthrough is highly dependent on the physical environment of the delay line. Obviously, a packaged delay line containing a well-grounded crystal presents much different surroundings to the transducers than a poorly grounded probed delay line on an 80-element wafer. Preliminary testing is not meant to provide precise electrical measurements. Its purpose is to determine which devices will meet final specifications. The probes are positioned on the wafer using the micro-manipulator shown in figure 31. The center prong is positioned on a bonding pad on the inductor and the outer two prongs are placed in contact with the ground plane. The details of the pulse-testing procedure are described in the next section.

Pulse Test Procedure.--A block diagram of the pulse test measurement is shown in figure 32. The HP 610B generator puts out a cw signal which is pulse modulated by two series connected rf switches. The switches are controlled by an EH 139 pulse generator. The pulse generator is set for a 30 ns width pulse at a 30 kHz repetition rate. Two rf switches are used in series to provide 80-dB isolation between the on and off states. The pulse train passes through a variable attenuator and then can be switched through a reference arm or through the delay line. The signal is then amplified, detected, and displayed on the oscilloscope screen.

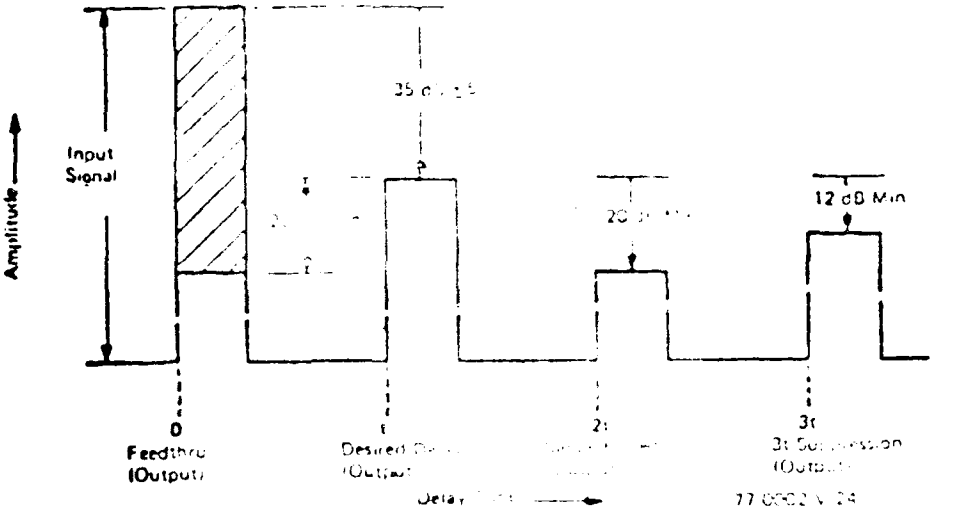
Amplitude
Input
Signal
12 dB Min
0
Feedthru
(Output)
Delay
77-0502-V-24

Figure 23.

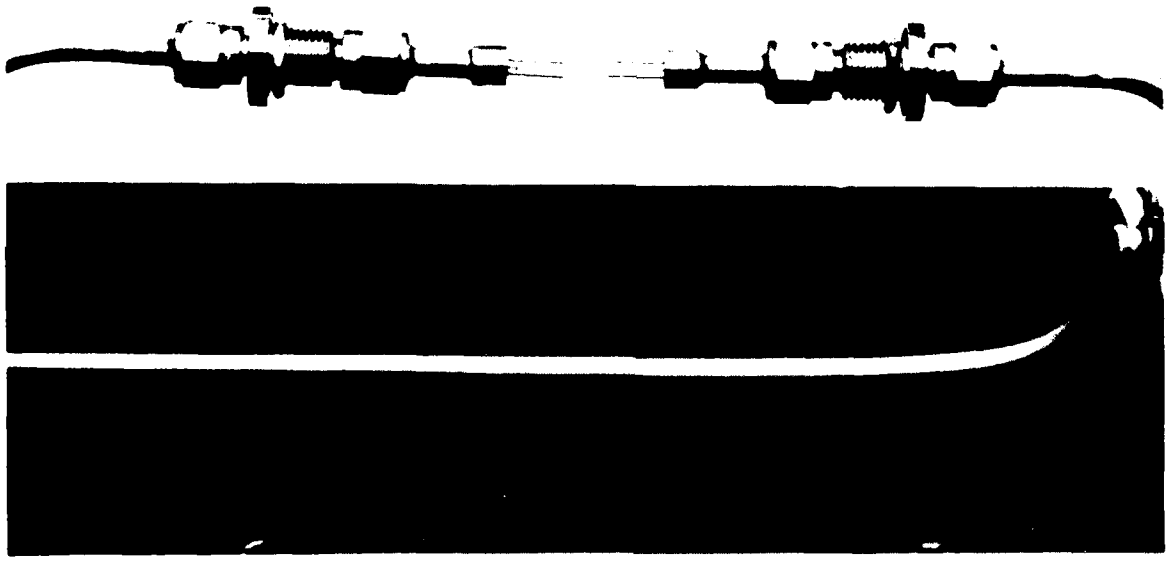

Figure 30. RF test probe

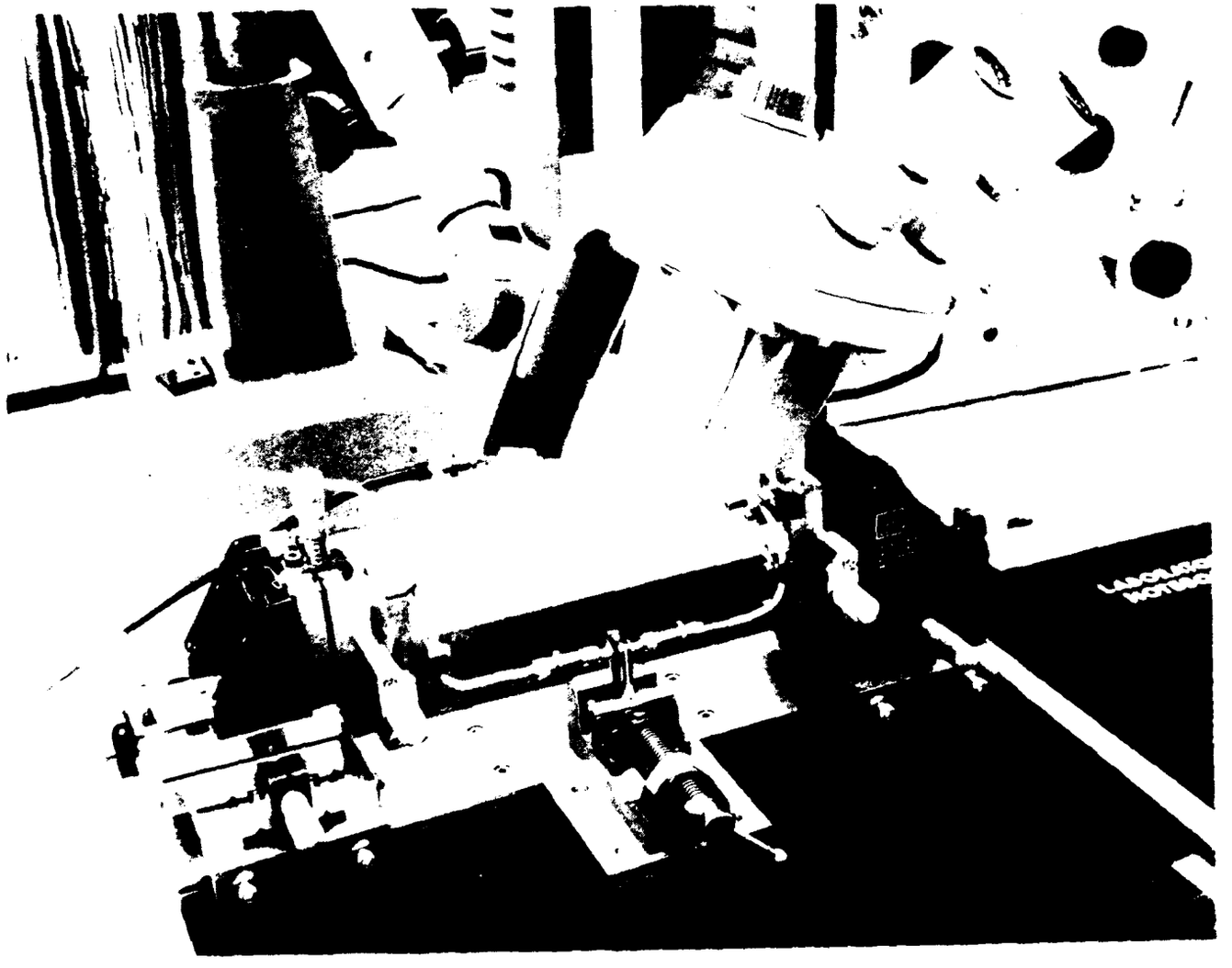

Figure 31. Probe station.

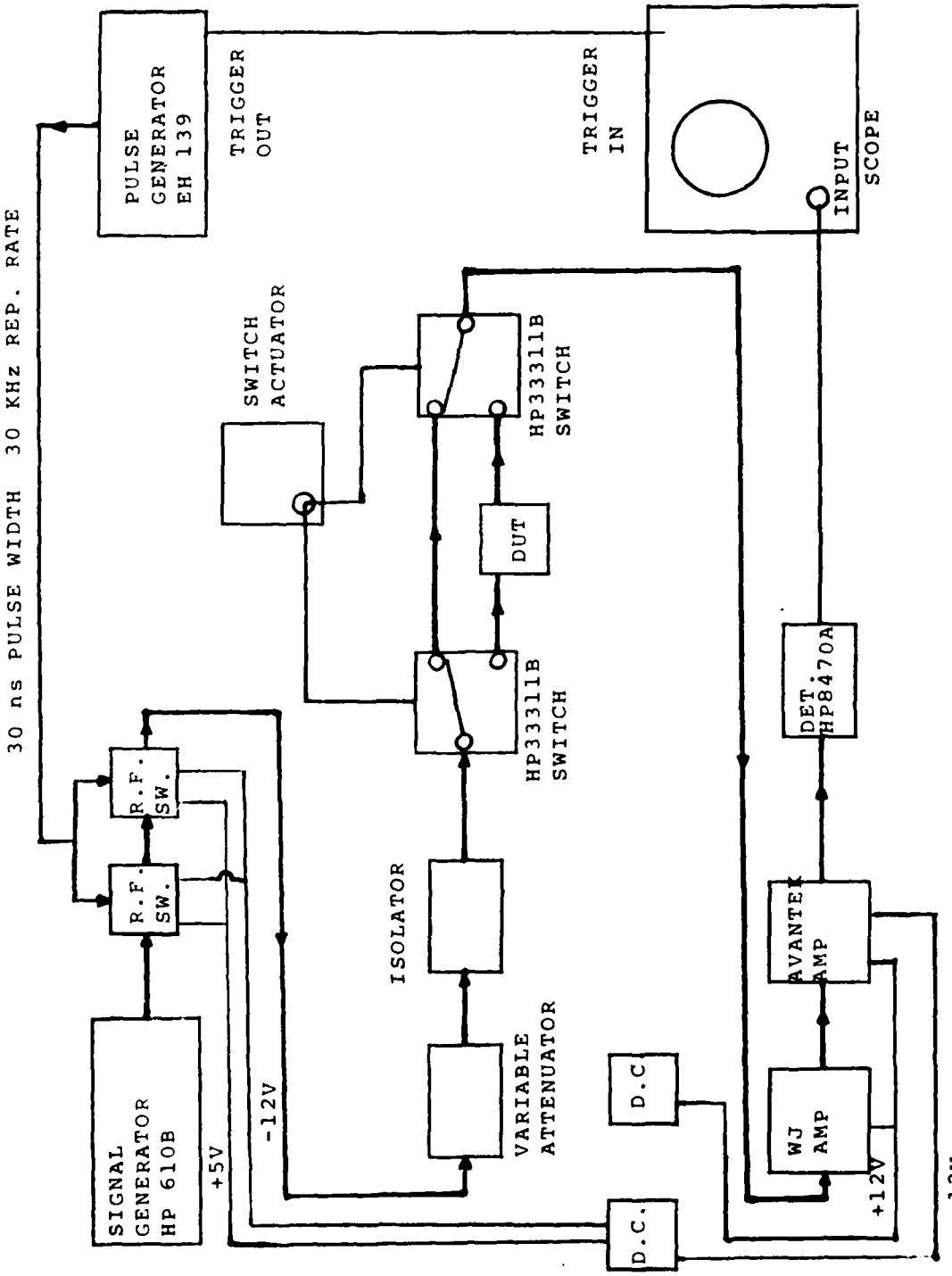

Figure 32. Block diagram of pulse test measurement.

TABLE 1. COMPARISON OF PROBED TO AS PACKAGED ELECTRICAL MEASUREMENTS FOR A TYPICAL WAFER.

DEVICE #	FEEDTHROUGH SUPPRESSION (dB)		INSERTION LOSS (dB)		3T SUPPRESSION (dB)	
	PROBES	FIXTURE	PROBES	FIXTURE	PROBES	FIXTURE
55	15	16	36	38	39	35
65	19	11	37	39	39	39
39	17	30	40	39	32	31
49	18	23	40	37	43	47
53	22	31	37	37	43	45
70	22	31	38	37	49	45
72	22	24	37	38	28	23
73	21	24	40	40	47	40
33	24	22	36	40	40	40
36	24	35	33	35	42	44
37	22	36	35	36	35	38
69	22	36	37	36	36	38
38	22	17	37	41	34	31
A	20	16	39	40	33	35
C	19	14	41	44	27	27
D	20	17	36	36	35	40

Prior to any tests, the reference arm must be calibrated. This is done without a wafer in the setup. The attenuation is set to zero and the probes are brought together. The signal is switched through the probes and the output level of the signal generator is adjusted until a two-division high pulse is displayed on the oscilloscope. The signal is then switched through the reference arm, and the variable attenuator is increased until a two-division high pulse is displayed. The attenuator setting is the insertion loss of the probes relative to the reference arm. This has been measured to be 2 dB over both A and B frequency bands. This means that the measured insertion loss magnitude must be reduced by 2 dB to give the actual value. This does not affect the triple transit suppression measurement nor the feedthrough suppression measurement.

The insertion loss measurement is identical to the reference arm calibration just described. The attenuator is set to zero. The probes are brought into contact with the delay line on the wafer, the signal is switched through the delay line, and the generator adjusted for a two-division high once-delayed pulse. The signal is then switched through the reference arm and the attenuator is increased until the pulse is two divisions high. The insertion loss is then 2 dB less than the attenuator setting.

To measure feedthrough suppression, the attenuator is set to zero and the generator amplitude adjusted for a two-division high feedthrough pulse. The attenuator is increased until the once-delayed signal is two divisions high. The attenuator reading is the feedthrough suppression in decibels.

The triple transit suppression is done the same way. With the attenuator set to zero, the triple transit pulse is adjusted to be two divisions high and the attenuator is increased until the once-delayed

pulse is two divisions high. Again, the attenuator setting is the triple transit suppression.

All of these measurements are performed at center frequency and both band edges. The devices on the wafer are numbered so that after the wafer is diced, the good devices can be identified and packaged.

1.9.6 Wafer Dicing

After probing, the wafer is prepared for sawing, the surfaces are protected with crystal bond 509 which melts at 71 ^{o}C and is soluble in acetone. It is also transparent, which is important since the initial saw cut is aligned visually. The wafer is attached to a glass plate with International Micro Industries Number 75 wafer mounting wax. This wax is applied as a liquid and is soluble in trichloroethane.

The wafer is cut with a Tempress model 604 dicing saw pictured in figure 33. This saw is microprocessor controlled and can be programmed to make a specified number of equally spaced cuts in one direction and then automatically rotate 90 degrees and make the remaining cuts. The spindle speed ranges from 10000 RPM to 40000 RPM. The sawblades used to dice the quartz wafers are 2 1/4 in. diameter Aremco Diamond Blades. These blades consist of a sintered nickel matrix with 325 grit diamond particles embedded uniformly throughout the outer 1/8 in. of the blade. The 6-mil thick blades produce a 10-to 12-mil kerf. The quartz is cut completely through. The crystal bond and mounting wax are dissolved, which frees the individual delay lines. They are thoroughly cleaned and the good devices set aside for bonding and mounting. At the beginning of the program, the quartz wafers were cut partially through from both sides. This was done prior to the deposition of the transducers. After processing and preliminary electrical testing, the individual devices were obtained by snapping apart the wafer using a

wedge mounted on an arbor. This works reasonably well with thin substrates but the "A" lines are 100 mils thick and the separation process only had about 50% yield. Because of this poor yield it was decided to saw completely through the quartz wafers after completion of thin processing and electrical testing. Very few devices have been lost during the dicing operation since then.

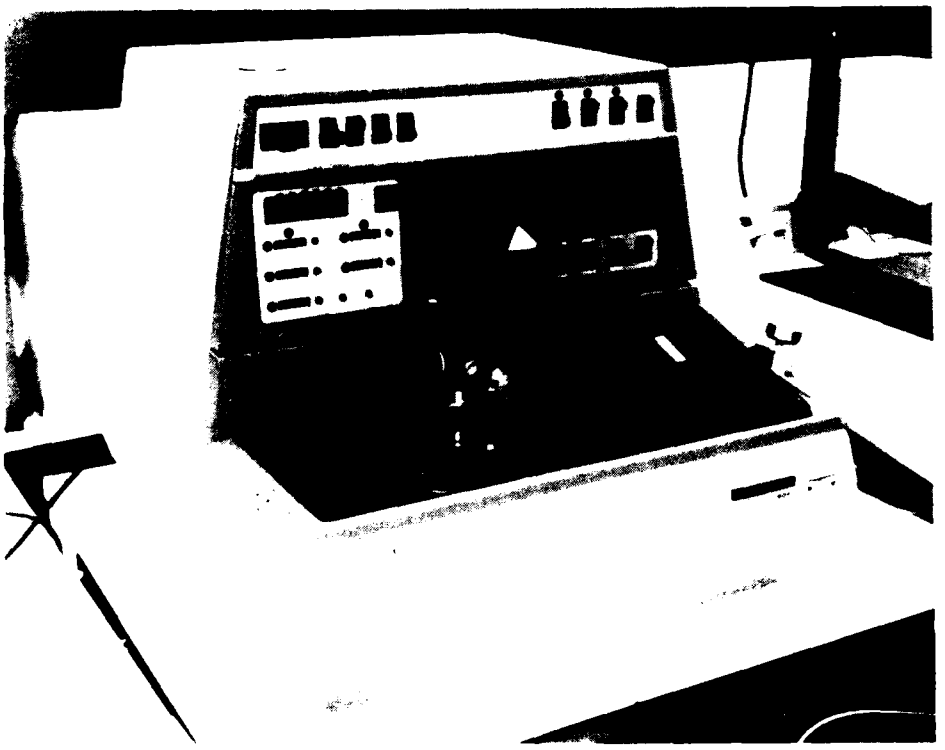

Figure 33. Tempress Model 600 wafer dicing saw.

Sawing would be faster and easier if thicker blades were used. However, it is desirable to have as many devices as possible on one wafer. This places each device close to another and limits the allowable saw kerf. Figure 34 shows the separation between the edges of a series tuned delay line and the edge of a perfectly positioned 10-mil-wide saw cut. There is only a 3 1/2 mil distance between the edge of the saw cut and the edge of the series inductor. Obviously, alignment during sawing is crucial and so is minimizing the saw kerf.

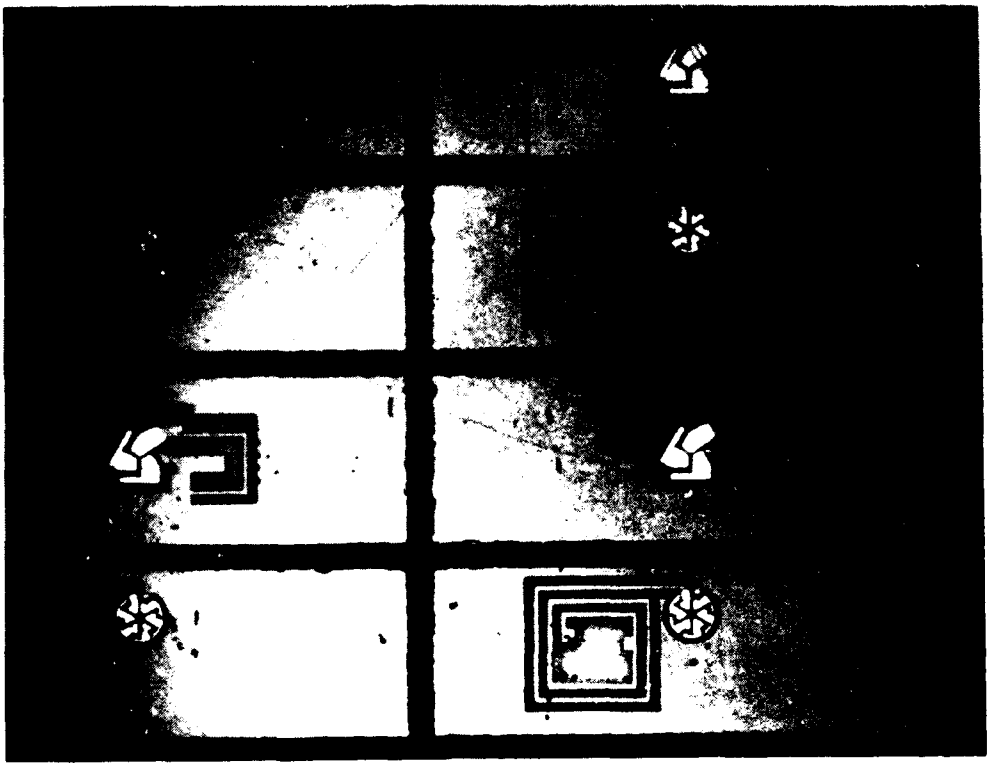

Figure 34. Separation between the edges of a series tuned delay-line.

1.9.7 Packaging

Packaging Fabrication.--During this program, three different package designs have been used. Originally, the contract called for 1/2 x 1/4 x 1/8 in. outside dimensions for the package. However, permission was officially granted to use 3/8 x 1/4 x 1/8 in. packages because they were commercially available and the 1/2 in. packages were not. Near the end of the program, 1/2 in. packages were fabricated so that they delay lines could be officially gun qualified by the government. Since delivery time for special packages is very long, the 1/2 in. packages were completely fabricated at Westinghouse. A small cavity was machined into the packages to accommodate the thin substrate for the short delay time of type "B" devices. A larger cavity was provided for the thick substrate of type "A" lines. Figure 35 compares all three packages and figure 36 is a drawing of the 1/2 in. packages.

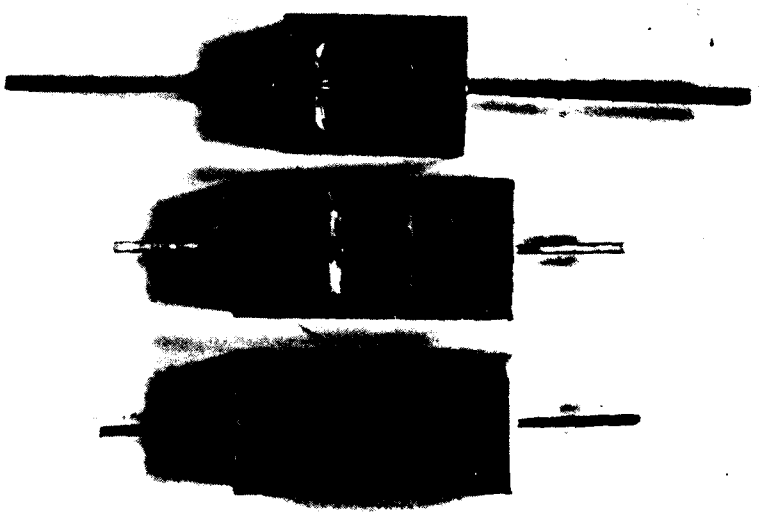

Figure 35. Comparison of the three packages.

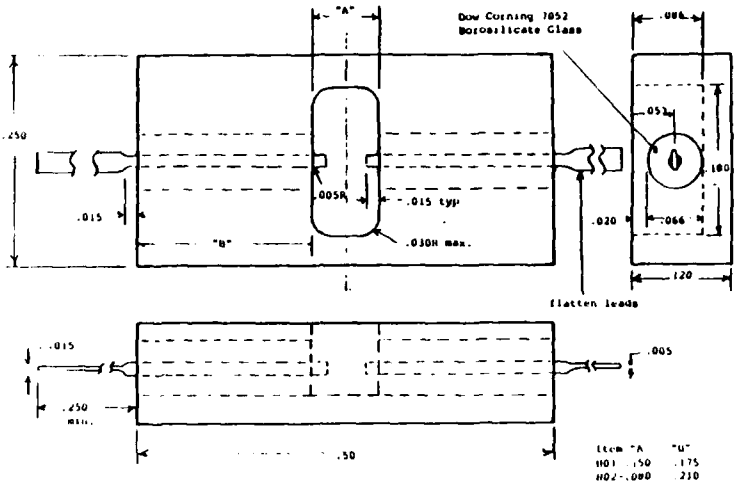

Figure 36. Drawing of the 1/2 in. package.

The packages were machined from Kovar and the input and output ports were glass-sealed. This was done by inserting Corning 7052 hollow glass beads and Kovar center conductors into the cylindrical openings at each end of the package. The package was placed in a carbon boat with a carbon lid (figure 37) and heated with a torch until the glass liquified and sealed both ports. Glass was annealed by heating in an oven to 490 ^{o}C for an hour and then gradually cooling to room temperature over a 24-hour period.

After annealing, the packages were dipped in a descaling solution to remove carbon deposited during the glass-sealing operation. The packages were thoroughly cleaned and gold-plated.

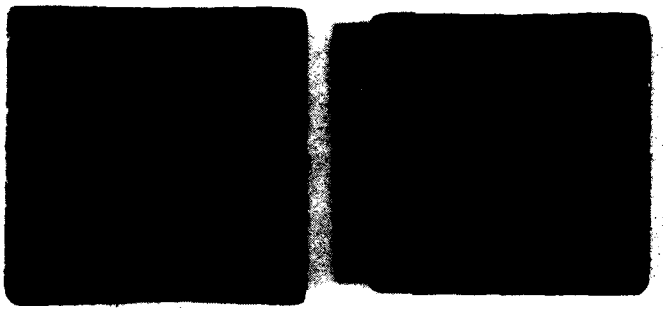

Figure 37. Carbon boat and lid

Mounting of Die in Package.--At this point, the delay line substrates are ready for bonding. The bonding machine is a Jade thermocompression bonder. Figure 38 is a photograph of this machine. A diagram of a thermocompression bonding system is shown in figure 39. The bonder uses 0.0007 in. diameter gold wire. The heating stage is kept at 90 ^{o}C and the capillary tip at 350 ^{o}C. The bonding force is adjusted to 35 grams and the actual bonding time is 2 to 3 seconds. Since the substrate has a transducer on opposite sides, a special jig is employed to permit bonding to the second side. This simple jig is a block of metal with a small hole drilled into its center. This block is placed on the heater stage with the substrate on top and the temperature of the substrate is allowed to heat up to 90 ^{o}C. The gold wire is bonded to the bonding pad on the tuning inductor on side one of the crystal. The crystal is flipped over and the gold wire on side one is inserted into

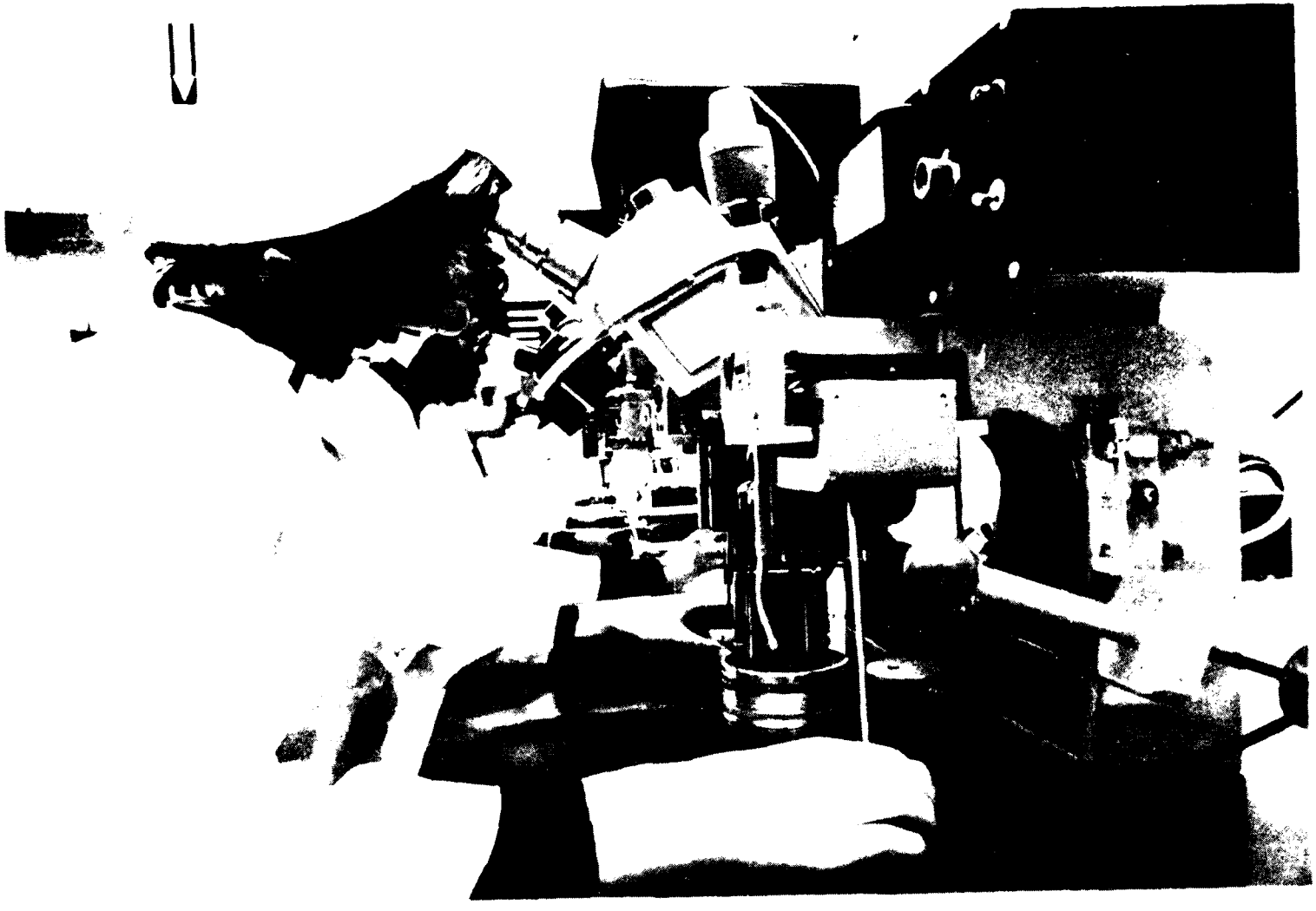

Figure 38. Thermocompression bonder.

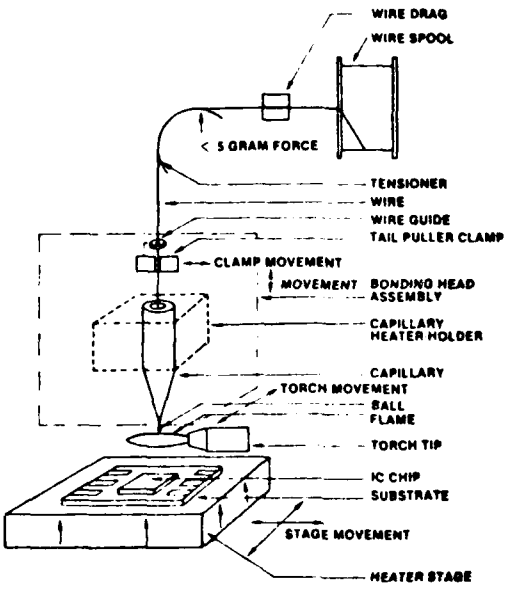

Figure 39. Thermocompression bonding system.

the hole in the fixture. Thus, a bond wire can be attached to side two without disturbing the bond wire on side one. It should be emphasized that because of integral tuning, only two bond wires are required. This is important because it improves reliability, reduces packaging time, and provides a sturdier device and a potentially smaller device.

The delay-line crystals are mounted in the package by coating the edges of each quartz die with A25 conductive polyimide and inserting them into the package. The bond wires are thermocompression bonded to the package center conductors and reinforced with polyimide. The assembly is placed in an oven and cured at 150 ^{o}C for 16 hours.

Feedthrough Reduction.--Polyimide was used instead of epoxy because of its low resistivity, low outgassing properties, and superior physical properties. Also, polyimide cured better than epoxy at

temperatures less than 200 ^{o}C for extended periods of time. The low resistivity is significant because it will help improve feedthrough suppression by improving the ground. Referring to figure 40, if the ground resistance (R) is finite, the input and output loops are not isolated and currents will be set up in the output loop. This results in feedthrough. Feedthrough suppression based on the ground resistance (R) can be found by comparing the output voltage for finite resistance to the ideal output voltage. In decibels this is:

$$20 \log 100R/(10^4+200R) \qquad (9)$$

Table 2 lists ground resistance and the associated feedthrough suppression.

TABLE 2 COMPARISON OF GROUND RESISTANCE AND THE ASSOCIATED FEEDTHROUGH SUPPRESSION.

R (Ohms)	Feedthrough Suppression (dB)
.01	-80.0
.1	-60.0
1.0	-40.2
10.0	-21.6

Of course, poor ground is only one of many causes of feedthrough. However, it does point out the need for a low resistance adhesive.

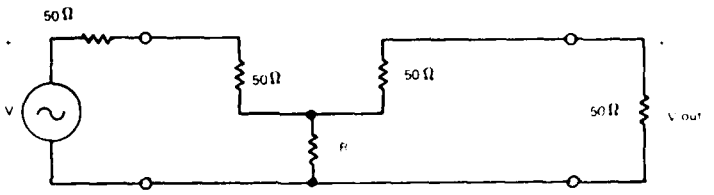

Figure 40. Feedthru isolation schematic

Comparison of Epoxy And Polyimide.--Table 3 is a comparison of resistivity for two types of polymide and two commonly used types of conductive epoxy.

TABLE 3 RESISTIVITY COMPARISON OF POLYIMIDE AND EPOXY

Adhesive	Sample #	Resistivity (ohm-cm)
Epoxy H31D	1	1.2×10^{-4}
	2	0.9×10^{-4}
Epoxy H20E	1	3.2×10^{-3}
	2	6.3×10^{-3}
Polyimide 71-1	1	4.8×10^{-4}
	2	1.5×10^{-3}
	3	0.78×10^{-4}
	4	0.13×10^{-4}
Polyimide A25	1	1.4×10^{-5}
	2	0.88×10^{-5}

These materials were cured using the manufacturers recommended cure cycle. Based on this and the low outgassing properties, A25 polyimide manufactured by Electro-Science Laboratories has been used in the fabrication of the delay lines. The literature has provided important information on polyimide. Table 4[4] compares various properties of polyimide and epoxy. According to this information, polyimides are equal to or superior to epoxy in almost every mechanical and chemical

[4] [illegible]. Vig, "Polyimide Resonators", Proc. 32nd annual Symp. on Freq. [illegible], (1978), p. 291-298.

property. The outgassing properties are especially impressive. One published study, [5] stated that polyimide baked at 300 ^{o}C for 12 hours has an outgassing rate which is lower than that of baked Viton and is also lower than unbaked stainless steel. This should increase shelf life and the operational life of the delay line since the primary source of contaminants inside a hermetically sealed package is the adhesive.

TABLE 4 COMPARISON OF PROPERTIES OF POLYIMIDE AND EPOXY.

PROPERTY	POLYIMIDE	EPOXY
Tensile strength	6-9 x 10^7 Pa	3-9 x 10^7 Pa
elongation	4-9%	2-10%
tensile elastic modulus	3.1 x 10^9 Pa	2.4 x 10^9 Pa
Compressive Strength	1.68 x 10^8 Pa	1-1.4 x 10^8Pa
Deflection Temperature (1.8 x 10^6 Pa)	360 ^{o}C	260 ^{o}C
Water absorption	0.3%	0.08-0.15%
Resistance to solvents	Very Resistant	Attacked by some
Flexural yield strength	10-16 x 10^7 Pa	7-9 x 10^7 Pa

[5] L. I. Maissel, R. Glang, "Handbook of Thin Film Technology", McGraw-Hill Book C., NY (1970).

Lid Welding.--The final step in the packaging procedure is the welding of the package lids. Prior to welding, the sealing surfaces of the package and the lid are thoroughly cleaned using a lint-free swab and propanol. The package and lids are placed in a vacuum oven and baked for at least one hour at 125 ^{o}C at a pressure of 50 μm. After bakeout, the oven is filled with nitrogen and the door from the oven to the glovebox is opened and the packages and lids are brought into the glovebox. The package is mounted in a special brass jig with a magnet insert to hold the package in place. The lid is held down with a nonconductive clamp and the package lids are grounded to the welding jig. The welder is a Superior model 160 Automatic Seamwelder. This is pictured in figure 41. The specially designed wheel electrodes are brought into contact with two parallel edges of the package and the lids are automatically advanced by the welder table and welded in place. The packages are turned 90 degrees and the two remaining edges are sealed. The heat produced by the welding process is highly localized in the region of the lid/package interface. The actual temperature of the substrate does not rise much over room temperature.

After welding, the packages are visually inspected and also subjected to a leak test. The leak rate must not exceed 5 x 10^{-7} cc/min. If possible, failed packages are rewelded and tested again.

1.9.8 Final Electrical Test

The final electrical tests consist of both pulse tests in the time domain and swept tests in the frequency domain.

Test Fixture.--In order to test packaged delay lines, a suitable test fixture is required. The test fixture developed for this program is pictured in figure 42. Special care was taken to insure that a 50-ohm transmission line existed up to the delay line. Also, feedthrough due to

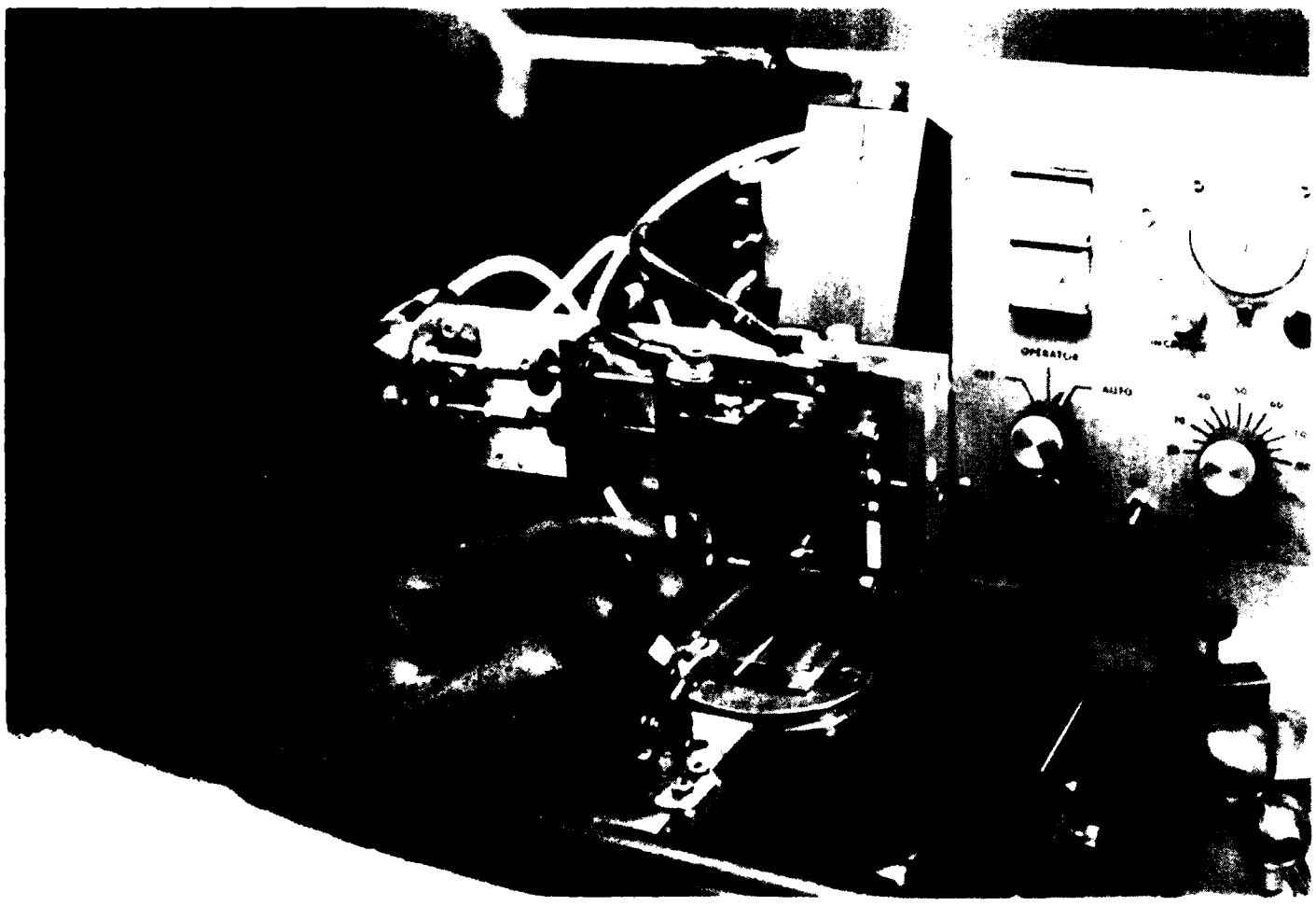

Figure 41. Experimental four automatic spot seam welder.

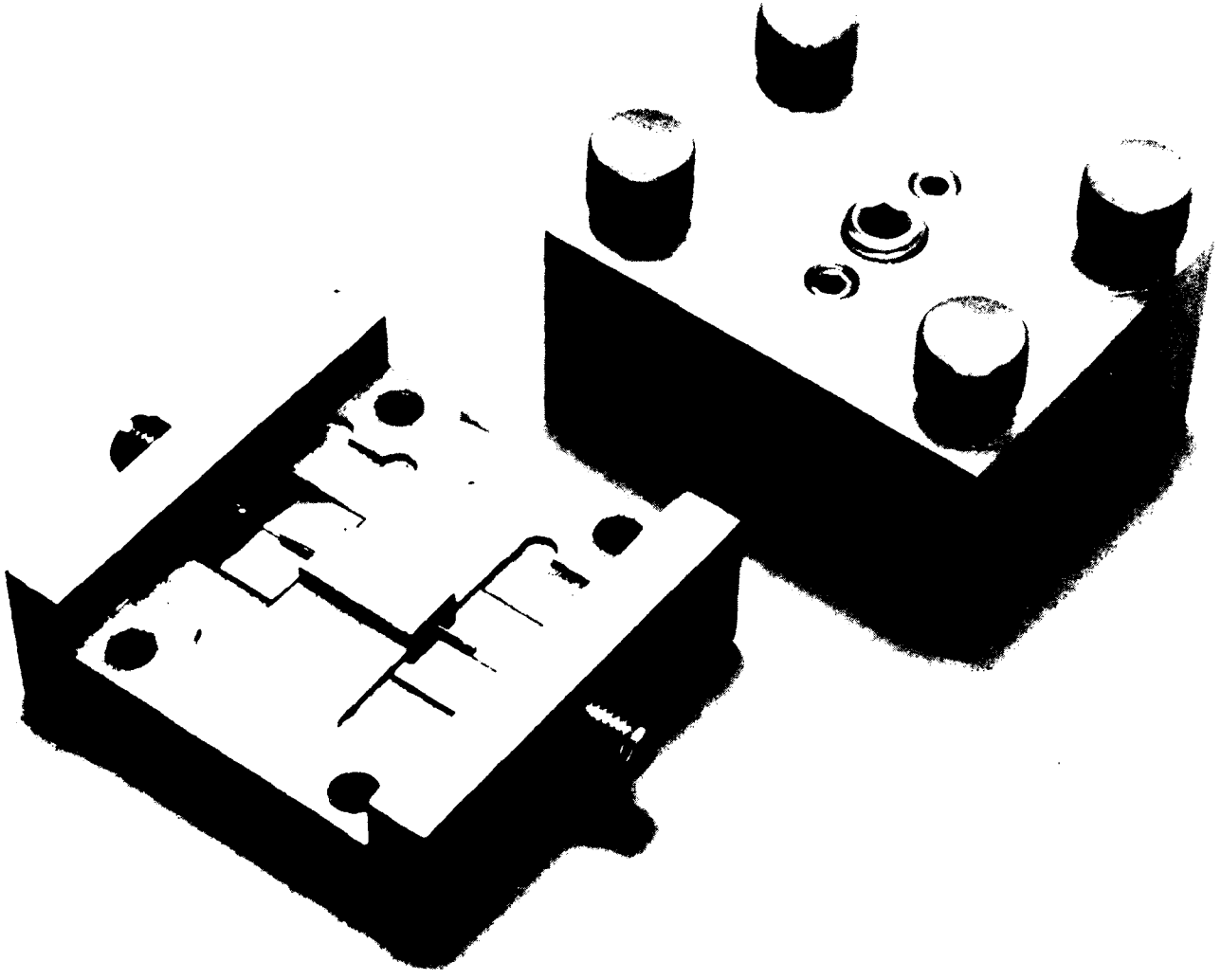

the fixture was a problem at first, but design improvements to the fixture have resulted in a minimum of 70 dB of feedthrough suppression over the frequency range of both types of delay lines.

The final pulse test procedure is identical to the preliminary pulse test described in Section 1.9.5 except the test fixture replaces the probe station.

Swept Test Specification.--All of the electrical specifications are summarized in Table 5.

TABLE 5 SWEPT TEST SPECIFICATIONS.

(1) Pulse width	1 μm
(2) Input level (Max)	1 W
(3) Frequency: Unit A Unit B	See SR 950-1 See SR 950-1
(4) Delay Time: Unit A Unit B	See SR 950-1 See SR 950-1
(5) Insertion loss	35 ± 5 dB
(6) VSWR (Max)	3:1
(7) Impedance: Input Output	50 ± jOΩ 50 ± jOΩ
(8) Leakage attenuation (direct feedthrough)	At least 20 dB greater than insertion loss
(9) Single ended insertions loss (twice delayed)	At least 20 dB greater than loss insertion loss
(10) Multiple delay attenuation (triple delay).	At least 12 dB greater than insertion loss

The swept tests determine if the delay lines exceed the 3:1 VSWR requirement over the bandwidth and also the insertion loss must lie between 30 and 40 dB over the bandwidth. The bandwidth is defined as center frequency $\pm$ 5%.

Swept Test Procedure.--The block diagram of the frequency-domain test is illustrated in figure 43. This diagram is practically self-explanatory. The VSWR is recorded by plotting the input impedance of both ports of the delay line. An example of this test is shown in figure 44. Also, a standard insertion loss measurement is made and figure 45 is an example. Both tests are performed over a $\pm$ 10% bandwidth.

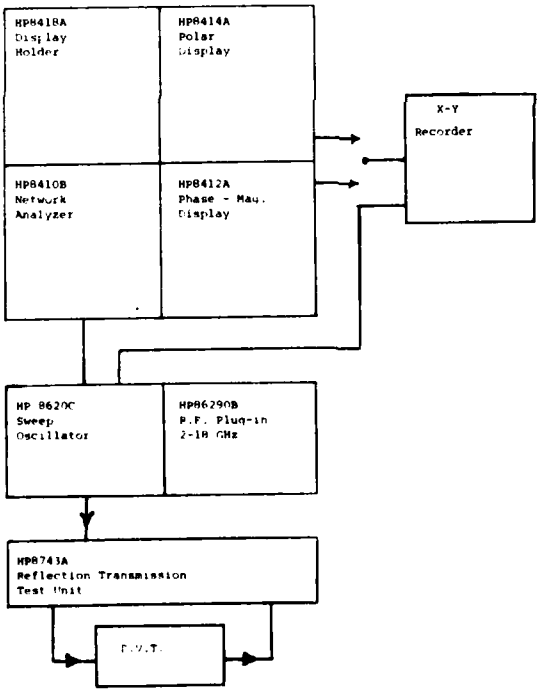

Figure 43. Block diagram of swept test setup.

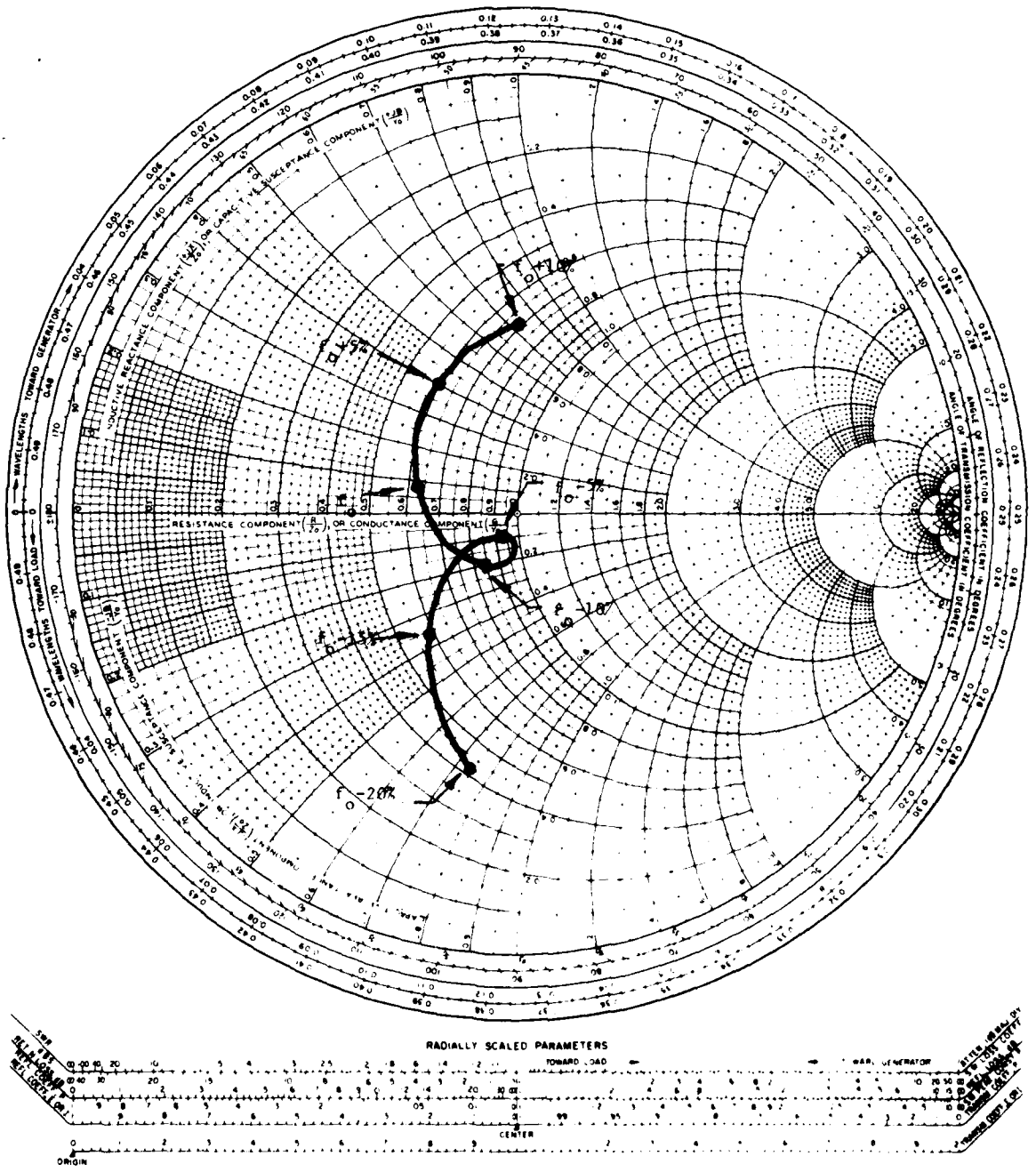

Figure 44 Typical VSWR plot.

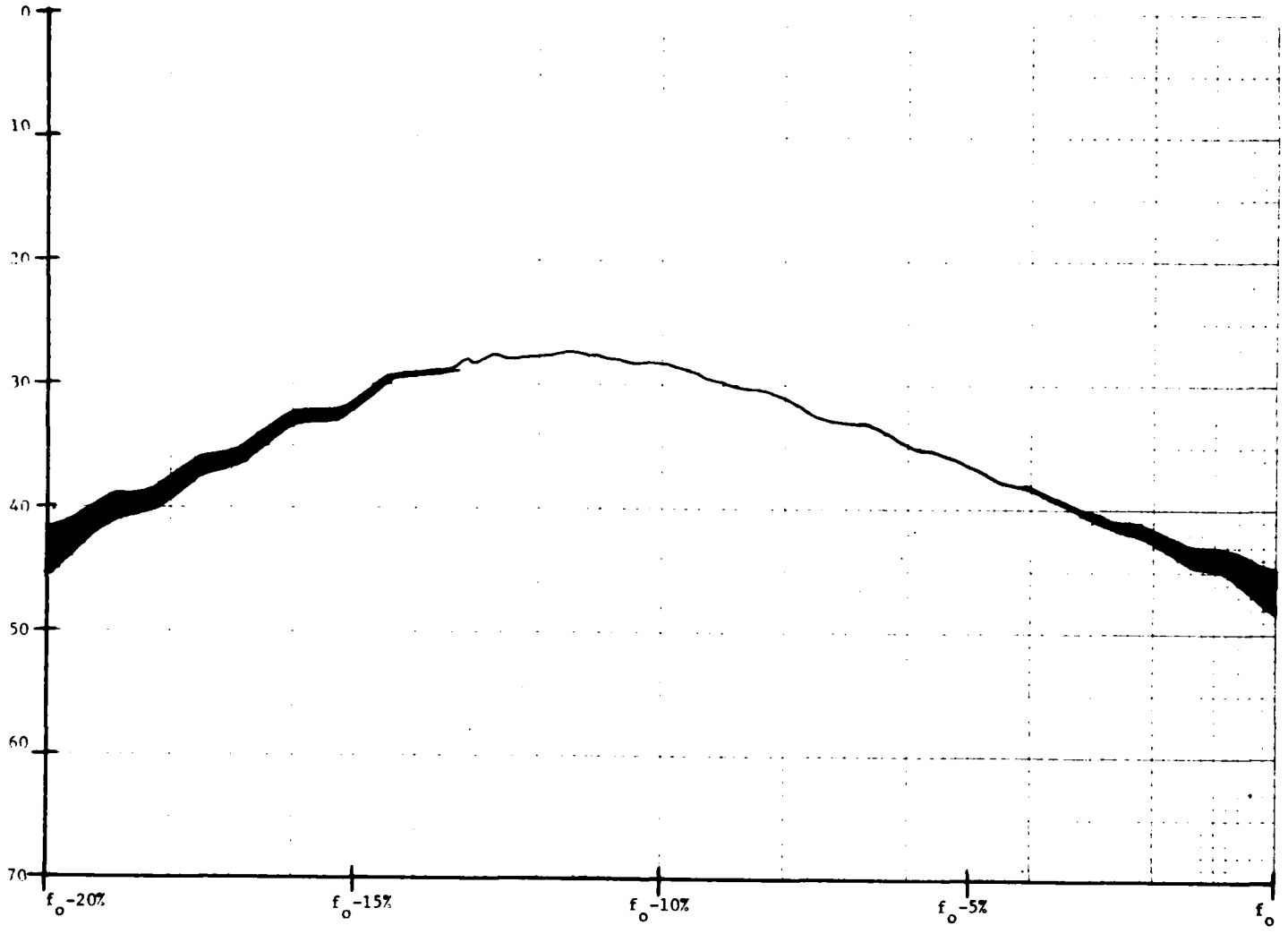

Figure 45 Typical insertion loss plot

2. DATA AND ANALYSIS

2.1 First Engineering Sample

The first engineering sample consisted of devices using the second iteration transducer design described in Section 1.3.3 and illustrated in figure 6. The type "A" delay line (low frequency, long delay time) insertion loss was above 40 dB but the triple transit suppression was within specifications. The type "B" delay line (high frequency, short delay time) did not perform as well. The insertion loss was greater than 70 dB. The VSWR for the type "A" lines was out of specification, but they could be inductively tuned to better than the required 3:1 VSWR.

2.2 Second Engineering Sample

This sample also consisted of the second iteration transducer design. A summary of the measured data is listed in Table 6. The two letters in the device I.D. column correspond to the four transducer designs depicted in figure 6 of Section 1.3.3. The insertion loss, feedthrough suppression, and triple transit suppression are measured in decibels, and the pulse specifications are shown in figure 29. The measurements are made at center frequency and at both the $\pm$ 5% band edges. The "B" lines exhibited very low insertion loss levels and two of the devices met the 20 dB feedthrough suppression requirement over the entire bandwidth. The triple transit suppression has never been a problem, and both "A" lines and "B" lines greatly exceed the 12 dB specification. The insertion loss for the "A" devices is high. The minimum value attained is 41 dB. The feedthrough suppression for the "A" lines was not as good as it was for the "B" lines. Finally, none of the devices met the VSWR requirement of less than 3:1 over the bandwidth, but one port of the "A" line 333-9 did have less than 2.8:1 VSWR.

TABLE 6 SECOND ENGINEERING SAMPLE

Device I.D.	Wafer	f_o-5% OT	1T	3T	VSWR	f_o OT	1T	3T	VSWR	f_o+5% OT	1T	3T	VSWR
333-7	CQX8A	18.0	50.0	30	6.3	16.5	50	30	5.8	17.0	50	28.0	6.0
PA					11.0				11.0				9.7
333-8	CQX8A	15.5	53.0	34	5.3	8.5	45	32	4.5	8.8	53	38.0	3.2
PB					8.3				7.0				5.3
333-9	CQX8A	26.0	46.5	42	2.7	20.5	41	40	2.8	20.0	49	40.0	2.8
SA					4.0				3.3				4.0
333-10	CQX3A	10.0	49.0	32	6.3	9.0	53	32	6.3	5.9	55	33.0	6.3
PB					6.3				6.2				7.0
333-11	CQX8A	41.0	54.0	37.5	3.2	4.0	42	32	3.0	37.0	53	40.0	3.6
SB					2.0				2.0				2.5
334-7	CFQ7B	25.0	20.0	24.0	3.2	25.0	20	22	2.6	27.5	23	24.5	3.7
SB					4.0				3.6				4.4
334-8	CFQ7B	27.0	19.5	22.5	3.2	27.5	17.5	24	2.6	26.5	26	24.0	3.6
SB					4.0				3.6				4.6
334-9	CFQ7B	7.0	25.0	21.0	4.2	8.0	24.0	21	4.6	4.0	31	21.5	5.8
PB					5.9				5.2				5.9
334-10	CFQ7B	20.0	21.0	26.0	3.5	19.0	20.0	25.5	3.3	16.5	24	27.5	3.4
SA					4.2				3.3				4.0
334-11	CFQ7B	15.0	32.0	25.0	5.2	14.5	31.5	24.5	5.0	12.5	33.5	24.5	5.0
PA					7.0				6.3				6.3

2.3 Third Engineering Sample

These delay lines utilized the third iteration transducer design described in Section 1.3.4 and pictured in figure 7.

Table 7 is a summary of the final electrical measurements. The insertion loss of the third sample "A" lines is much improved over the second engineering sample. Once again the triple transit suppression is well within specifications for both "A" lines and "B" lines. The VSWR is also improved except for the three parallel tuned "B" lines. It was decided that the series-tuned design was superior to the parallel-tuned design because of consistently better electrical parameters (especially VSWR).

2.4 Miscellaneous Test Data

All of the engineering samples were mounted in 3/8 x 1/4 x 1/8 in. packages. However, additional delay lines were delivered in 1/2 x 1/4 x 1/8 in. packages. These were all "A" length lines and the 1/2 in. package was required in order to gun qualify the delay line. Table 8 is a summary of the measurements made on photolithographically processed type "A" lines in 1/2 in. packages. These devices were fabricated using wafers CQX12A and CQX21A.

Also, a successful metal mask processed wafer was produced. From this wafer, 19 delay lines were mounted in 1/2 in. packages. The test results are shown in Table 9. All of the devices are parallel tuned. This is because alignment problems occurred with the initial metal masks and holders, but the alignment problems were more serious for the series tuned devices. It is interesting that nine of these devices met the pulse specifications over the bandwidth and also the VSWR requirement for at least one port. Five of the devices met all of the electrical specifications.

TABLE 7 THIRD ENGINEERING SAMPLE

Device I.D.	Wafer	f_o-5% OT	1T	3T	VSWR	f_o OT	1T	3T	VSWR	f_o+5% OT	1T	3T	VSWR
155-23	CQX9A	33	36	43	1.7	33	33.0	43	1.4	27	35	32	1.7
Series													
155-24	CQX9A	23	43	30	3.4	24	40.0	38	3.1	26	41	40	4.5
Parallel													
155-25	CQX9A	31	36	44	3.4	30	33.0	33	2.6	28	37	42	2.0
Series													
155-22	CQX9A	21	42	26	4.0	22	40.0	39	3.0	19	44	35	3.1
Parallel													
155-37	CQX9A		35		2.2		31.0		1.9		34		3.5
Series													
162-22	CFQ8B	26	30	20	14.0	27	31.5	23.5	10.0	23	34	24	7.0
Parallel													
162-24	CFQ8B	36	31	33	10.5	35	31.0	39.0	8.5	39	33	24	6.4
Parallel													
162-26	CFQ8B	37	27	19	12.5	38	28.0	22.0	9.5	38.5	31	23.5	6.8
Parallel													
162-27	CFQ8B	29	22	19.5	2.9	28	21.0	27.0	3.8	25.5	24	26.5	4.2
Series													
162-43	CFQ8B	24.5	26	19.5	2.8	24	23.0	30.0	4.6	22.0	25	20.0	6.8
Series													

TABLE 8 DELIVERED "A" LINES (WET PROCESS)

Device I.D.	Wafer	f_o-5% OT	1T	3T	VSWR	f_o OT	1T	3T	VSWR	f_o+5% OT	1T	3T	VSWR
24	CQX12A	22	33	21	1.15	30	27	34	1.65	32	35	42	2.1
Parallel					2.1				2.8				3.1
21	CQX12A	17	40	24	1.35	24	35	34	1.75	23	43	35	1.75
Series					2.3				3.0				2.8
57	CQX21A	43	35	27	2.9	46	31	42	1.9	41	34	38	2.6
Series					2.7				2.9				3.0
11	CQX21A	20	33	27		23	28	43		21	30	40	
Series													
23	CQX21A	27	30	32		29	29	38		21	34	45	
Series													
27	CQX21A	31	30	32		35	28	40		28	33	46	
Series													
17	CQX21A	20	36	29		20	34	42		18	35	38	
Series													
69	CQX21A	25	34	37		23	34	39		20	37	48	
Series													
71	CQX21A	14	35	38		13	34	36		10	35	36	
Series													

AD-A107 339 WESTINGHOUSE DEFENSE AND ELECTRONIC SYSTEMS CENTER B--ETC F/G 9/5
ESTABLISHMENT OF PRODUCTION TECHNIQUES FOR TRANSDUCER ACOUSTIC --ETC(U)
JUN 81 A F ZAHORCHAK, R A MOORE, R N SUNDELIN DAAB07-77-C-0569

UNCLASSIFIED HDL-CR-81-569-1 NL

2 OF 2
AD A
107339

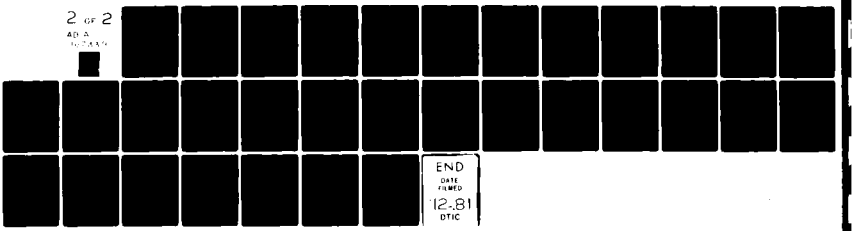

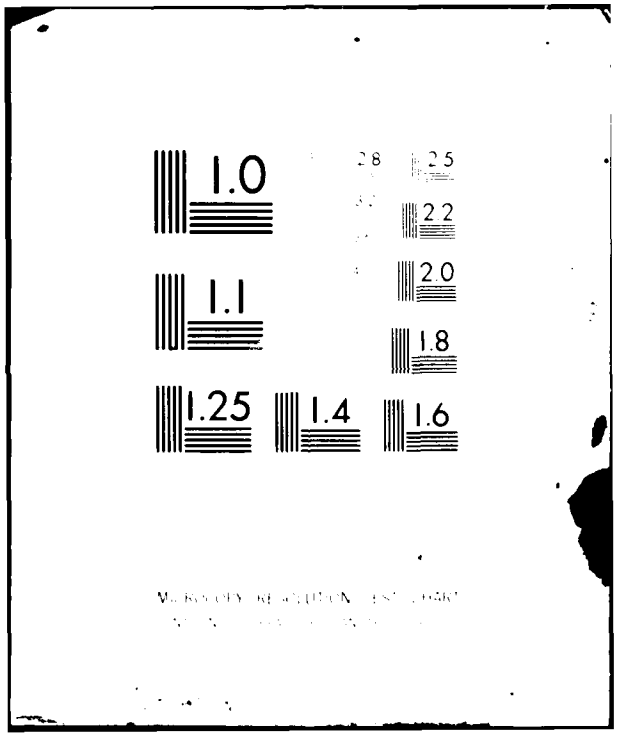
1.0
1.1
1.25
1.4
1.6
2.0
1.8
2.2
2.5

Table 9 Delivered "A" Lines (Dry Process)

Device I.D.	Wafer	f_o-5% OT	f_o-5% 1T	f_o-5% 3T	f_o-5% VSWR	f_o OT	f_o 1T	f_o 3T	f_o VSWR	f_o+5% OT	f_o+5% 1T	f_o+5% 3T	f_o+5% VSWR
33	CQX27A	12	41	26	2.6 4.0	16	38	45	1.55 4.1	22	40	40	1.5 3.9
36		14	37	28	2.0 2.7	35	35	44	1.4 3.0	39	36	47	1.15 3.2
37		48	37	27	2.1 2.5	36	36	38	1.6 2.8	27	39	47	1.3 3.0
69		34	38	24	1.9 2.7	4.3	36	33	1.5 3.2	36	36	36	1.5 3.5
38		16	43	26	1.55 1.3	17	41	31	1.8 1.2	17	40	45	2.0 1.3
39		29	40	31	1.5 3.2	28	37	46	2.1 3.5	25	41	45	2.6 3.7
49		42	38	26	2.8 3.0	47	37	36	2.0 3.2	40	40	46	2.1 3.2
53		30	40	28	1.5 1.2	30	38	40	1.2 1.15	29	40	46	1.25 1.15
54		16	40	26	6.0 2.5	17	40	35	6.0 2.6	17	40	47	5.5 2.8
65		11	40	24	3.2 2.6	13	38	41	2.7 2.8	11	39	39	3.0 2.9
70		32	39	23	1.8 2.2	31	37	31	1.2 2.5	31	37	40	1.2 2.7
72		22	40	22	2.2 3.6	28	39	28	1.4 3.6	28	39	44	1.3 3.6
73		24	41	23	4.0 2.8	25	39	29	4.4 1.7	24	38	42	4.5 1.9
A		15	40	24	3.0 2.1	16	39	33	3.4 1.9	14	40	35	3.4 1.9
B		22	40	25	2.3 1.8	30	38	42	2.0 2.0	25	40	34	2.2 2.1

Since it is difficult to glance at Tables 8 and 9 and digest the columns of numbers, Table 10 summarizes the results.

Table 10 SUMMARIZED RESULTS

Wafer	I.L. at f_o	OT at f_o	3T at f_o
CQX12A and CQX21A	Avg. = 31.1 dB Max. = 35.0 dB Min. = 27 dB	Avg. = 27 dB Max. = 46 dB Min. = 13 dB	Avg. = 38.7 dB Max. = 43.0 dB Min. = 34 dB
CQX07A	Avg. = 37.5 dB Max. = 91 dB Min. = 35 dB	Avg. = 28.4 dB Max. = 47 dB Min. = 13 dB	Avg. = 36.7 dB Max. = 46 dB Min. = 28 dB

3. CONCLUSIONS

The objectives of the program were low cost processing and fabrication of delay lines to reduce handwork operations as much as possible and automate where possible. In a limited scope program such as this, progressing toward these objectives was a matter of identifying and resolving key problems. Complete implementation of many of the solutions in the sense of taking maximum advantage of potential cost savings, such as process mounting and automatic electrical testing, will have to await actual production activities, (In both of these cases the key improvements have proven feasible and are fully tested.) Further, total elimination of certain operations, such as post process tuning, has been

achieved through a design that provides for monolithic tuning and allows much wider tolerances on the process parameters than had been previously possible. Full implementation of the automation allowed by these improvements will have to await a production program where automation costs can be amortized into the actual program costs. The automation associated with these improvements is now clearly feasible and can be projected into any new production programs. Further, even without automation, these improvements lead to cost savings.

Beyond the above mentioned improvements, work to date has identified specific areas where improved process definitions can provide savings and make possible more complete automation. Even without improved process definitions, mechanization of some areas of processing is being carried out. Once this mechanization is in place, automation will be carried out to the extent current process definitions allow. Additional automation may be provided with improved definitions. As mentioned in the previous paragraph, circuit improvements have allowed a major relaxation in process tolerances with an accompanying improvement in yield. There is still a significant need for detailed examination of the process parameters and their relationship to process results. Expressed another way, there is a major need to advance zinc oxide processing from a black art to a science, particularly in thin films suitable for microwave delay lines. Ultimately the degree to which this is done will have a major influence on the ability to process microwave delay lines at a cost compatible with their widespread use in systems. This is as opposed to the current procedure of using a bulk delay line only where nothing else will work.

Design.--Improved impedance matching with mosaic transducers can be simplified and carried out monolithically. Though originally this design was somewhat empirically carried out, subsequent modelling has

provided an analytical basis for certain key parameters. It is recommended that optimization be carried out over all key parameters to provide a complete design basis.

Test.--A probe which maintains 50 Ω through the probe right up to the chip has been tested. It is so successful that both transmission and impedance parameters can be evaluated to normal measurement accuracy on the wafer, with results comparable to a packaged device. Only leakage cannot be accurately tested on the wafer. As the delay line requires probes on both sides of the wafer, automation would be more complex than that of simple IC mechanics. However, a variation should be possible and should be the objective of a major production program.

Packaging.--High conductivity polyimide was identified and adapted to packaging of the delay line chip. The key factor in the use of a polyimide is that curing to a high conductivity is possible below 200 ^{o}C which is a safe temperature for delay lines with zinc oxide transducers. This replaces conductive epoxy which could not be fully processed below 200 ^{o}C and eliminates the need for extensive ground electrode bonding, a very labor intensive operation. Currently, even the application of the polyimide is more labor intensive than should be and indicates an area for an automation application. The labor savings from the present process could be substantial.

Processing.--This is the area of continuing greatest need. There are almost as many approaches to processing zinc oxide as there are active workers. Though there are favorite deposition systems among various active groups, there is seldom common ground as to system operating parameters even among those who operate a given system. Most popular systems seem to be rf diode, dc triode and magnetron. Parameters which seem to work for various groups have been identified by each group using a given system. During the industry information meeting conducted

for this program, it was clear there is little agreement among workers active in the field. Variability of results has been the rule rather than the exception. An advance by Westinghouse was the introduction of an online mass spectrometer to its zinc oxide deposition system. This identified certain impurities which require control. Further investigation is needed to reduce zinc oxide deposition to a science. This will be a task for a future program.

APPENDIX A.--MEDIA MODELING PROGRAM DATA FOR ALPHA QUARTZ.

PLANE NORMAL
(90.0, .0, .0)
(.000, 1.000, .000)

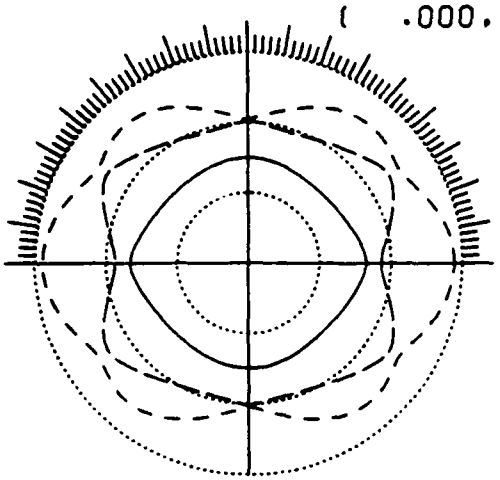

SLOWNESS
DIV =.105-03 SEC/M

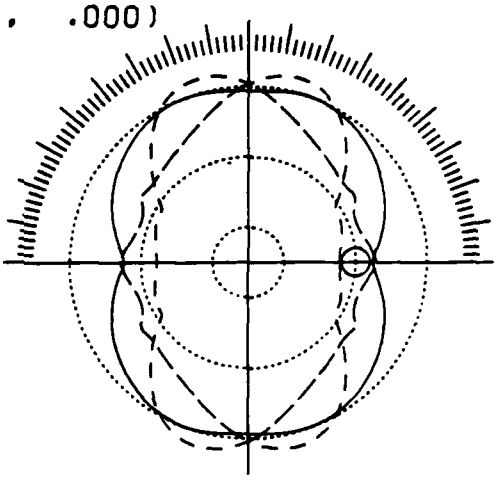

TEMPERATURE COEF. OF DELAY
DIV = .750-04/DEG C

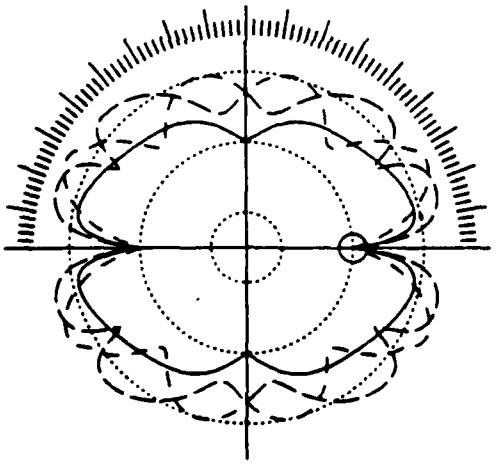

POWER FLOW ANGLE
DIV = 24.500 DEGREES

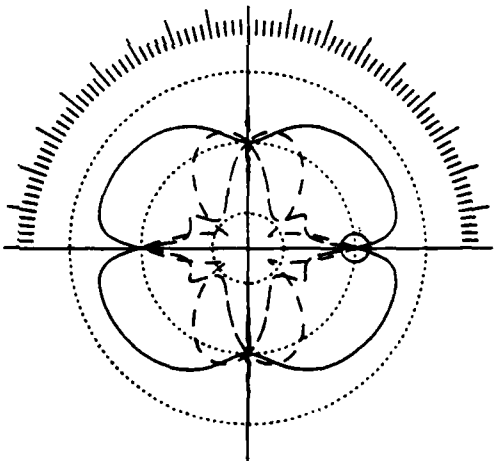

OUT-OF-PLANE ANGLE
DIV = 24.500 DEGREES

T1 T2 L

BULK ACOUSTIC WAVES IN ALPHA QUARTZ
SYMMETRY TYPE: TRIGONAL (32)

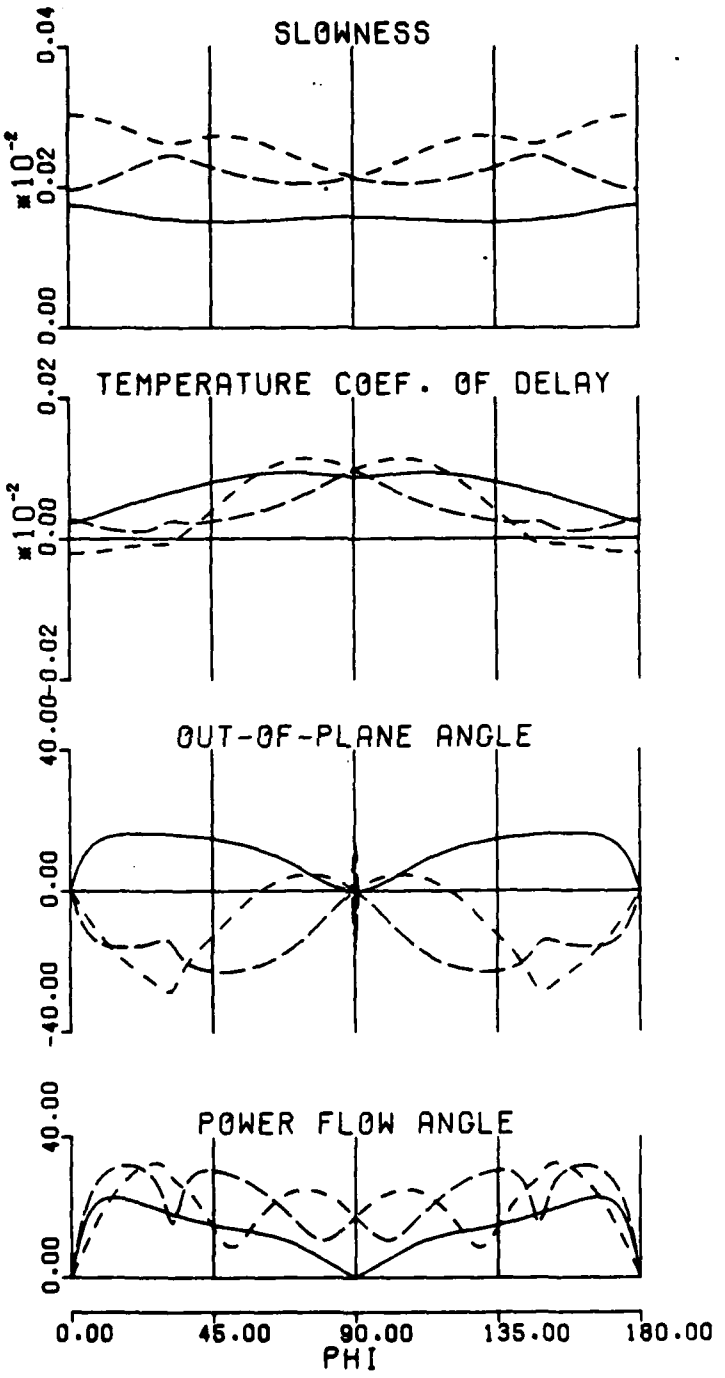
SLOWNESS
0.04
0.02
0.00
x10^-2
TEMPERATURE COEF. OF DELAY
0.02
0.00
-0.02
x10^-2
OUT-OF-PLANE ANGLE
40.00
0.00
-40.00
POWER FLOW ANGLE
40.00
0.00
0.00
45.00
90.00
135.00
180.00
PHI

PLANE NORMAL
(90.0, .0, 5.0)
(-.087, .996, .000)

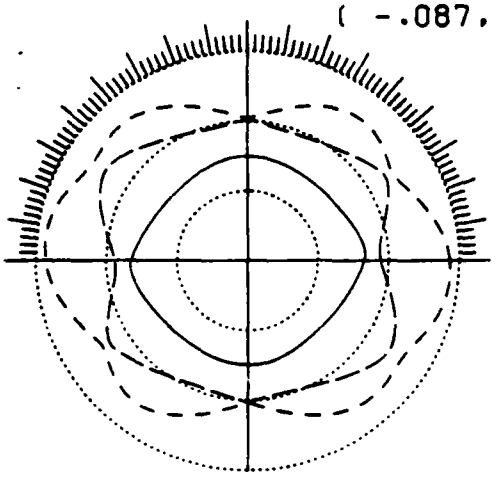

SLOWNESS
DIV =.105-03 SEC/M

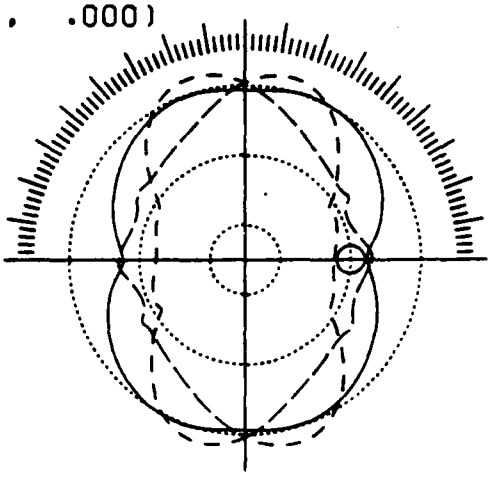

TEMPERATURE COEF. OF DELAY
DIV = .750-04/DEG C

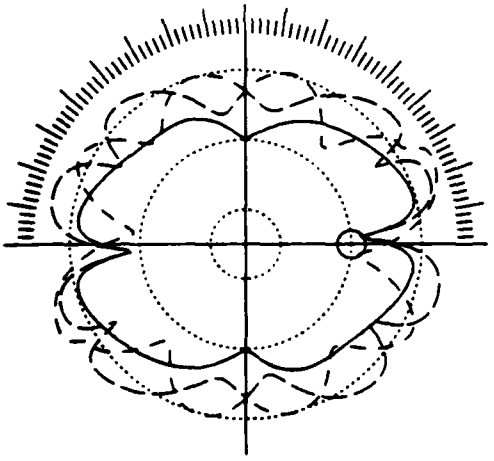

POWER FLOW ANGLE
DIV = 24.500 DEGREES

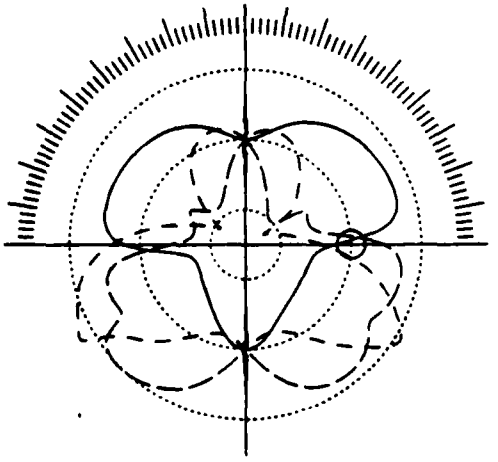

OUT-OF-PLANE ANGLE
DIV = 24.500 DEGREES

T1 T2 L

BULK ACOUSTIC WAVES IN ALPHA QUARTZ
SYMMETRY TYPE: TRIGONAL (32)

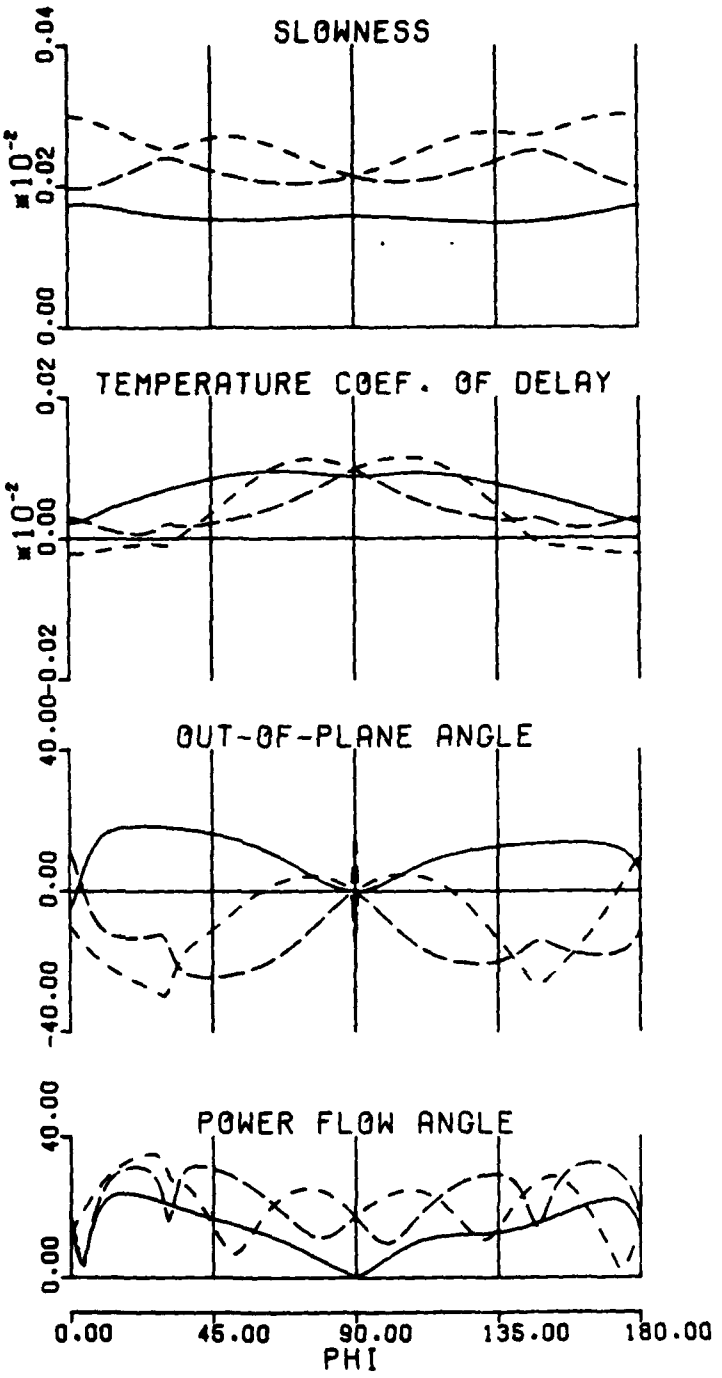
SLOWNESS
0.04
0.02
0.00
x10^-2
TEMPERATURE COEF. OF DELAY
0.02
0.00
-0.02
x10^-2
OUT-OF-PLANE ANGLE
40.00
0.00
-40.00
POWER FLOW ANGLE
40.00
0.00
0.00
45.00
90.00
135.00
180.00
PHI

PLANE NORMAL
(90.0, .0, 10.0)
(-.174, .985, .000)

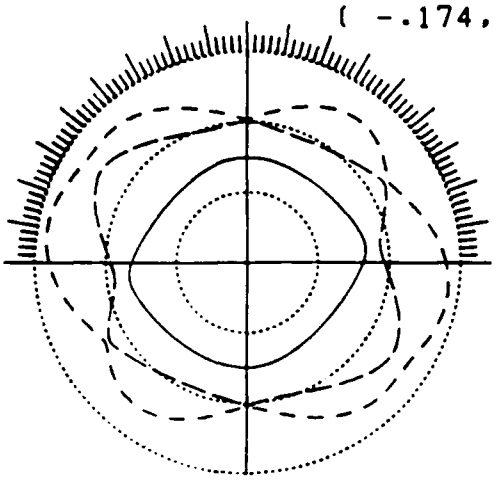

SLOWNESS
DIV =.105-03 SEC/M

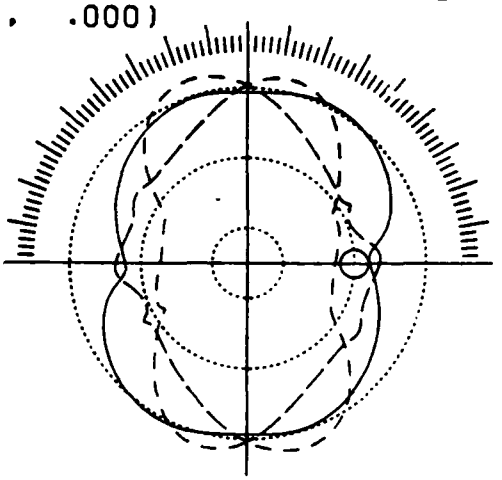

TEMPERATURE COEF. OF DELAY
DIV = .750-04/DEG C

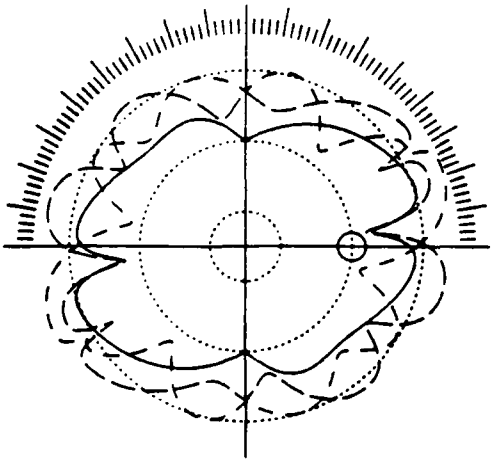

POWER FLOW ANGLE
DIV = 24.500 DEGREES

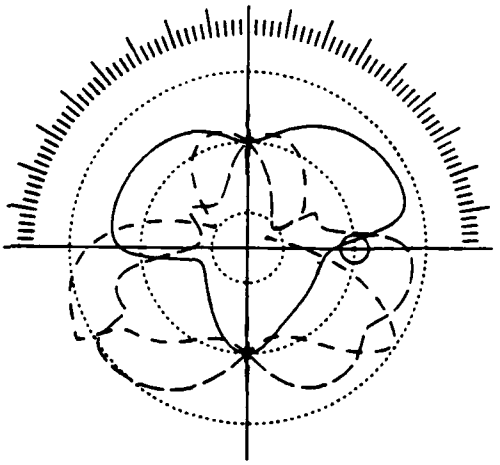

OUT-OF-PLANE ANGLE
DIV = 24.500 DEGREES

----- T1 ------ T2 ———— L

BULK ACOUSTIC WAVES IN ALPHA QUARTZ
SYMMETRY TYPE: TRIGONAL (32)

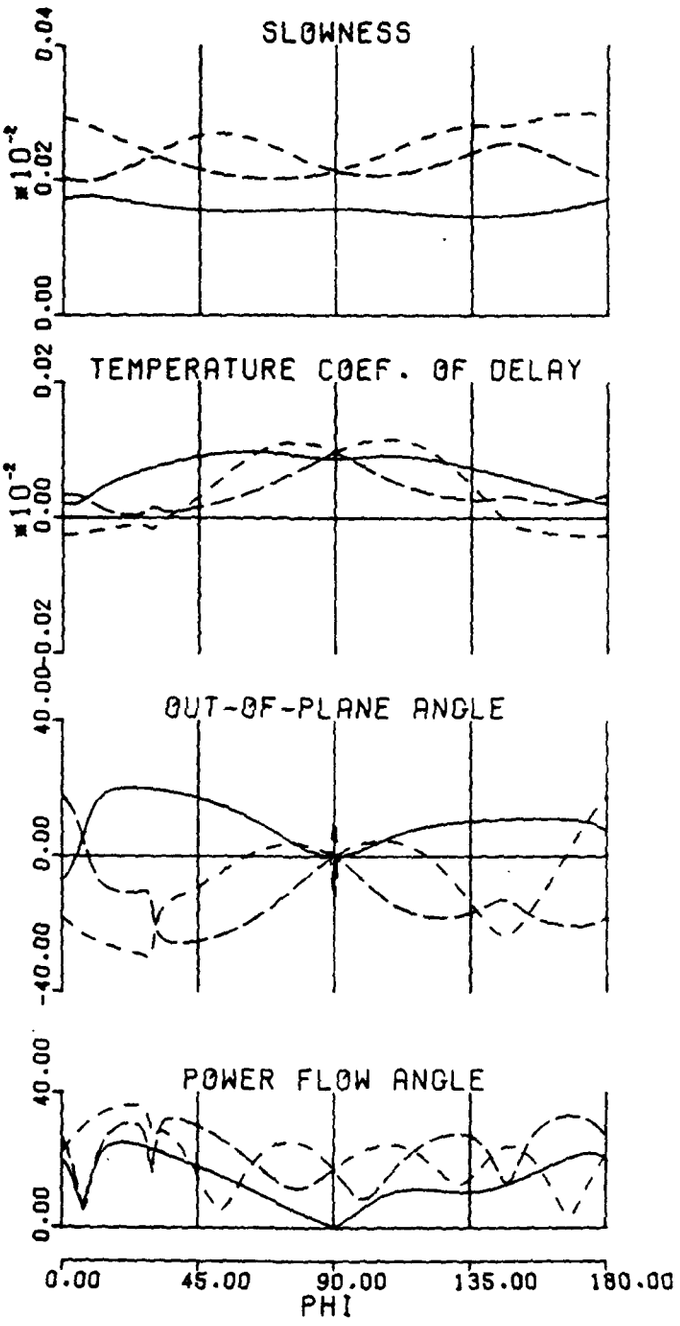
SLOWNESS
0.04
0.02
0.00
*10⁻²
TEMPERATURE COEF. OF DELAY
0.02
0.00
-0.02
*10⁻²
OUT-OF-PLANE ANGLE
40.00
0.00
-40.00
POWER FLOW ANGLE
40.00
0.00
0.00
45.00
90.00
135.00
180.00
PHI

PLANE NORMAL
(90.0, .0, 15.0)
(-.259, .966, .000)

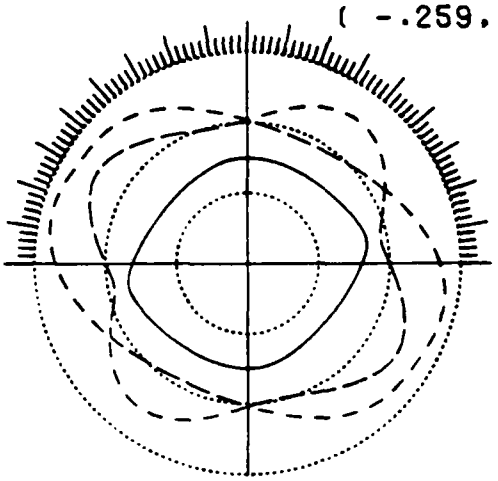

SLOWNESS
DIV =.105-03 SEC/M

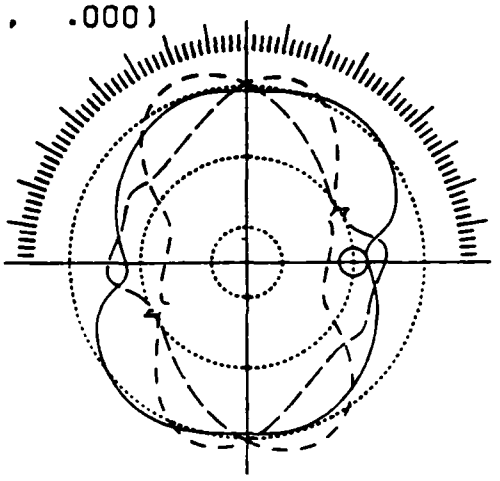

TEMPERATURE COEF. OF DELAY
DIV = .750-04/DEG C

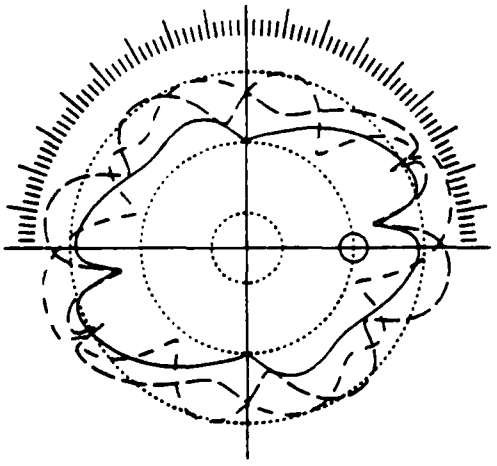

POWER FLOW ANGLE
DIV = 24.500 DEGREES

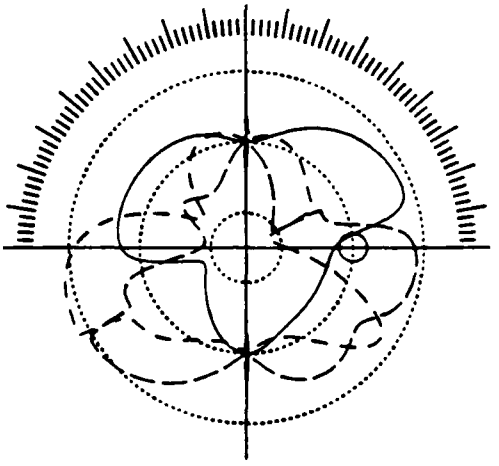

OUT-OF-PLANE ANGLE
DIV = 24.500 DEGREES

- - - - - - T1 ——— T2 ——— L

BULK ACOUSTIC WAVES IN ALPHA QUARTZ
SYMMETRY TYPE: TRIGONAL (32)

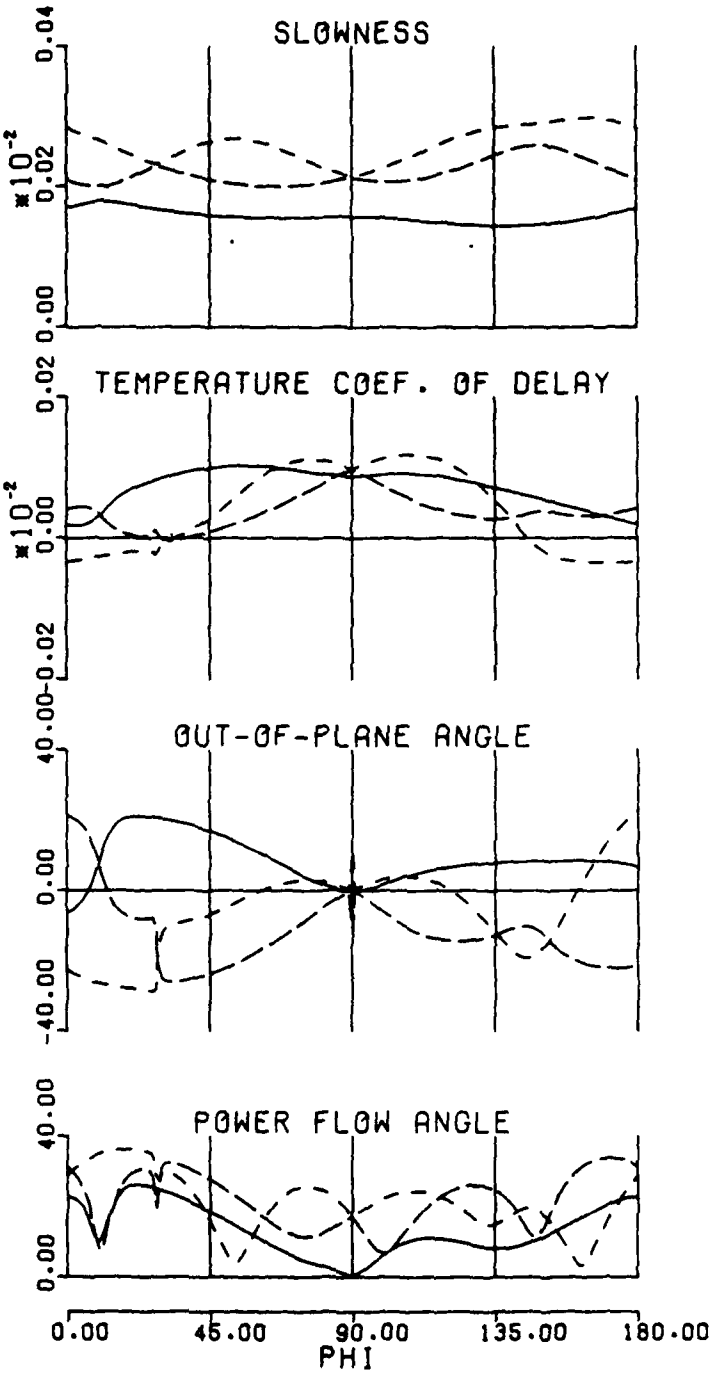
SLOWNESS
0.04
0.02
0.00
×10⁻²
TEMPERATURE COEF. OF DELAY
0.02
0.00
-0.02
×10⁻²
OUT-OF-PLANE ANGLE
40.00
0.00
-40.00
POWER FLOW ANGLE
40.00
0.00
0.00
45.00
90.00
135.00
180.00
PHI

PLANE NORMAL
(90.0, .0, 20.0)
(-.342, .940, .000)

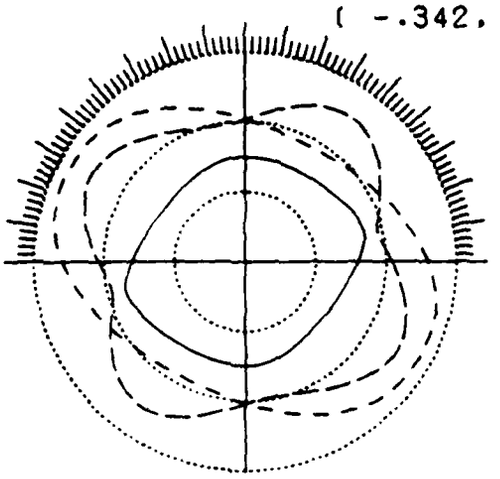

SLOWNESS
DIV =.105-03 SEC/M

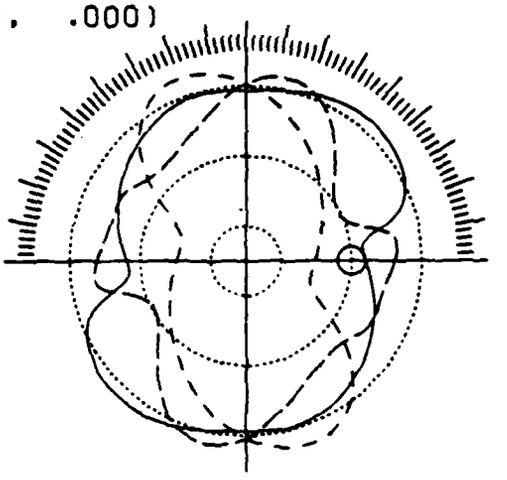

TEMPERATURE COEF. OF DELAY
DIV = .750-04/DEG C

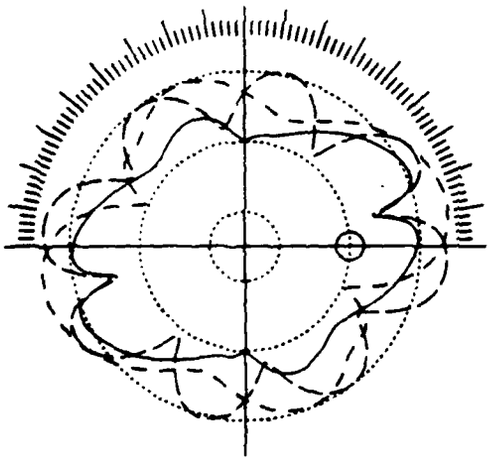

POWER FLOW ANGLE
DIV = 24.500 DEGREES

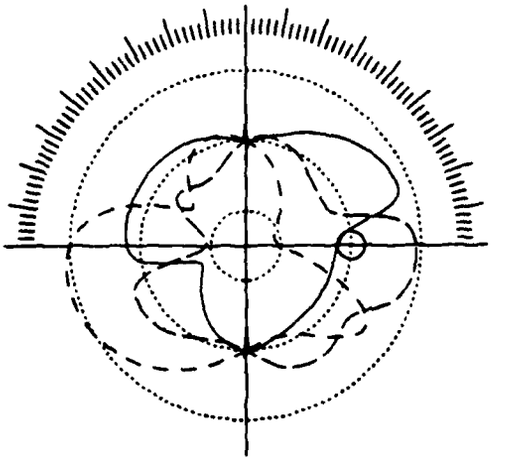

OUT-OF-PLANE ANGLE
DIV = 24.500 DEGREES

------ T1 ——— T2 ——— L

BULK ACOUSTIC WAVES IN ALPHA QUARTZ
SYMMETRY TYPE: TRIGONAL (32)

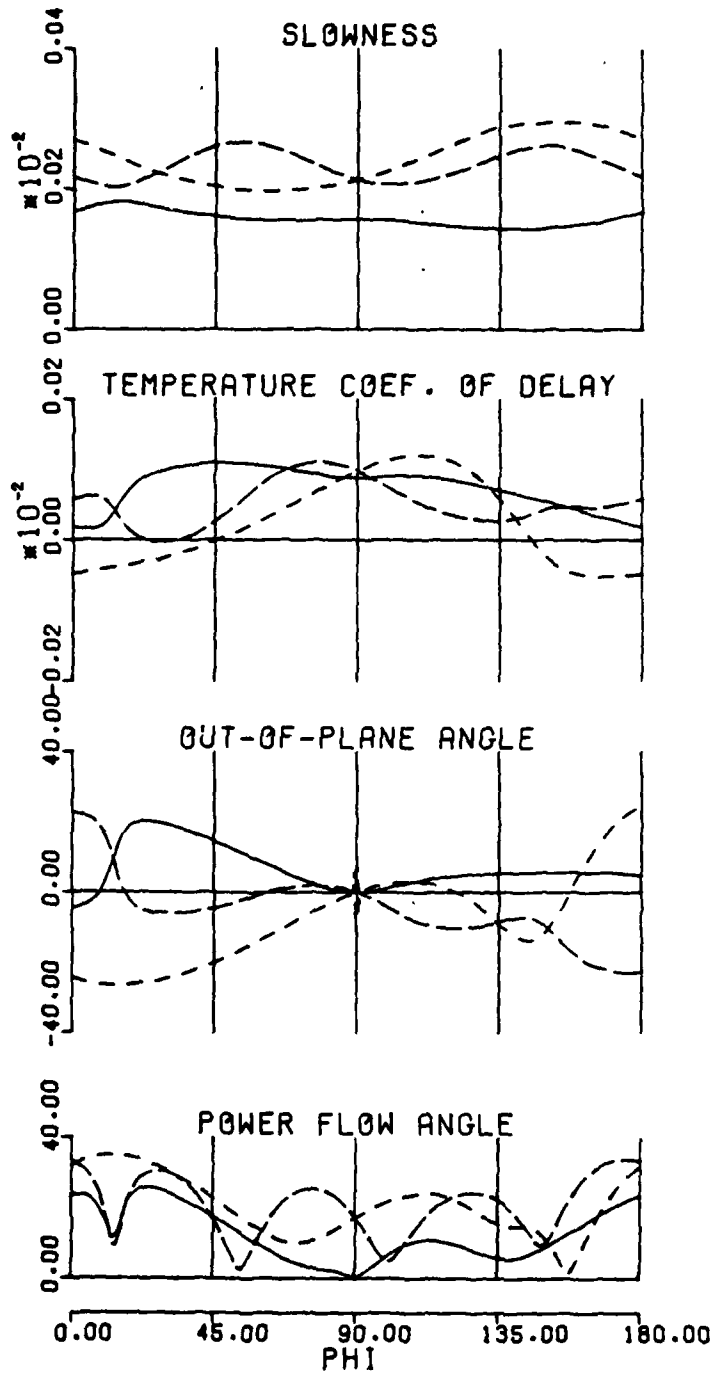
SLOWNESS
0.04
0.02
0.00
x10^-2
TEMPERATURE COEF. OF DELAY
0.02
0.00
-0.02
x10^-2
OUT-OF-PLANE ANGLE
40.00
0.00
-40.00
POWER FLOW ANGLE
40.00
0.00
0.00
45.00
90.00
135.00
180.00
PHI

PLANE NORMAL
(90.0, .0, 25.0)
(-.423, .906, .000)

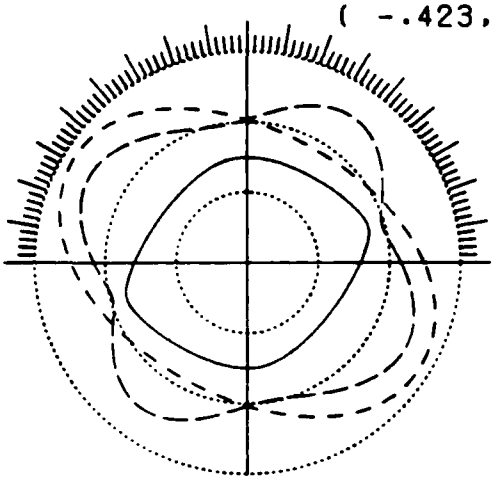

SLOWNESS
DIV =.105-03 SEC/M

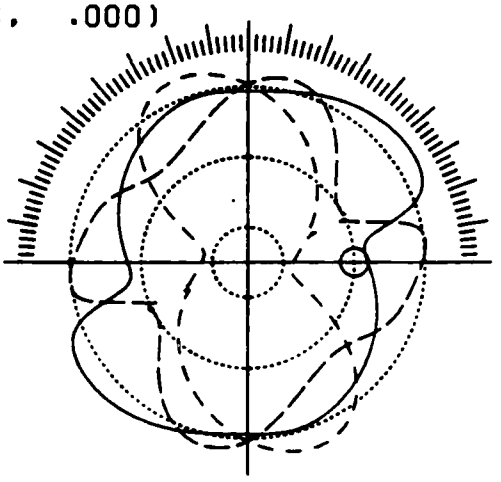

TEMPERATURE COEF. OF DELAY
DIV = .750-04/DEG C

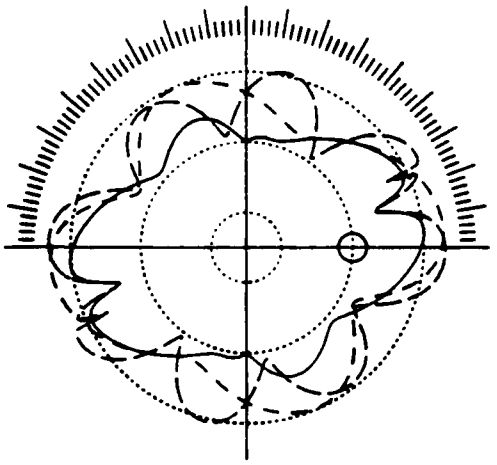

POWER FLOW ANGLE
DIV = 24.500 DEGREES

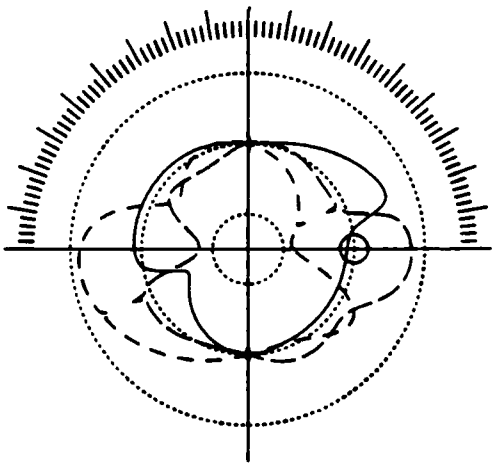

OUT-OF-PLANE ANGLE
DIV = 24.500 DEGREES

- - - - - - T1 ——— T2 ——— L

BULK ACOUSTIC WAVES IN ALPHA QUARTZ
SYMMETRY TYPE: TRIGONAL (32)

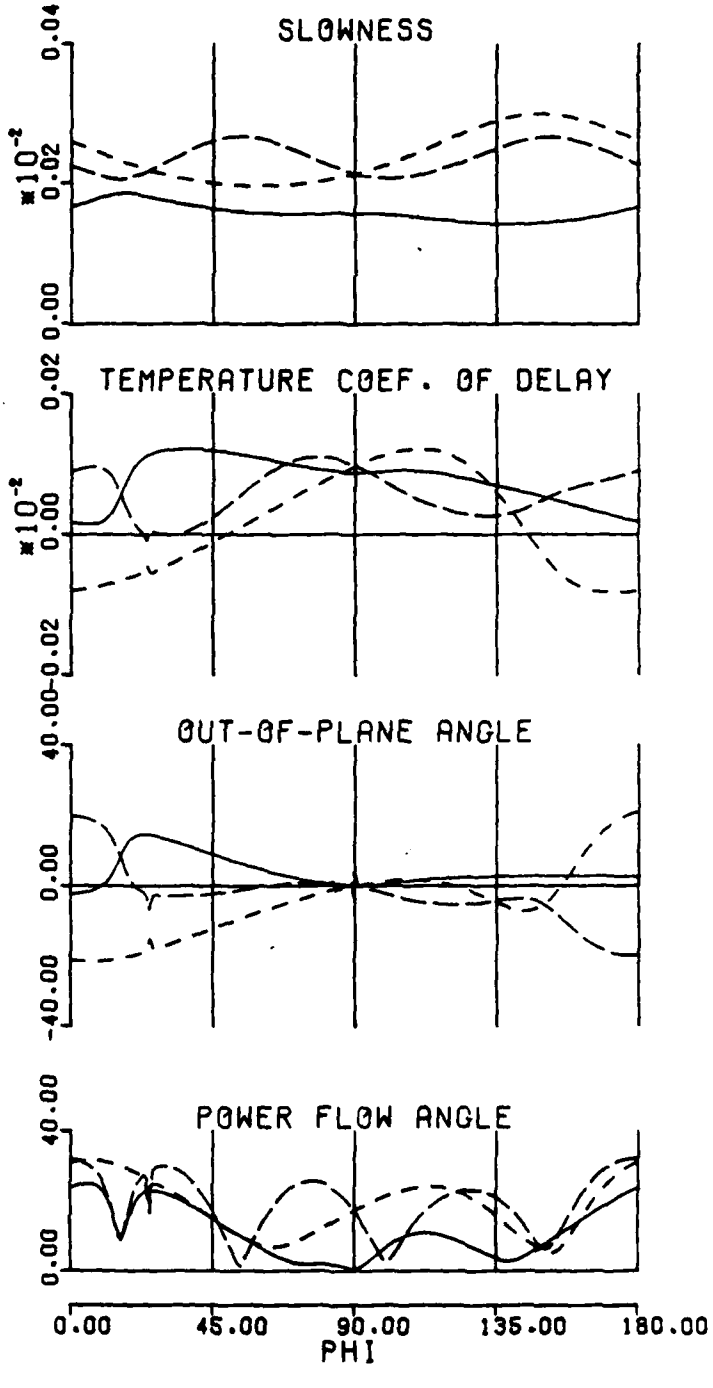
SLOWNESS
0.04
0.02
0.00
x10^-2
TEMPERATURE COEF. OF DELAY
0.02
0.00
-0.02
x10^-2
OUT-OF-PLANE ANGLE
40.00
0.00
-40.00
POWER FLOW ANGLE
40.00
0.00
0.00
45.00
90.00
135.00
180.00
PHI

PLANE NORMAL
(90.0, .0, 30.0)
(-.500, .866, .000)

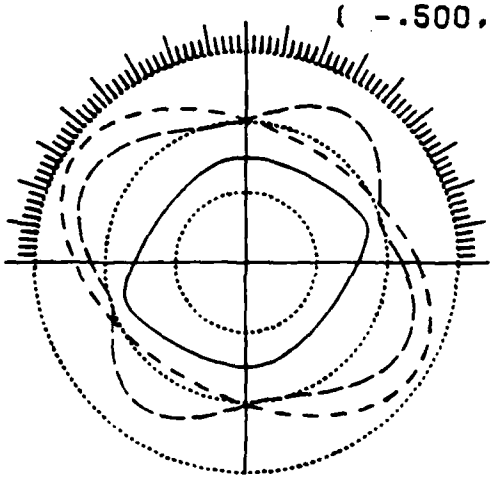

SLOWNESS
DIV =.105-03 SEC/M

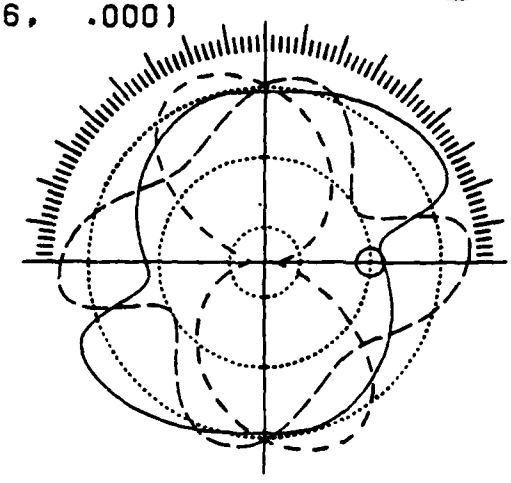

TEMPERATURE COEF. OF DELAY
DIV = .750-04/DEG C

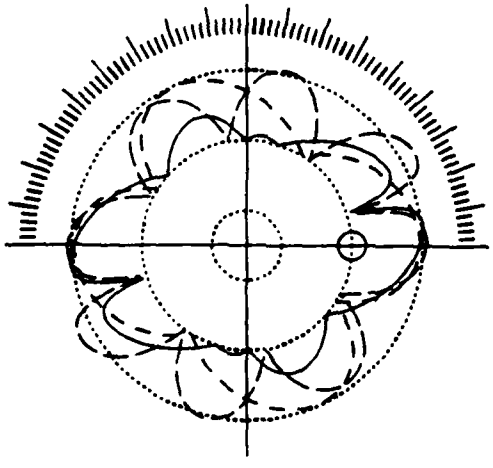

POWER FLOW ANGLE
DIV = 24.500 DEGREES

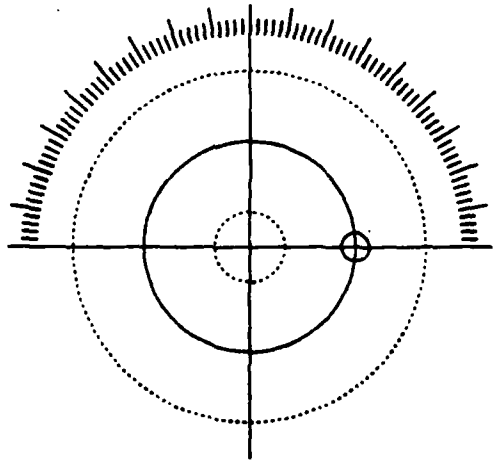

OUT-OF-PLANE ANGLE
DIV = 24.500 DEGREES

- - - - - - T1 ——— T2 ——— L

BULK ACOUSTIC WAVES IN ALPHA QUARTZ
SYMMETRY TYPE: TRIGONAL (32)

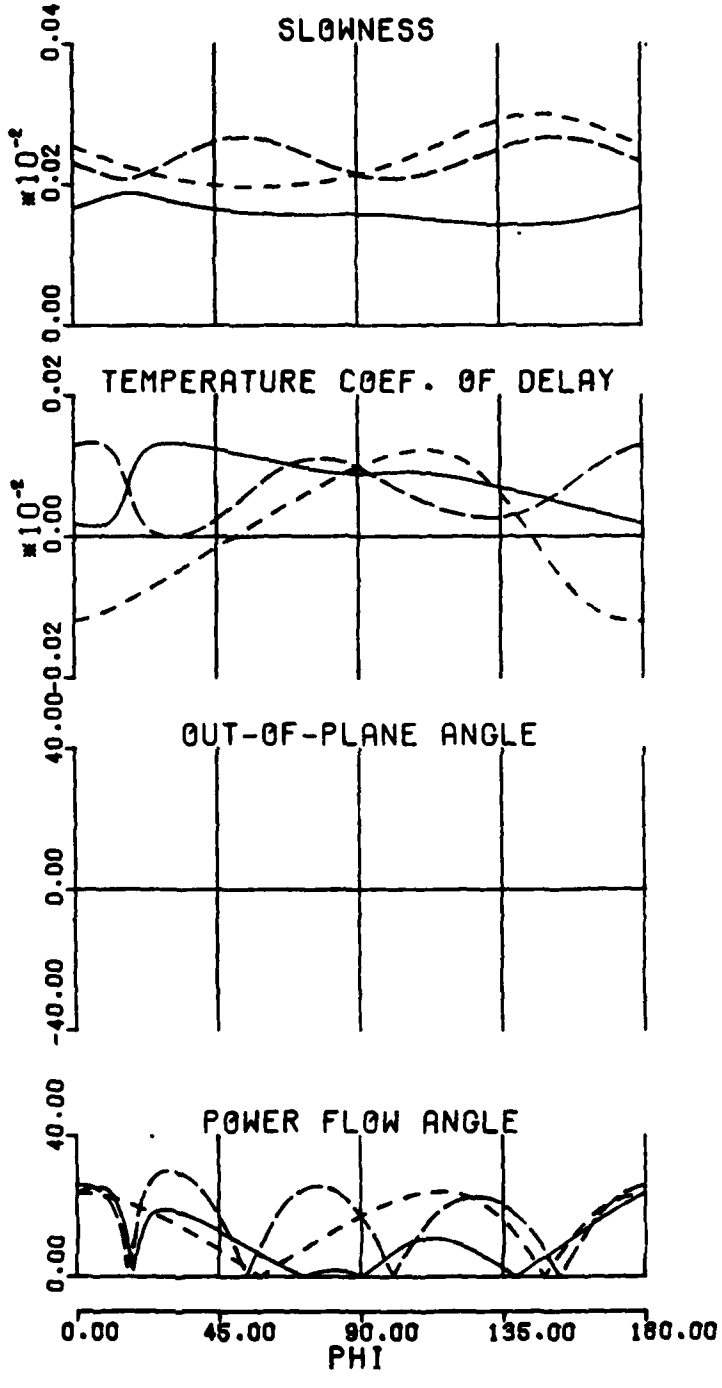
SLOWNESS
0.04
0.02
0.00
×10⁻²
TEMPERATURE COEF. OF DELAY
0.02
0.00
-0.02
×10⁻²
OUT-OF-PLANE ANGLE
40.00
0.00
-40.00
POWER FLOW ANGLE
40.00
0.00
0.00
45.00
90.00
135.00
180.00
PHI

PLANE NORMAL
(90.0, .0, 35.0)
(-.574, .819, .000)

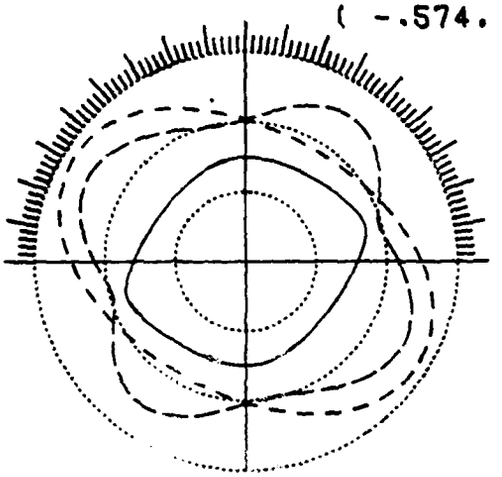

SLOWNESS
DIV = .705-03 SEC/M

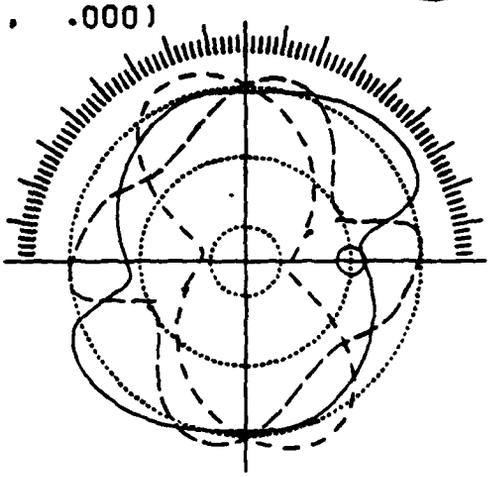

TEMPERATURE COEF. OF DELAY
DIV = .750-04/DEG C

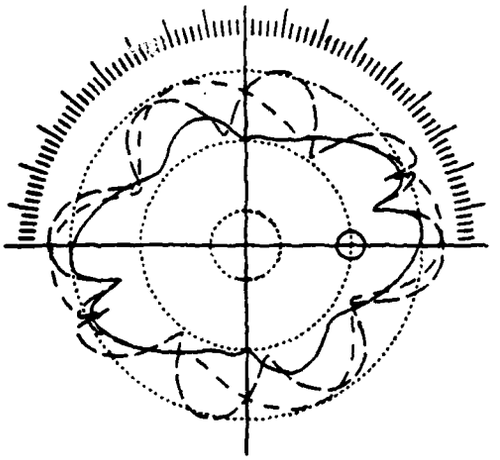

POWER FLOW ANGLE
DIV = 24.500 DEGREES

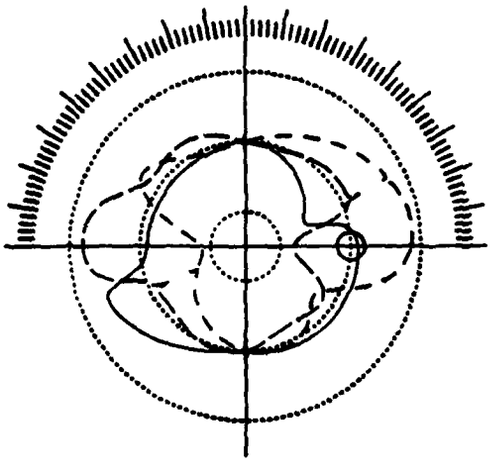

OUT-OF-PLANE ANGLE
DIV = 24.500 DEGREES

- - - - - - T1 ——— T2 ——— L

BULK ACOUSTIC WAVES IN ALPHA QUARTZ
SYMMETRY TYPE: TRIGONAL (32)

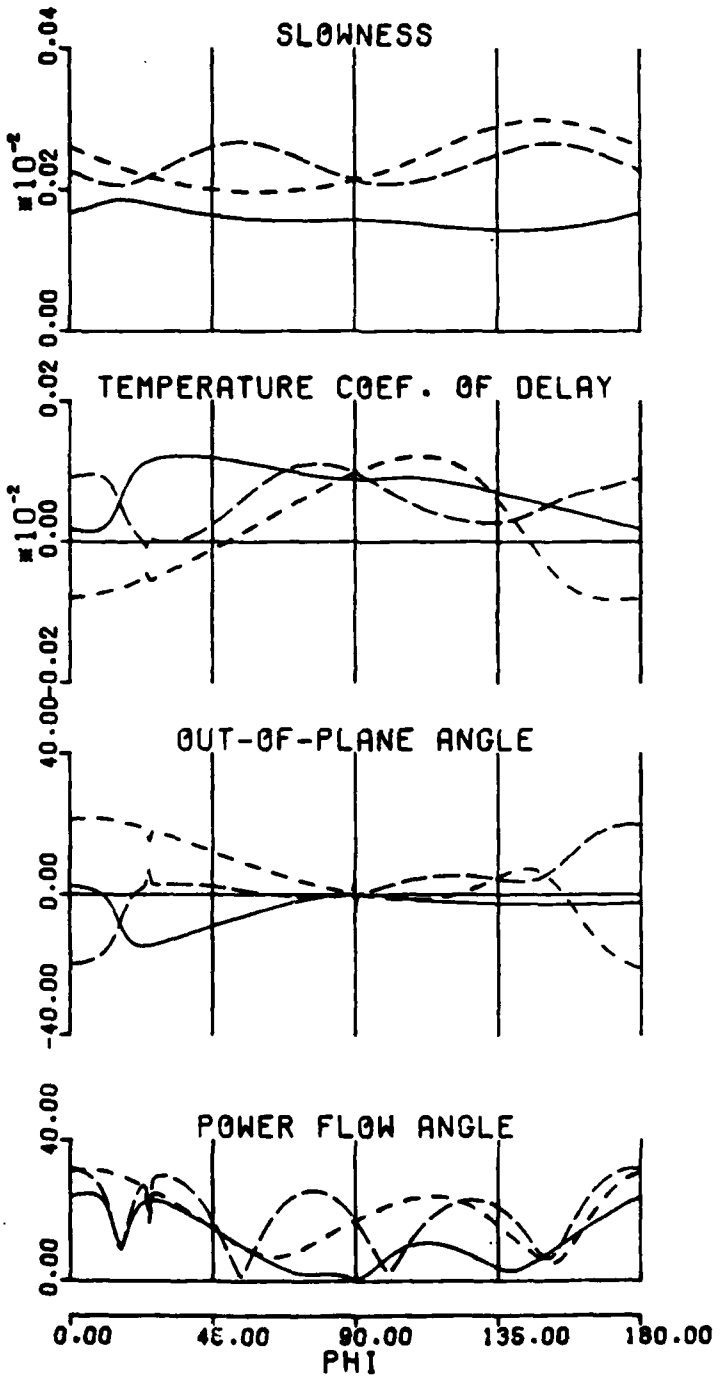
SLOWNESS
0.04
0.02
0.00
x10^-2
TEMPERATURE COEF. OF DELAY
0.02
0.00
-0.02
x10^-2
OUT-OF-PLANE ANGLE
40.00
0.00
-40.00
POWER FLOW ANGLE
40.00
0.00
0.00
45.00
90.00
135.00
180.00
PHI

PLANE NORMAL
(90.0, .0, 40.0)
(-.643, .766, .000)

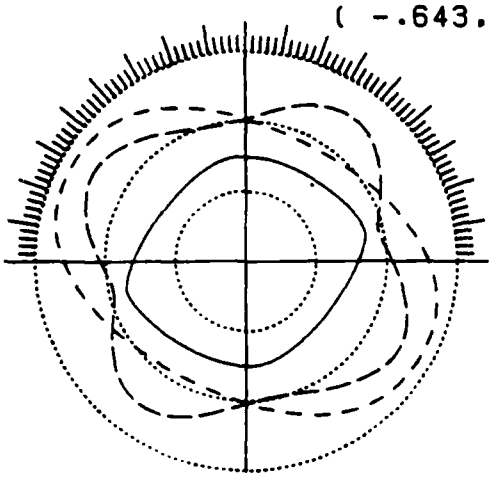

SLOWNESS
DIV =.105-03 SEC/M

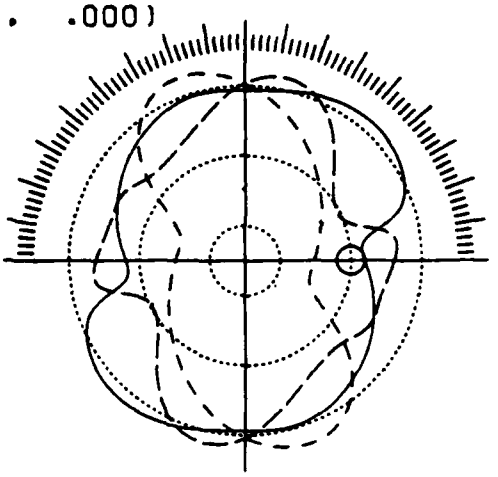

TEMPERATURE COEF. OF DELAY
DIV = .750-04/DEG C

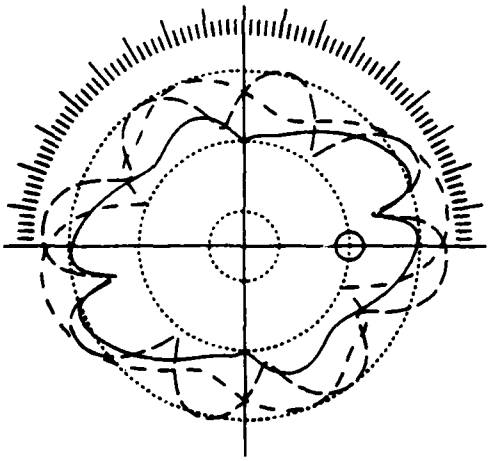

POWER FLOW ANGLE
DIV = 24.500 DEGREES

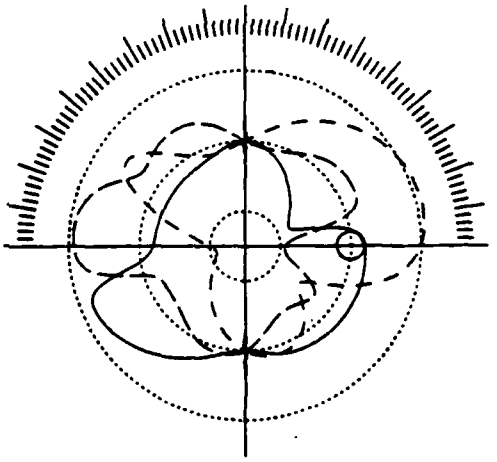

OUT-OF-PLANE ANGLE
DIV = 24.500 DEGREES

- - - - - - T1 ——— T2 ——— L

BULK ACOUSTIC WAVES IN ALPHA QUARTZ
SYMMETRY TYPE: TRIGONAL (32)

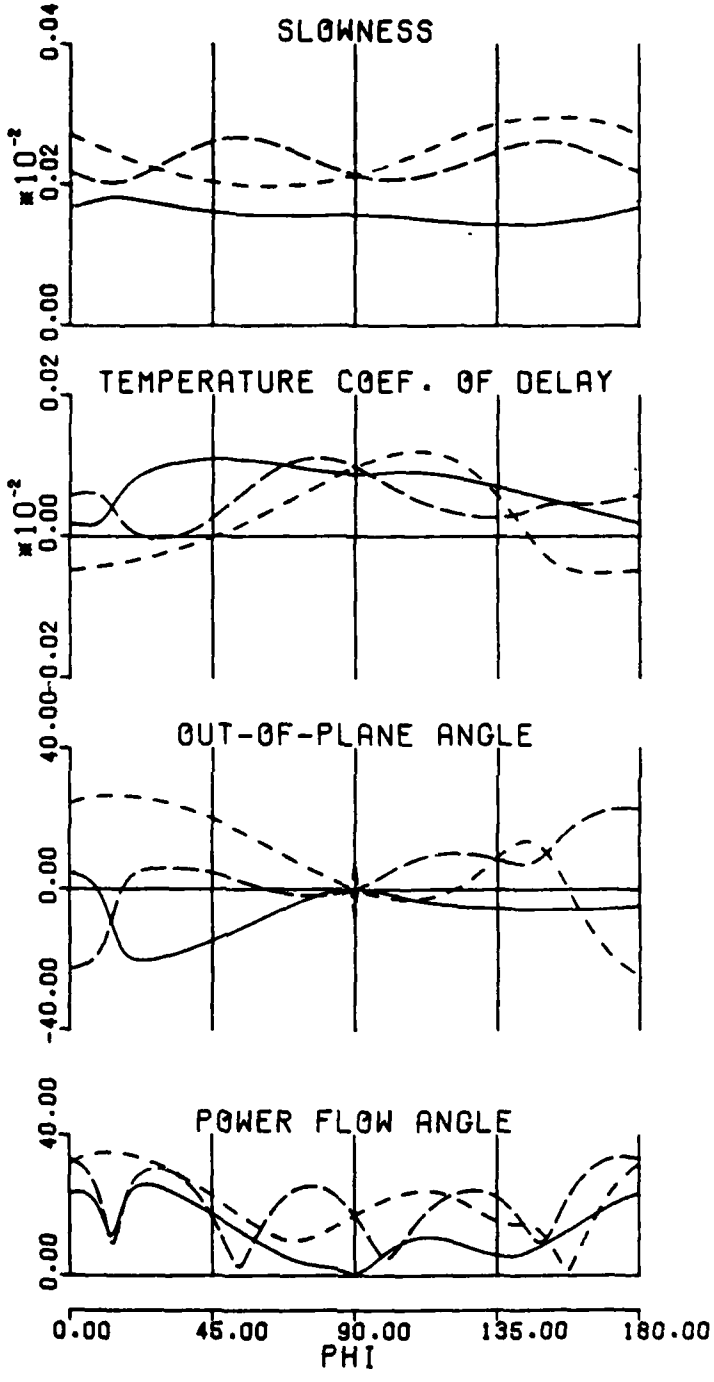
SLOWNESS
0.04
0.02
0.00
x10⁻²
TEMPERATURE COEF. OF DELAY
0.02
0.00
-0.02
x10⁻²
OUT-OF-PLANE ANGLE
40.00
0.00
-40.00
POWER FLOW ANGLE
40.00
0.00
0.00
45.00
90.00
135.00
180.00
PHI

PLANE NORMAL
(90.0, .0, 45.0)
(-.707, .707, .000)

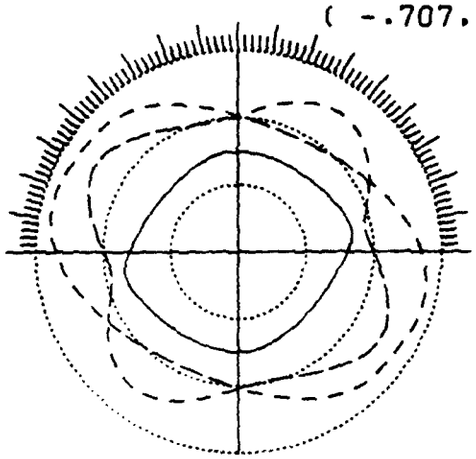

SLOWNESS
DIV =.105-03 SEC/M

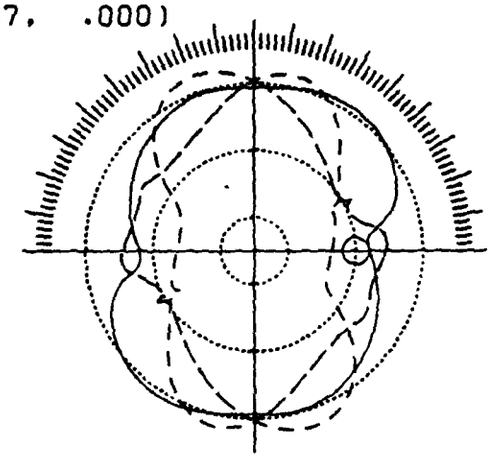

TEMPERATURE COEF. OF DELAY
DIV = .750-04/DEG C

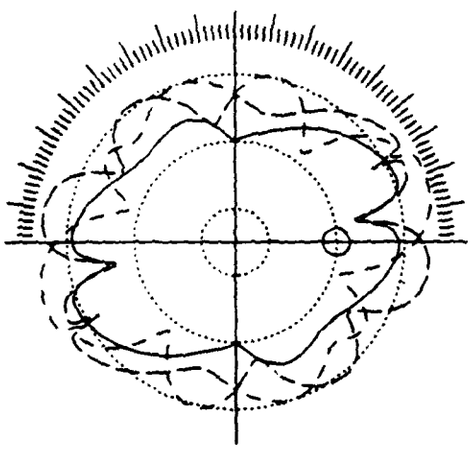

POWER FLOW ANGLE
DIV = 24.500 DEGREES

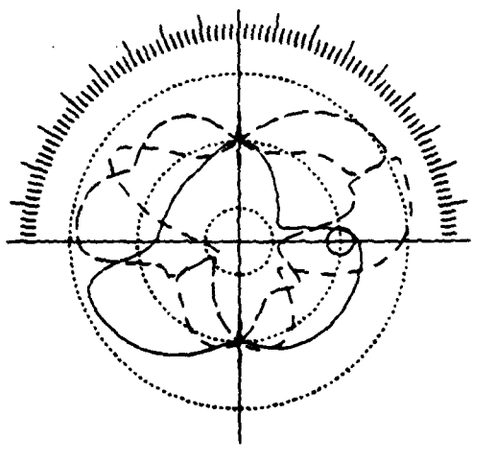

OUT-OF-PLANE ANGLE
DIV = 24.500 DEGREES

T1 T2 L

BULK ACOUSTIC WAVES IN ALPHA QUARTZ
SYMMETRY TYPE: TRIGONAL (32)

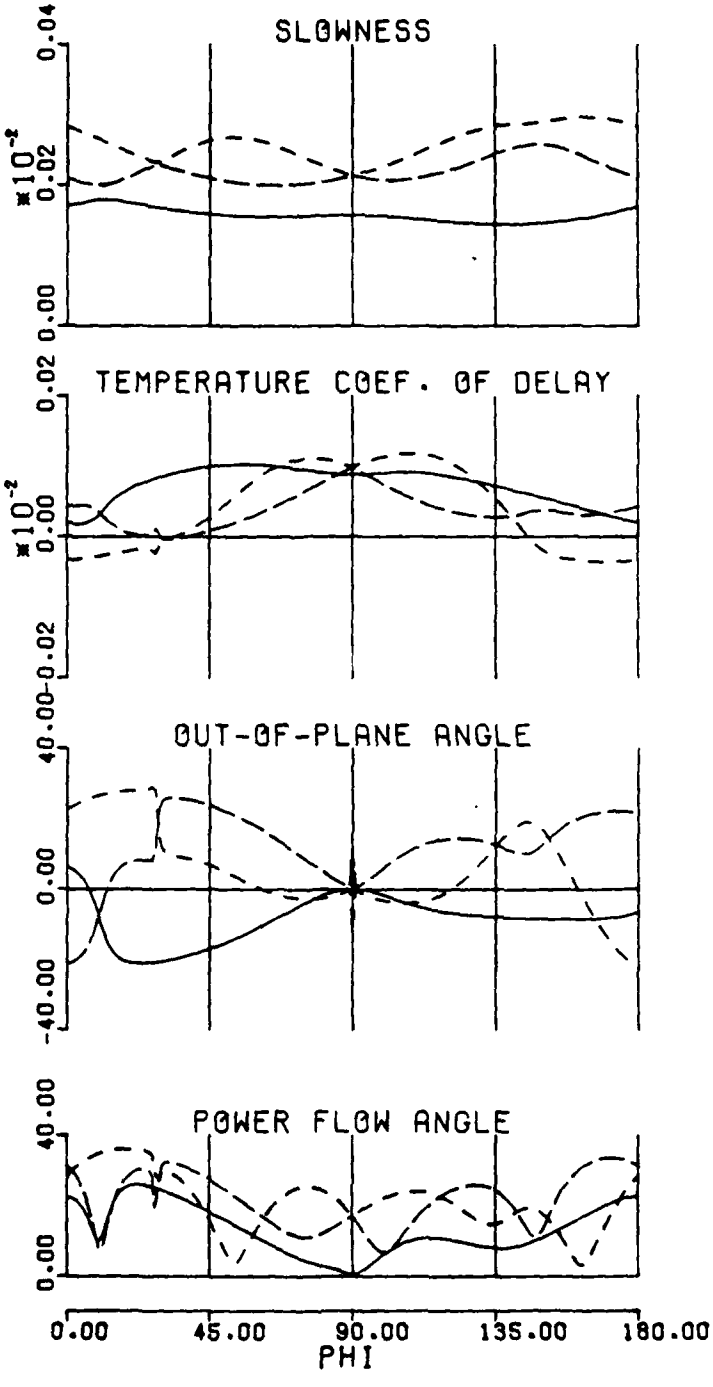
SLOWNESS
0.04
0.02
0.00
x10⁻²
TEMPERATURE COEF. OF DELAY
0.02
0.00
-0.02
x10⁻²
OUT-OF-PLANE ANGLE
40.00
0.00
-40.00
POWER FLOW ANGLE
40.00
0.00
0.00
45.00
90.00
135.00
180.00
PHI

PLANE NORMAL
(90.0, .0, 50.0)
(-.766, .643, .000)

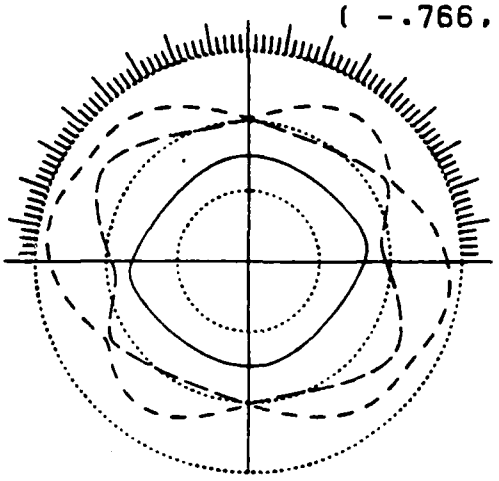

SLOWNESS
DIV =.105-03 SEC/M

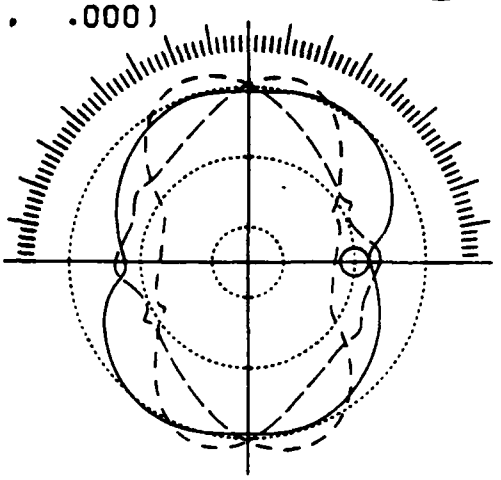

TEMPERATURE COEF. OF DELAY
DIV = .750-04/DEG C

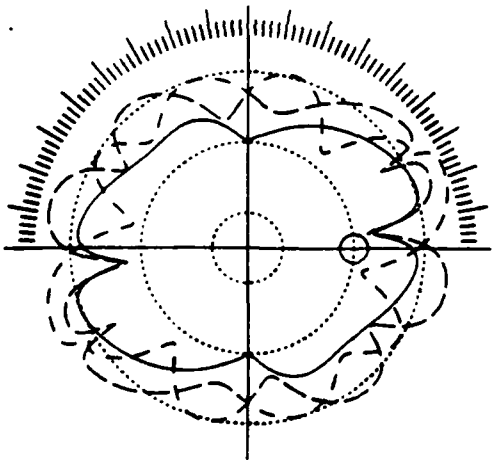

POWER FLOW ANGLE
DIV = 24.500 DEGREES

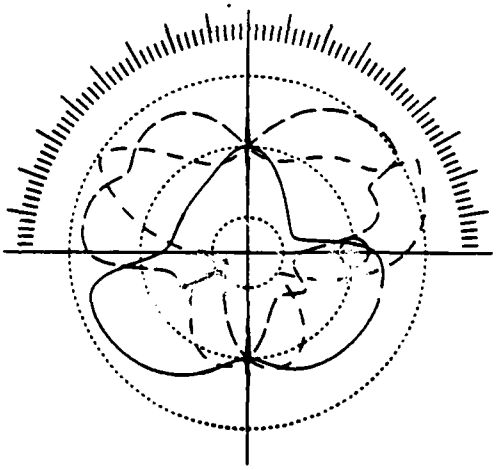

OUT-OF-PLANE ANGLE
DIV = 24.500 DEGREES

T1 T2 L

BULK ACOUSTIC WAVES IN ALPHA QUARTZ
SYMMETRY TYPE: TRIGONAL (32)

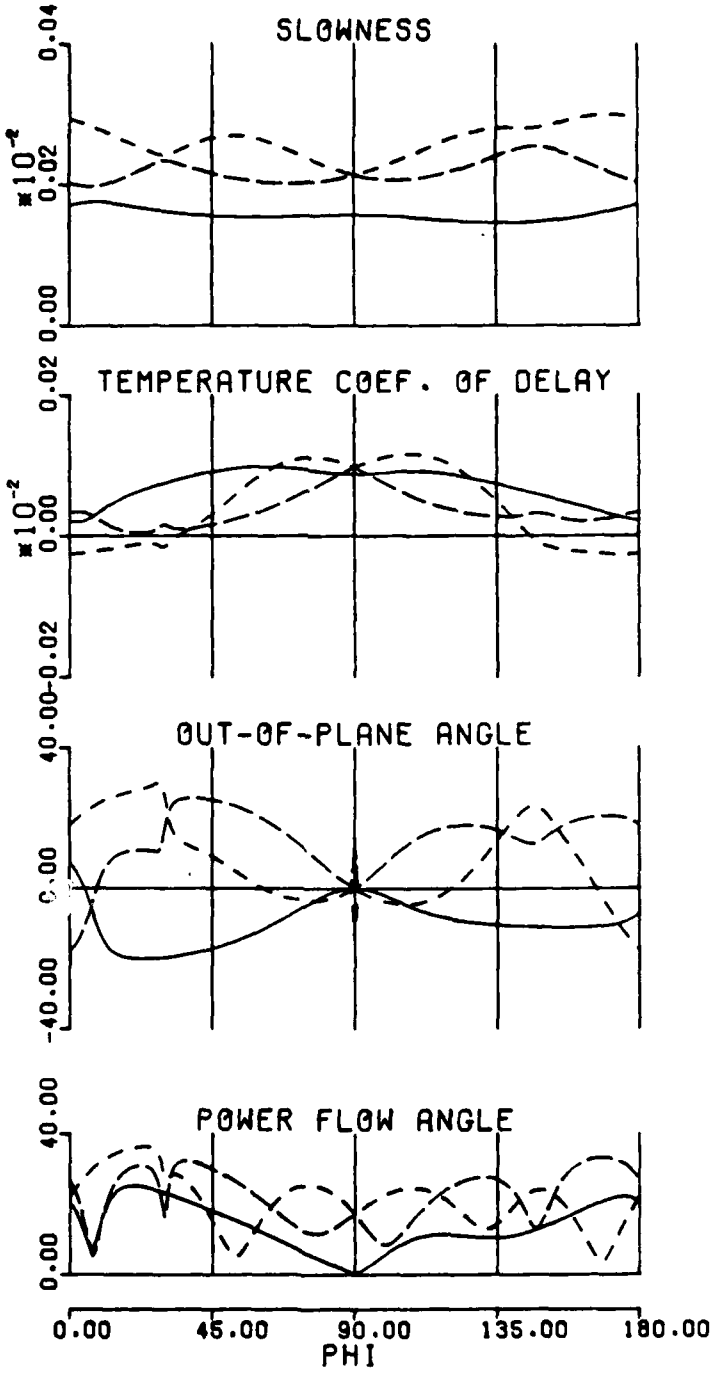
SLOWNESS
0.04
0.02
0.00
x10⁻²
TEMPERATURE COEF. OF DELAY
0.02
0.00
-0.02
x10⁻²
OUT-OF-PLANE ANGLE
40.00
0.00
-40.00
POWER FLOW ANGLE
40.00
0.00
0.00
45.00
90.00
135.00
180.00
PHI

PLANE NORMAL
(90.0, .0, 55.0)
(-.819, .574, .000)

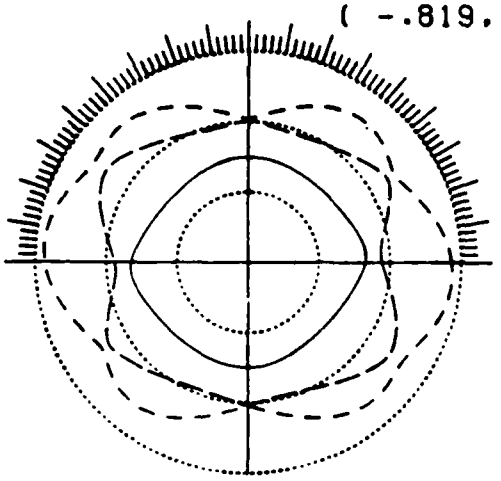

SLOWNESS
DIV =.105-03 SEC/M

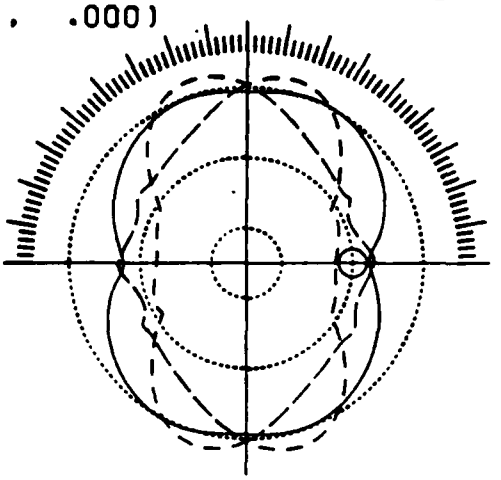

TEMPERATURE COEF. OF DELAY
DIV = .750-04/DEG C

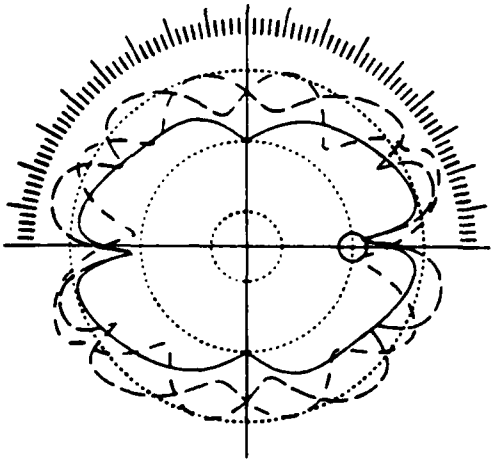

POWER FLOW ANGLE
DIV = 24.500 DEGREES

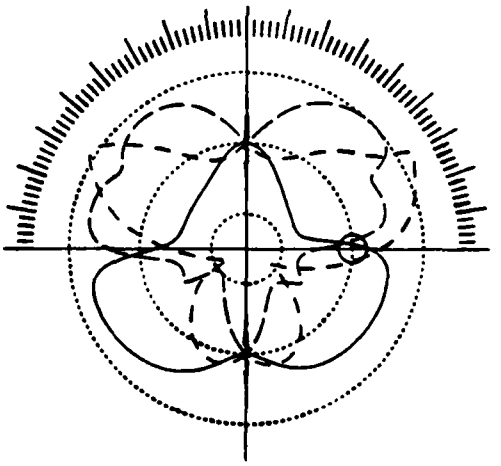

OUT-OF-PLANE ANGLE
DIV = 24.500 DEGREES

T1 T2 L

BULK ACOUSTIC WAVES IN ALPHA QUARTZ
SYMMETRY TYPE: TRIGONAL (32)

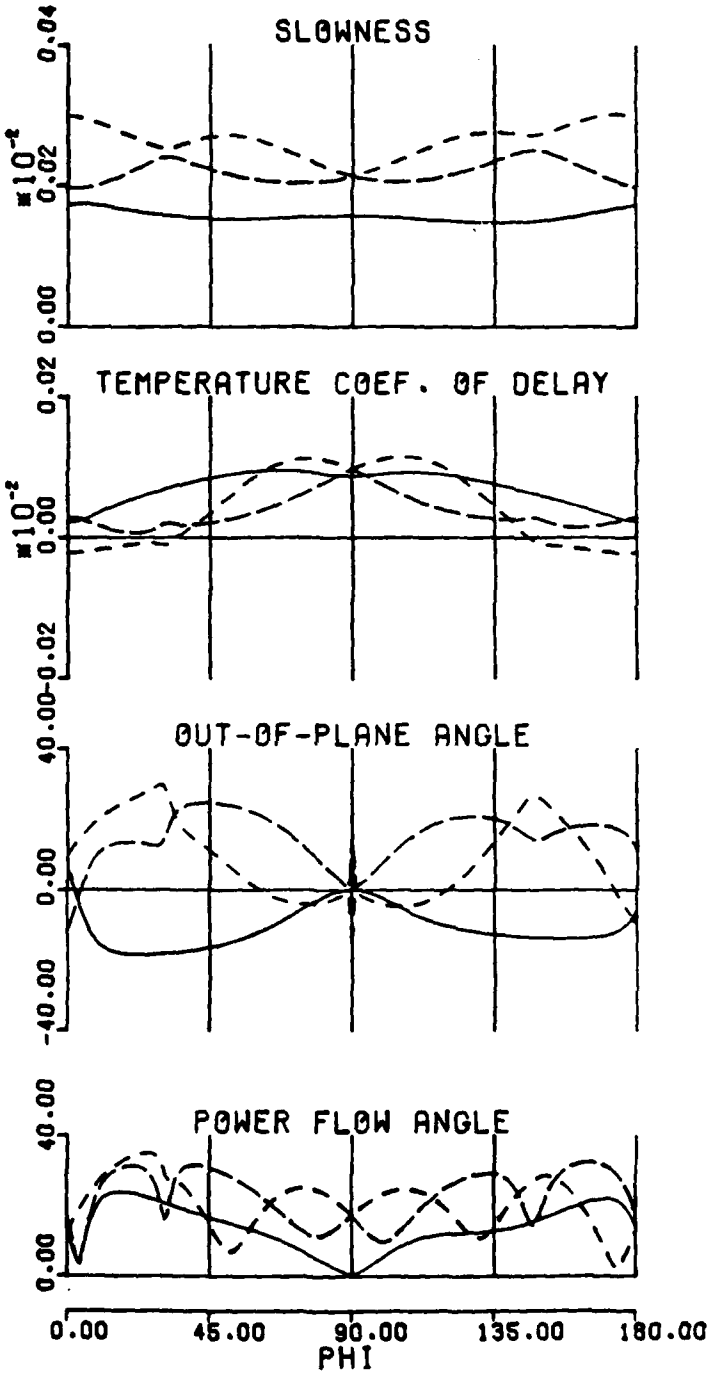
SLOWNESS
0.04
0.02
0.00
x10⁻²
TEMPERATURE COEF. OF DELAY
0.02
0.00
-0.02
x10⁻²
OUT-OF-PLANE ANGLE
40.00
0.00
-40.00
POWER FLOW ANGLE
40.00
0.00
0.00
45.00
90.00
135.00
180.00
PHI

PLANE NORMAL
(90.0, .0, 60.0)
(-.866, .500, .000)

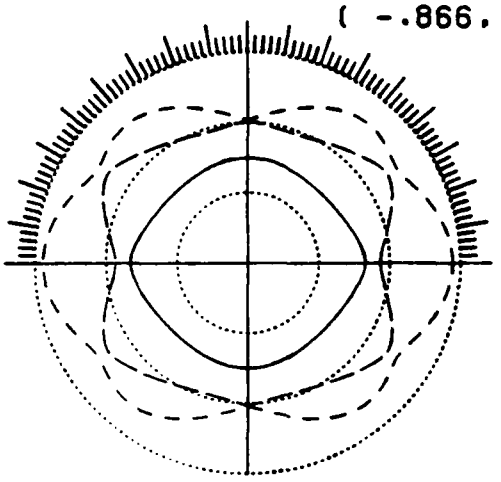

SLOWNESS
DIV =.105-03 SEC/M

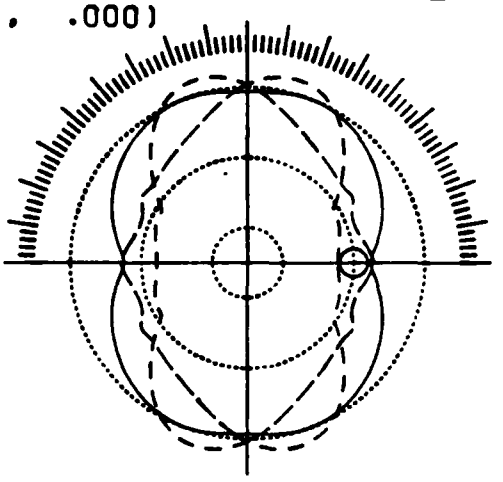

TEMPERATURE COEF. OF DELAY
DIV = .750-04/DEG C

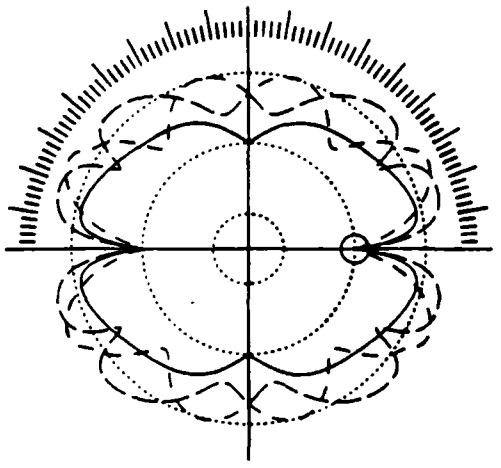

POWER FLOW ANGLE
DIV = 24.500 DEGREES

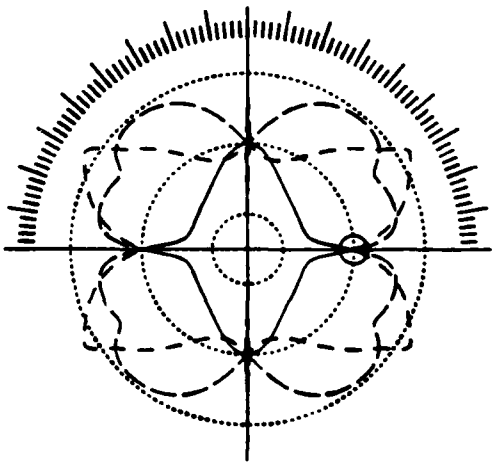

OUT-OF-PLANE ANGLE
DIV = 24.500 DEGREES

- - - - - T1 ——— T2 ——— L

BULK ACOUSTIC WAVES IN ALPHA QUARTZ
SYMMETRY TYPE: TRIGONAL (32)

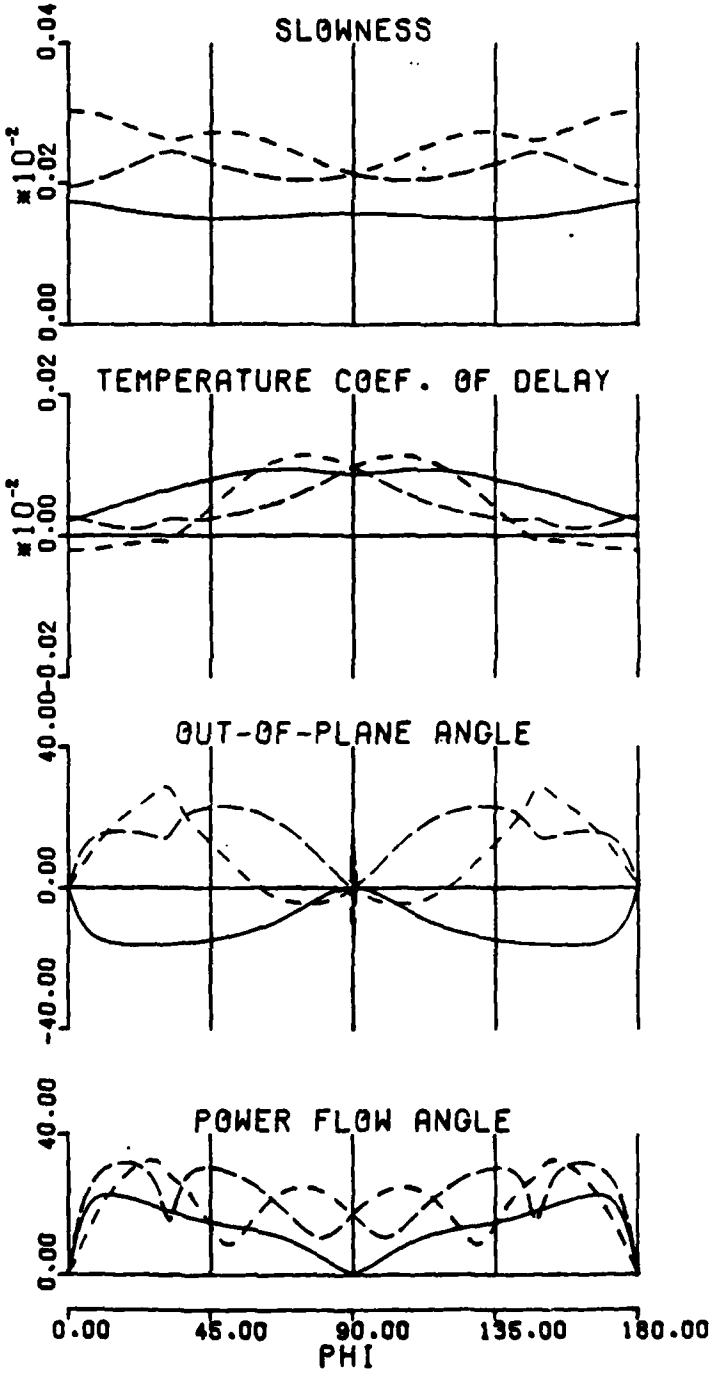
SLOWNESS
0.04
0.02
0.00
x10⁻²
TEMPERATURE COEF. OF DELAY
0.02
0.00
-0.02
x10⁻²
OUT-OF-PLANE ANGLE
40.00
0.00
-40.00
POWER FLOW ANGLE
40.00
0.00
0.00
45.00
90.00
135.00
180.00
PHI

DISTRIBUTION LIST

Administrator
Defense Technical Information Center
Attn: DTIC-DDA (12 copies)
Cameron Station, Building 5
Alexandria, Virginia 22314

Harry Diamond Laboratories
Attn: CO/TD/TSO/Division Direction

Attn: Record Copy, 81200

Attn: HDL Library, 81100 (3 copies)

Attn: HDL Library, 81100 (Woodbridge)

Attn: Technical Reports Branch, 81300

Attn: Chairman, Editorial Committee

Attn: Legal Office, 97000

Attn: Chief, 20240